Static and dynamic properties of the pion from continuum modelling of strong QCD

COBOS-MARTINEZ, JESUS,JAVIER

Static and dynamic properties of the pion from continuum modelling of strong QCD

A thesis presented for the degree of

Doctor of Philosophy

by

Jesus Javier Cobos-Martinez

Institute for Particle Physics Phenomenology

Durham University

November 2010

Abstract

We present nonperturbative numerical solutions for the quark propagator Schwinger-Dyson equation (SDE) and pseudoscalar meson Bethe-Salpeter equation (BSE) at and beyond the rainbow-ladder truncation level of this system of equations. We solve this coupled system of integral equations using a phenomenological model for the dressed gluon propagator in Landau gauge as input. In the rainbow-ladder truncation scheme, we systematically calculate static properties of the pion and kaon. After combining the rainbow-ladder truncation for the SDE-BSE system with the impulse approximation for the pion-photon vertex, we present numerical results for the pion form factor using the Ball-Chiu and bare vertices for the nonperturbative quark-photon vertex. We find that the Ball-Chiu vertex satisfies electromagnetic current conservation automatically, however, this vertex gives a charge pion radius that is less than its experimental value, leaving room for further improvement. We go beyond the rainbow-ladder truncation by including pion cloud effects into the quark propagation, and then all the way up into the pion form factor. Here we find significant changes for the mass and decay constant of the pion. For the pion form factor, on the other hand, we find no qualitative changes in the Q^2 region studied for both vertices. Nevertheless, more work remains to be done at and beyond the rainbow-ladder truncation in order to connect the pion form factor to the model-independent perturbative result.

Declaration

This dissertation is the result of my own work, except where explicit reference is made to the work of others, and has not been submitted for another qualification to this or any other university

Acknowledgements

First and foremost, my thanks go to my supervisor, Mike Pennington, for providing me the opportunity to work with him, for suggesting the research carried out in this thesis, and for his help and patience during my PhD studies.

Thanks go to my office mates, specially Aoife Bharucha, David Wilson, and Richard Williams, for their friendship, and for making our office a lively place to work in. My gratitude goes also to all my fellow PhD students and staff of the IPPP for providing a lively and friendly atmosphere in which to work.

My thanks must also go to my family for their encouragement, patience, and support throughout all my studies. A special mention goes to Maria Elena and Carlos for their friendship, support, and guidance during my undergraduate and postgraduate studies.

I must also thank all of my friends accumulated during my time in Durham: Iris, Genesis, Cesar, Maria, Misha, and Jorge. A special mention must go to Jean and her family for always being there to give a hand and their love, and for all those nice walks on the beautiful Durham country side. Last but not least, to my girlfriend Francesca for being such a lovely and enthusiastic person.

My studies in Durham would have been impossible without a CONACyT studentship which is gratefully acknowledged.

Contents

Chapter 1.

Introduction

Quantum Chromodynamics (QCD), the theory of quarks, gluons, and their interactions, is the accepted theory of the strong interactions at the fundamental level. It is a self-contained part of the Standard Model of elementary particles, whose only input parameters are the masses of the quarks and the coupling constant between these and the gluons[1]. QCD is a consistent quantum field theory with a simple and elegant Lagrangian, based entirely on the invariance under the local non-Abelian $SU(3)$ colour gauge group, and renormalisability. Out of this Lagrangian emerges an enormously rich variety of physical phenomena, structures, and phases. Exploring and *understanding* these phenomena is undoubtedly one of the most exciting challenges in modern science.

At high temperatures, above a critical temperature T_c of about 200 MeV, the elementary quark and gluon degrees of freedom are released from their confinement in hadrons. Correlations between these basic constituents are expected still to persist up to quite high temperatures, above which matter presumably exists in the form of the quark-gluon plasma. At temperatures below T_c and low baryon density, matter exists in aggregates of quarks and gluons with their colour degrees of freedom combined to form colour-singlet objects. This is the domain of low energy QCD, the physics of the hadron phase in which mesons, baryons, and nuclei exist. In this phase, the QCD vacuum has undergone a qualitative change to a ground state characterised by strong condensates of quark-antiquark pairs and gluons. In another sector, at very high baryon chemical potential, i.e. at large quark densities and Fermi momenta, it is expected that Cooper pairing of

[1]The fundamental scale $\Lambda_{\rm QCD}$, or equivalently the running coupling constant α_S, emerges from QCD through the phenomenon of dimensional transmutation; the masses of the quarks arise from the vacuum expectation values of the Higgs field, through Yukawa couplings of the Higgs boson with the quarks. Since QCD is a confining theory, the masses of the quarks are not observable, and must be determined indirectly, e.g. through the masses of the hadrons.

quark sets in and induces transitions to a complex pattern of colour superconducting and superfluid phases.

However, the Lagrangian written on the blackboard does not by itself explain the data of strongly interacting matter, and it is not clear how the plethora of the observed bound state objects, the hadrons, and their static and dynamic properties, arise from the fundamental quark and gluon fields of QCD. This is the ambitious goal of the field of hadron physics: the understanding of the properties of strongly interacting matter in all of its manifestations in terms of the underlying fundamental theory, Quantum Chromodynamics.

For "hard processes", i.e. at large momentum transfers, due to the property of asymptotic freedom of QCD, one could use the familiar perturbative language, the Feynman diagrams and the like, to describe hadron interactions. At these small distances, hadrons and their reactions, are pictured as bound states of weakly interacting quarks and gluons. This picture, however, starts to break down at energies around 1-2 GeV, and is surely inadequate at length scales corresponding to the size of the nucleon. At such scales, the strong coupling constant is large enough to invalidate perturbation theory, and one has to employ different methods to deal with what is called strong QCD.

QCD posses two important mechanisms that lie at the heart of this theory: confinement and dynamical chiral symmetry breaking. Understanding these mechanisms from first principles will surely provide the foundation for an understanding of hadron physics. Confinement is the remarkable fact that the fundamental constituents of hadrons, the quarks and gluons, cannot be removed from them and studied in isolation. Dynamical chiral symmetry breaking is responsible for the existence of light pions, and from the generation of quark masses via interactions. Neither of these phenomena can be accounted for in perturbation theory, and are therefore genuine effects of strong QCD.

In order to go from the nonperturbative quarks and gluons to the study of hadron physics, we need special tools such as QCD *correlation functions*, a bridge between the theory and the experiment. At present, our choices for the nonperturbative calculation these correlation functions are the Lattice-QCD theory and the Schwinger-Dyson equations, both of which have their own advantages and drawbacks. Lattice-QCD Monte Carlo methods, based on the discretisation of spacetime, include all the nonperturbative physics, and are therefore the only ab initio calculation method available so far. However, the simulations suffer from limitation at small momenta due to finite volume effects: one has to rely on extrapolation methods to obtain the infinite volume limit.

Furthermore, calculations including quarks use unphysically large values for the quark masses, and extrapolations to the physical values are required. On the other hand, with the Schwinger-Dyson equations (SDE), which are the quantum equations of motion for the correlation functions of the theory, we can work either in Minkowski or Euclidean space for any value of the quark masses. However, here we are working with an infinite number of coupled integral equations, and in order to obtain a closed system of equations we must introduce ansatze for the higher correlation functions that are not explicitly solved for, introducing a model dependence that is difficult to quantify. Nevertheless, these two methods are entirely complementary in their strengths and weaknesses.

As quarks and gluons are confined, we need to study the bound states of the theory since the hadrons and their properties are the objects that are observable. Bound state calculations based on the Bethe-Salpeter equation (BSE) for mesons, or on the Faddeev equation for baryons, will be the bridge between the fundamental theory, QCD, and hadron phenomenology. Drawing a connection between QCD and hadron observables, through the SDE-BSE system, is difficult due to the infinite number of equations we need to confront, and that is why modelling remains a keystone in hadron physics. Modern comparisons with and predictions of experimental data can properly be said to rest on model assumptions but they can be tested within the framework and also via comparisons with lattice-QCD simulations, and the predictions are very good. Furthermore, progress in understanding the intimate connection between symmetries and truncation schemes has enabled the proof of exact results.

In this thesis we will be concerned with the SDE-BSE approach to hadron physics, by focusing on the static and dynamic properties of the pion as a bound state of a nonperturbative quark-antiquark pair. In Chapter 2, we will introduce some basic aspects of strong QCD that will serve to set up the notation, and introduce two very important equations that will be the basis for most of the work of this thesis: the Schwinger-Dyson equation (SDE) for the quark propagator, and the Ward-Takahashi identity (WTI) for the quark-photon vertex. Chapter 3 will introduce another two important equations, supplementary to those in Chapter 2. These are the meson bound state equation, known as the Bethe-Salpeter equation (BSE), and the axial-vector Ward-Takahashi identity (axWTI). These four equations (in fact, two equations and two constraints) will illustrate the main characteristics of the SDE-BSE approach: an infinite number of integral equation that must be truncated. In Chapter 4 we will introduce the rainbow-ladder truncation of the SDE-BSE system, and solve the quark SDE and meson BSE numerically. Here, we will also present results for the static properties of pseudoscalar mesons. Moving to

dynamic properties of the pion, in Chapter 5 we will introduce the general setting of the impulse approximation of the pion-photon vertex in the SDE-BSE approach, and show that this truncation is consistent with the rainbow-ladder truncation, in the sense that electromagnetic current is conserved automatically. Furthermore, we will present numerical results for the pion form factor in this approximation. Finally, in Chapter 6 we will introduce pion cloud effects into the approach by extending the rainbow-ladder truncation with the inclusion of the pion back-reaction in the quark SDE, and then all the way into the pion BSE and pion form factor. We will accompany these with numerical results for the quark propagator, and static and dynamic properties of the pion. In Chapter 7 we give our conclusions and outlook.

Chapter 2.

Aspects of strong QCD

2.1. Introduction

Quantum Chromodynamics (QCD) is the accepted theory of the strong interactions. It is local non-Abelian gauge field theory whose gauge group is that of colour $SU(3)$. The non-Abelian nature of its gauge group not only dictates the interactions between quarks and gluons, but also induces self-interactions amongst gluons themselves.

Gluons experience colour interactions only, being blind to electroweak interactions. Quarks on the other hand, experience electromagnetic interactions. These are described by the Abelian gauge theory of Quantum Electrodynamics (QED). The gauge invariance of this theory is manifested in relations between different Green's functions, and in the physical world as the conservation of the electromagnetic charge. These not only prove to be useful in the renormalisability of the theory, but also constrain the form of the quark-photon interaction.

The Schwinger-Dyson equations of QCD also relate different Green's functions of the theory, but stem from a different origin. These are the quantum field equations of the theory, and can in principle be solved in a perturbative expansion. However, their main usefulness is in the strong coupling regime where, for example, the nonperturbative solution of the SDE for the quark propagator serves as a main input for bound state calculations.

In addition to gauge invariance, the Lagrangian of QCD possesses several symmetries. Of these, chiral symmetry and its spontaneous breakdown are fundamental in the study of bound states.

This chapter introduces the basic aspects of strong QCD that will serve as a starting point for the study of hadrons, and their electromagnetic interactions, as bound states of fully-dressed nonperturbative constituent quarks.

2.2. Gauge principle in electrodynamics

Gauge field theories are a particular class of field theories based on the gauge principle. The gauge principle requires that the theory be invariant under a local gauge transformation. A prototypical example of a gauge theory is the familiar Quantum Electrodynamics (QED). In its classical version, the theory is described by the Lagrangian

$$\mathcal{L}_{\rm QED} = \overline{\psi}(x)\left(\mathrm{i}\gamma^\mu D_\mu - m\right)\psi(x) - \frac{1}{4}F_{\mu\nu}F^{\mu\nu}, \tag{2.1}$$

where $\psi(x)$ is a spin-1/2 Dirac field with mass parameter m, $F_{\mu\nu}$ is the field strength tensor, and D_μ is the covariant derivative. These are explicitly given by

$$F_{\mu\nu} = \partial_\mu A_\nu - \partial_\nu A_\mu, \tag{2.2}$$

$$D_\mu = \partial_\mu + \mathrm{i}QeA_\mu, \tag{2.3}$$

where $A_\mu(x)$ is the electromagnetic vector potential. After gauge-fixing and quantisation, $\mathcal{L}_{\rm QED}$ successfully describes the quantum theory of electromagnetic interactions [1].

It is interesting that classical electrodynamics, and indeed its quantised version, described by Eq. (2.1), is invariant under the Abelian local (gauge) transformation

$$\psi(x) \rightarrow U(x)\psi(x), \quad U(x) = \exp\left(-\mathrm{i}Q\theta(x)\right), \tag{2.4}$$

$$A_\mu \rightarrow A_\mu + \frac{1}{e}\partial_\mu\theta(x), \tag{2.5}$$

where $\theta(x)$ is an arbitrary function of the space-time coordinate x. The name Abelian gauge transformation stems from the fact that θ is x-dependent, and that the (infinite)

set of transformations Eq. (2.4) forms the commutative (Abelian) $U(1)$ group. That is, the electric charges Q satisfy the commutative algebra corresponding to the $U(1)$ group.

Alternatively, by taking the modern viewpoint, we can postulate that the Abelian gauge transformation, Eq. (2.4), is obeyed by the Dirac field ψ, and require that the free Dirac Lagrangian

$$\mathcal{L}_{\text{fermion}} = \overline{\psi}(x)\left(\mathrm{i}\gamma^{\mu}\partial_{\mu} - m\right)\psi(x), \tag{2.6}$$

and its physical predictions, are invariant under Eqs. (2.4,2.5). This is the gauge principle. By imposing this gauge symmetry, we will be forced to introduce the vector gauge potential A_{μ}, through the covariant derivative Eq. (2.3), subject to the transformation rule Eq. (2.5). After supplementing the A_{μ} field with a kinetic term, invariant under Eq. (2.5), we will uniquely arrive at Eq. (2.1). Here, it is assumed that the Lagrangian is invariant under Lorentz transformations, the discrete symmetries* of space inversion and time reversal, and is renormalisable†.

It therefore seems that the principle of ($U(1)$) gauge invariance, applied to $\mathcal{L}_{\text{fermion}}$, has led to the correct electromagnetic interactions of the Dirac field ψ. Of course, it just happens that the $U(1)$ gauge invariance is realised in the electromagnetic interactions, but other more general (gauge) transformations could lead to other more interesting Lagrangians, that could in principle be realised in nature. This is the case of Quantum Chromodynamics, the modern theory of the strong interactions, which we now describe.

2.3. Yang-Mills theories

In the previous section we saw how the principle of gauge invariance leads to the correct form of the Lagrangian for electrodynamics. There, the gauge group from was that of $U(1)$. This is in fact the simplest possible gauge transformation. Here, we consider the gauge group $SU(N)$ since we have in mind Quantum Chromodynamics, the accepted

*A term that violates the discrete symmetries P and T is $\epsilon^{\alpha\beta\mu\nu}F_{\alpha\beta}F_{\mu\nu}$.

†The requirement of renormalisability further constrains the type of terms that can appear in $\mathcal{L}_{\text{QED}}$. For example, if the renormalisability of the theory is not required, as in so-called effective field theories, then there is no reason for the term $\overline{\psi}\sigma^{\mu\nu}F_{\mu\nu}\psi$ to be absent.

theory of the strong interactions. This theory is invariant under the colour $SU(3)$ gauge group with N_f spin-1/2 quark flavours.

We consider the Dirac fermion field $\psi(x)$, with mass parameter m, in the N-dimensional fundamental representation of the group $SU(N)$. This restricts our discussion to semi-simple Lie algebras[1], and when convenient we will write the corresponding infinitesimal expressions in order to be more explicit. The fermion field $\psi(x)$ thus has N components $\psi_i(x),\ i = 1, 2, \ldots, N$, each of them being a Dirac field. According to the gauge principle, we postulate that the Lagrangian describing the free Dirac field $\psi(x)$ be invariant under the non-Abelian gauge transformation

$$\psi_i(x) \to \psi_i'(x) = U_{ij}(x)\psi_j(x), \quad U(x) = \exp\left(-\mathrm{i}t^a\theta^a(x)\right), \tag{2.7}$$

where $\theta^a(x)$ are N^2-1 arbitrary functions of x, and the $t^a,\ a = 1, 2, \ldots, N^2-1$, are the generators associated to the $SU(N)$ group. The generators t^a satisfy the Lie algebra

$$\left[t^a, t^b\right] = \mathrm{i}f^{abc}t^c, \tag{2.8}$$

where f^{abc} are the totally antisymmetric structure constants characterising the group algebra.

The Lagrangian for the fermion field, $\mathcal{L}_{\text{fermion}}$, is clearly invariant under the corresponding global transformation Eq. (2.7). For $\theta^a(x)$ x-dependent, however, $\mathcal{L}_{\text{fermion}}$ is no longer invariant due to the derivative term. Nevertheless, it may be made invariant under the non-Abelian gauge transformation, Eq. (2.7), by replacing the ordinary derivative with the covariant one:

$$\partial_\mu \to D_\mu = \partial_\mu - \mathrm{i}gt^a A_\mu^a, \tag{2.9}$$

where A_μ^a are N^2-1 vector gauge fields, and g is the coupling constant between ψ and A_μ^a. In component form $(D_\mu)_{ij} = \delta_{ij}\partial_\mu - \mathrm{i}g(t^a)_{ij}A_\mu^a$, where $(t^a)_{ij}$ is the representation of t^a in the fundamental representation. We now replace the Lagrangian $\mathcal{L}_{\text{fermion}}$ with

$$\mathcal{L}_{\text{fermion}} = \overline{\psi}_i(x)\left(\mathrm{i}\gamma^\mu D_\mu - m\right)_{ij}\psi_j(x). \tag{2.10}$$

The Lagrangian Eq. (2.10) is invariant under Eq. (2.7) provided the $A^a_\mu(x)$ obey the transformation rule

$$t^a A^a_\mu \to t^a A'^a_\mu = U\left(t^a A^a_\mu - \frac{\mathrm{i}}{g}U^{-1}\partial_\mu U\right)U^{-1}. \tag{2.11}$$

For infinitesimal $\theta^a(x)$, we have $U(x) \approx 1 - \mathrm{i}t^a\theta^a(x)$, and Eq. (2.11) gives

$$\delta A^a_\mu \equiv A'^a_\mu - A^a_\mu = f^{abc}\theta^b A^c_\mu - \frac{1}{g}\partial_\mu\theta^a, \tag{2.12}$$

where we have used the commutation relations Eq. (2.8). We note that the infinitesimal transformation rule for A^a_μ involves only the structure constants f^{abc}, and hence the gauge fields A^a_μ belong to the adjoint representation of the algebra of $SU(N)$, where $(t^a)_{bc} = -\mathrm{i}f^{abc}$.

The Lagrangian Eq. (2.10) describes the fermion fields in interaction with the gauge fields $A^a_\mu(x)$, but in order to construct a complete theory, we still need to supplement the gauge fields $A^a_\mu(x)$ with a kinetic term. In order to do so, we first note that the covariant derivatives for the $U(1)$ gauge group of electrodynamics satisfy $[D_\mu, D_\nu] = \mathrm{i}QeF_{\mu\nu}$, where $F_{\mu\nu}$ and D_μ are given by Eqs. (2.2,2.3), respectively. Clearly the form $F^{a\mu\nu}F^a_{\mu\nu}$, with $F^a_{\mu\nu} = \partial_\mu A^a_\nu - \partial_\nu A^a_\mu$, is not invariant under Eq. (2.11) due to the non-commutative nature of the gauge group $SU(N)$. Following the case of electrodynamics, we calculate the commutator of covariant derivatives to find

$$[D_\mu, D_\nu] = -\mathrm{i}gt^a F^a_{\mu\nu}, \quad \text{where} \quad F^a_{\mu\nu} = \partial_\mu A^a_\nu - \partial_\nu A^a_\mu + g f^{abc}A^b_\mu A^c_\nu. \tag{2.13}$$

Thus, in analogy with QED, $F^a_{\mu\nu}$ may be regarded as the field strength tensor for the non-Abelian gauge fields $A^a_\mu(x)$. To work out the transformation law for $F^a_{\mu\nu}$ it is more

convenient to use the infinitesimal version of $U(x)$. Using the infinitesimal transformation law for $A^a_\mu(x)$, Eq. (2.12), and the antisymmetry of the structure constants f^{abc}, the infinitesimal transformation law for the field strength tensor is $\delta F^a_{\mu\nu} = f^{abc}\theta^b F^c_{\mu\nu}$. Hence, $F^{a\mu\nu}F^a_{\mu\nu}$ is gauge invariant, since $\delta\left(F^{a\mu\nu}F^a_{\mu\nu}\right) = 2F^{a\mu\nu}\delta F^a_{\mu\nu} = 2f^{abc}\theta^b F^{a\mu\nu}F^c_{\mu\nu} = 0$ due to the anti-symmetry of f^{abc}. Therefore, $F^{a\mu\nu}F^a_{\mu\nu}$, conventionally normalised, can be added to the Lagrangian Eq. (2.10). We thus arrive at the general form of the Lagrangian invariant under the non-Abelian gauge transformations Eqs. (2.7,2.11)

$$\mathcal{L}_{\rm QCD} = \overline{\psi}(x)\left(\mathrm{i}\gamma_\mu D^\mu - m\right)\psi(x) - \frac{1}{4}F^{a\mu\nu}F^a_{\mu\nu}. \tag{2.14}$$

In QCD, the gauge group is colour $SU(3)$, and the quarks ψ and gluons A^a_μ, belong to the fundamental and adjoint representation, respectively. The classical Lagrangian of QCD is thus given by

$$\mathcal{L}_{\rm QCD} = \sum_{k=1}^{N_f}\overline{\psi}_k(x)\left(\mathrm{i}\gamma_\mu D^\mu - m_k\right)\psi_k(x) - \frac{1}{4}F^a_{\mu\nu}F^{a\mu\nu}, \tag{2.15}$$

where the summation is over the N_f quark flavours.

There are two remarkable consequences of gauge invariance. The first one is that in the Lagrangian Eq. (2.14) there exists only one coupling constant, g, between quarks and gluons. The second is the self-interaction amongst the gauge fields A^a_μ, through the term $gf^{abc}A^{b\mu}A^{c\nu}$ in $F^{a\mu\nu}$, giving rise to cubic and quartic terms. In QCD, this self-interaction of gluons is the main source of asymptotic freedom, and possibly confinement. This last feature was not present in electrodynamics. It is entirely new, and is due solely to the non-Abelian character of the gauge transformations, Eq. (2.7). However, the non-Abelian nature of the gauge group introduces further elements into the theory, which are as remarkable as the ones just described. These new features of the theory enter through the process of quantisation, as we now describe.

2.4. Quantisation in the functional approach

In the previous section we constructed the classical non-Abelian gauge theory, Eq. (2.15), that is the basis for Quantum Chromodynamics. This is the first step in setting up QCD and we must quantise the classical Lagrangian $\mathcal{L}_{\rm QCD}$.

There are two well-known quantisation procedures. In the canonical approach to quantisation of field theories, one regards fields as operators and sets up commutation relations for them. All the Green's functions, which characterise the quantum theory, may be then calculated as vacuum expectation values of the time-ordered product of field operators. On the other hand, in the functional integral approach, fields are c-numbers and the Lagrangian is in its classical form. The Green's functions are then obtained by integrating the fields over all their functional forms with a suitable weight. Even though these are well established methods, there are some subtleties that need to be addressed in order to properly quantise the theory. One of these is the gauge invariance of the Lagrangian itself, related to the fact that there are an infinite set of gauge field configurations that are physically equivalent. In order to see this, we will concentrate below on the functional integral approach to quantisation.

For simplicity, and to set up the notation, consider only a real scalar field $\phi(x)$. The n-point Green's functions for the field $\phi(x)$ are given by the vacuum expectation value of the time-ordered product of n field operators $\hat{\phi}(x)$: $\langle 0|T\left[\hat{\phi}(x_1)\cdots\hat{\phi}(x_n)\right]|0\rangle$. In the functional integral formalism [1], these n-point Green's functions can be written as

$$\langle 0|T\left[\hat{\phi}(x_1)\cdots\hat{\phi}(x_n)\right]|0\rangle = \frac{\int \mathcal{D}\phi\phi(x_1)\cdots\phi(x_n)\exp\left(\mathrm{i}S\right)}{\int \mathcal{D}\phi\exp\left(\mathrm{i}S\right)}, \tag{2.16}$$

where S is the classical action $S = \int \mathrm{d}^4x\mathcal{L}(\phi,\partial\phi)$. The expression Eq. (2.16) may be rewritten in a more compact form by using the generating functional formalism[1]. Here, we introduce an artificial source function $J(x)$ into the functional integral through the term $\phi(x)J(x)$:

$$\mathcal{Z}[J(x)] = \int \mathcal{D}\phi\exp\left\{\mathrm{i}\int \mathrm{d}^4x(\mathcal{L}+\phi J)\right\}, \tag{2.17}$$

where $\mathcal{Z}[J(x)]$, called the generating functional, is a functional of $J(x)$. By functional differentiation of $\mathcal{Z}$ with respect to J, we can generate all the n-point functions of the theory:

$$\langle 0|T\left[\hat{\phi}(x_1)\cdots\hat{\phi}(x_n)\right]|0\rangle = \frac{(-\mathrm{i})^n}{\mathcal{Z}[0]}\frac{\delta^n\mathcal{Z}[J]}{\delta J(x_1)\cdots\delta J(x_n)}\bigg|_{J=0}. \tag{2.18}$$

In the case of gauge fields, the generating functional is given by

$$\mathcal{Z}[J(x)] = \int \mathcal{D}A \exp\left\{\mathrm{i}\int \mathrm{d}^4x \left(\mathcal{L} + A^a_\mu J^{a\mu}\right)\right\}, \tag{2.19}$$

where, for the moment, $\mathcal{L}$ is the Lagrangian for the pure gauge theory, and $\mathcal{D}A$ is a compact notation for $\prod_x \prod_{a,\mu} \mathrm{d}A^a_\mu(x)$. Note that the source term $A^a_\mu J^{a\mu}(x)$ is not gauge invariant, however the physical predictions stemming from $\mathcal{Z}[J(x)]$ must be gauge invariant.

In order to see what the main problem with gauge invariance is in the process of quantisation, set $J = 0$ in Eq. (2.19). In this case the generating functional is given by

$$\mathcal{Z}[0] = \int \mathcal{D}A \exp\left(\mathrm{i}S\right). \tag{2.20}$$

The action S is invariant under the gauge transformation $A^a_\mu \to A^{\theta a}_\mu$, where $A^{\theta a}_\mu$ denotes the gauge-transformed field, Eq. (2.11), that depends on the arbitrary functions $\theta^a(x)$. This means that if we start with a fixed A^a_μ, we can generate a continuous infinity $A^{\theta a}_\mu$ of field configurations by applying to A^a_μ the gauge transformation $U(\theta)$, Eq. (2.11). According to the above invariance, the action S is constant for all $A^{\theta a}_\mu$ in this subset, and the functional integral is badly divergent, as we are redundantly integrating over a continuous infinity of physically equivalent field configurations. To fix the problem, we would like to isolate the interesting part of the functional integral, which counts each physical configuration only once, and factor out a divergent constant. We can achieve this by means of a trick due to Faddeev and Popov [2]. This consists in applying the following restriction on A^a_μ:

$$G^\mu A^a_\mu = B^a. \tag{2.21}$$

Here, G^μ and B^a should be chosen appropriately, and we assume that Eq. (2.21) gives a unique $\theta^a(x)$ for fixed A^a_μ and B^a. In order to incorporate the constraint Eq. (2.21) into Eq. (2.20), we insert 1 under the functional integral in the form

$$1 = \int \mathcal{D}\theta(x)\delta\left(G^\mu A^{\theta a}_\mu - B^a\right)\det M_G, \quad (M_G(x,y))^{ab} = \left(\frac{\delta(G^\mu A^{\theta a}_\mu(x))}{\delta\theta^b(y)}\right), \tag{2.22}$$

where the functional integral is performed over the gauge group, and $\mathcal{D}\theta(x)$ is the invariant measure of the gauge group space [3]. Inserting Eq. (2.22) into Eq. (2.20) we obtain

$$\mathcal{Z}[0] = \int \mathcal{D}A \prod_{a,x} \mathcal{D}\theta^a(x)\delta\left(G^\mu A^{\theta a}_\mu - B^a\right)\det M_G \exp\left\{\mathrm{i}\int \mathrm{d}^4x\mathcal{L}\right\}. \tag{2.23}$$

In Eq. (2.23), everything but the argument of the delta function is gauge invariant [3], and hence we may replace $A^{\theta a}_\mu$ by A^a_μ in the argument of the delta function. Thus we have

$$\mathcal{Z}[0] = \int \mathcal{D}A \int \prod_{a,x} \mathcal{D}\theta^a(x)\delta\left(G^\mu A^a_\mu - B^a\right)\det M_G \exp\left\{\mathrm{i}\int \mathrm{d}^4x\mathcal{L}\right\}. \tag{2.24}$$

The integrand is now independent of the group parameters $\theta^a(x)$, so we can factor out the functional integral $\int \prod_{a,x} \mathcal{D}\theta^a(x)$, which is an infinite constant. The functional integral $\mathcal{Z}[0]$ is thus defined by extracting this infinite constant. The (infinite) factor $\int \mathcal{D}\theta$ will cancel out in the computation of correlation functions of gauge invariant operators [1]. Since B^a is arbitrary, we may average $\mathcal{Z}[J]$ over B^a in the sense of the functional integral, i.e. we integrate $\mathcal{Z}[J]$ in B^a with a suitable weight, which is commonly chosen to be $\exp\left\{-\frac{\mathrm{i}}{2\xi}\int \mathrm{d}^4x \left(B^a(x)\right)^2\right\}$, where ξ is the gauge parameter. Hence we obtain

$$\mathcal{Z}[J] = \int \mathcal{D}A \det M_G \exp\left\{ \mathrm{i} \int \mathrm{d}^4x \left(\mathcal{L} - \frac{1}{2\xi} \left(G^\mu A^a_\mu \right)^2 + A^a_\mu J^{a\mu} \right) \right\}. \tag{2.25}$$

In this way, we have succeeded in exponentiating the delta function representing the constraint Eq. (2.21). The resulting added term in the exponent is the so-called gauge-fixing term, with gauge parameter ξ. It is $\det M_G$ which makes the quantisation of non-Abelian gauge theories non-trivial. In Lorentz covariant gauges, which we shall use throughout this thesis, $G^\mu = \partial^\mu$ and

$$\left(M_G(x,y)\right)^{ab} = -\frac{1}{g} \left(\delta^{ab}\partial^2 - g f^{abc} \partial^\mu A^c_\mu \right) \delta^4(x-y). \tag{2.26}$$

Note that for non-Abelian gauge theories $f^{abc} = 0$, and therefore $\det M_G$ is independent of the gauge field A_μ. Thus, $\det M_G$ presents no further problems since it can be absorbed in the normalisation of the the functional integral. This is also true in temporal, Coulomb, and axial gauges, for Abelian and non-Abelian gauge theories [3].

We would like to exponentiate $\det M_G$ in a similar way as we did with the gauge-fixing condition, and regard it as part of our effective Lagrangian. This will lead us to introduce a fictitious field, called the Faddeev-Popov ghost, in the next section.

Including fermions fields, the generating functional Eq. (2.25) is given by

$$\begin{aligned} \mathcal{Z}[J,\overline{\eta},\eta] &= \int \mathcal{D}A\mathcal{D}\overline{\eta}\mathcal{D}\eta \det M_G \exp\left\{ \mathrm{i} \int \mathrm{d}^4x \left(\mathcal{L}_{\text{eff}} + A^a_\mu J^{a\mu} + \overline{\psi}\eta + \overline{\eta}\psi \right) \right\}, \\ \mathcal{L}_{\text{eff}} &= \mathcal{L}_{\text{QCD}} - \frac{1}{2\xi} \left(G^\mu A^a_\mu \right)^2, \end{aligned} \tag{2.27}$$

where η and $\overline{\eta}$ are anti-commuting source functions for the fermion fields ψ and $\overline{\psi}$, respectively, and $\mathcal{L}_{\text{QCD}}$ is given as in Eq. (2.15).

The fermion Green's functions are obtained in a similar way as in Eq. (2.16), by performing functional derivatives of Eq. (2.27) with respect to the sources η and $\overline{\eta}$. It should be stressed that ψ, $\overline{\psi}$, η, and $\overline{\eta}$ are all anti-commuting but classical c-numbers. Hence, proper account has to be taken of the sign coming from their anti-commutation

when defining correlation functions in which fermions are included. For example, the two-point Green's function (quark propagator) should be defined in the following way [3]

$$\langle 0|T\left[\hat{\psi}_\alpha(x)\overline{\hat{\psi}}_\beta(y)\right]|0\rangle = \frac{(-\mathrm{i})^2}{Z[0,0,0]}\left.\frac{\delta^2 Z[J,\overline{\eta},\eta]}{\delta\overline{\eta}_\alpha(x)\delta(-\eta_\beta(y))}\right|_{J=\eta=\overline{\eta}=0}. \tag{2.28}$$

2.4.1. Faddeev-Popov ghosts

As we mentioned above, we would like to exponentiate $\det M_G$ in a similar way as we did with the gauge-fixing condition, and regard it as part of our effective Lagrangian. Faddeev and Popov [2] chose to represent this determinant as a functional integral over a new set of anti-commuting fields $\chi^a(x)$:

$$\det M_G = \int \mathcal{D}\chi\mathcal{D}\chi^* \exp\left\{-\mathrm{i}\int \mathrm{d}^4x\mathrm{d}^4y\chi^{a*}(x)\left(M_G(x,y)\right)^{ab}\chi^b(y)\right\}, \tag{2.29}$$

where M_G is given by Eq. (2.26), and $\chi^a(x)$ is a complex fictitious field that obeys the Grassmann algebra, and belongs to the adjoint representation of the non-Abelian gauge group. The field $\chi^a(x)$ is called the Faddeev-Popov ghost, and its quantum excitations have the wrong relation between spin and statistics to be physical particles [2]. The exponent of the integrand in Eq. (2.29) may be rewritten by performing an integration by parts, such that

$$\int \mathrm{d}^4x\mathrm{d}^4y\chi^{a*}(x)\left(M_G(x,y)\right)^{ab}\chi^b(y) = -\int \mathrm{d}^4x\left(\partial^\mu\chi^a(x)\right)^* D_\mu^{ab}\chi^b(x), \tag{2.30}$$

where $D_\mu^{ab} = \delta^{ab}\partial_\mu - gf^{abc}A_\mu^c(x)$ is the covariant derivative, Eq. (2.9), in the adjoint representation. We now put all terms together. We insert Eq. (2.29) together with Eq. (2.30) into Eq. (2.27) to obtain the full generating functional of QCD:

$$\begin{aligned}
&\mathcal{Z}[J,\xi,\xi^*,\overline{\eta},\eta] = \int \mathcal{D}A\mathcal{D}\overline{\eta}\mathcal{D}\eta\mathcal{D}\xi\mathcal{D}\xi^* \exp\left\{\mathrm{i}\int \mathrm{d}^4x\,(\mathcal{L}_{\text{eff}} + \text{Sources})\right\}, \\
&\mathcal{L}_{\text{eff}} = \mathcal{L}_{\text{G}} + \mathcal{L}_{\text{GF}} + \mathcal{L}_{\text{FP}} + \mathcal{L}_{\text{F}},\ \text{Sources} = A^a_\mu J^{a\mu} + \chi^{a*}\xi^a + \xi^{a*}\chi^a + \overline{\psi}\eta + \overline{\eta}\psi,
\end{aligned} \tag{2.31}$$

where ξ^a and ξ^{*a} are Grassmann-valued source functions for the ghosts fields. Here, $\mathcal{L}_{\text{eff}}$ is a gauge-fixed quantum Lagrangian which includes the effect of $\det M_G$ through Eqs. (2.29,2.30), and

$$\mathcal{L}_{\text{G}} = -\frac{1}{4}F^a_{\mu\nu}F^{\mu\nu}_a, \qquad \mathcal{L}_{\text{GF}} = -\frac{1}{\xi}\left(\partial^\mu A^a_\mu\right)^2, \tag{2.32}$$

$$\mathcal{L}_{\text{FP}} = \left(\partial^\mu\chi^a\right)^* D^{ab}_\mu \chi^b, \qquad \mathcal{L}_{\text{F}} = \sum_{k=1}^{N_f}\overline{\psi}_k\left(\mathrm{i}\gamma_\mu D^\mu - m_k\right)\psi_k, \tag{2.33}$$

where the summation in the fermion Lagrangian $\mathcal{L}_{\text{F}}$ is over N_f quark flavours.

2.4.2. The Gribov ambiguity

When deriving $\mathcal{L}_{\text{eff}}$ in Eq. (2.31), it is was assumed that at any fixed A^a_μ and B^a, the equation $G^\mu A^a_\mu = B^a$ has a unique solution with respect to θ^a, i.e. the absence of any solution or the existence of several solutions were excluded. There are no examples of the first possibility, however, the existence of many gauge-equivalent fields obeying the same gauge condition, Eq. (2.21), was pointed out by Gribov [4, 5].

The simplest example presented by Gribov [4, 5] corresponds to Coulomb gauge, defined by the equation

$$\partial^i A_i = 0, \tag{2.34}$$

for the case of the $SU(2)$ colour gauge group. The existence of gauge-equivalent fields means that the equality

$$\partial^i A_i^{(\theta)} = 0, \tag{2.35}$$

where $A_i^{(\theta)}$ is the gauge-transformed field, is valid for non-trivial $\theta^a(x)$, and the matrix U tending to the identity matrix at $|\mathbf{r}| \to \infty$. From Eqs. (2.34,2.35) follows that

$$\left[D_i, \left(\partial_i U^{-1}\right) U\right] = 0, \tag{2.36}$$

where $D_i = \partial_i + igA_i$ is the covariant derivative, and U is given in Eq. (2.7).

Consider the case $A = 0$ and $U \in SU(2)$. One can look for spherically symmetric solutions of Eq. (2.36) in the form

$$U = \exp\left(\mathrm{i}\theta(r)\mathbf{n}\cdot\sigma\right) = \cos(\theta) + \mathrm{i}\mathbf{n}\cdot\sigma\sin(\theta), \tag{2.37}$$

where σ_k are the Pauli sigma matrices, and $\mathbf{n} = \mathbf{r}/r$. It follows[6] that the corresponding fields satisfying Eq. (2.36) are transverse fields, which are gauge equivalent to $A = 0$:

$$A_{ai}^{\theta} \overset{r\to\infty}{=} -\frac{1}{g}\epsilon_{aib}n_b\frac{1}{r}. \tag{2.38}$$

Thus, there is a family of pure gauge transverse fields, i.e. non-zero A^θ, which up to gauge transformations are equivalent to zero fields, and satisfy the gauge condition Eq. (2.35). This is a particular case of a general statement that the gauge condition Eq. (2.21) does not fix uniquely the field from a family of gauge-equivalent fields. The existence of a solution of Eq. (2.36) for an arbitrary field A_i^a can also be understood for large fields [6].

The problem of the existence of many gauge equivalent fields (Gribov copies) satisfying the same gauge condition is not particular to the Coulomb gauge, but it also occurs in covariant gauges [6]. On the other hand, axial gauges are found to be free of the Gribov ambiguity [7].

The existence of Gribov copies means that Eqs. (2.25,2.31) have to be improved. Gribov suggested [4, 5] that the problem of copies can be solved if the integration in the functional space is restricted by the potentials for which the Faddeev-Popov determinant $\det M_G$ is positive (in Euclidean space). This restriction does not concern small fields, and therefore is not significant for perturbation theory. In particular it is not significant for hard processes, where perturbation theory is applied. The existence of Gribov copies is evidently important for lattice QCD.

2.5. Symmetries of QCD

The Lagrangian of Quantum Chromodynamics possess a number of exact and approximate symmetries [8]. The most important of the exact symmetries of the Lagrangian of QCD are local gauge invariance, which we have described above, and Lorentz invariance. See [8] for a detailed account of the symmetries of QCD.

In addition to gauge symmetry, the Lagrangian of QCD, Eq. (2.15), possesses several other discrete symmetries. These are the operation of parity, charge conjugation, and time reversal. These discrete symmetries are in agreement with the observed properties of the strong interaction [**?**].

2.5.1. Strong CP problem

The analysis of the behaviour of the QCD Lagrangian, under these discrete symmetries, is considerably complicated at the quantum level, due to the fact that there is another gauge invariant operator of mass dimension four that can be added to the Lagrangian [9]:

$$\mathcal{L}_\theta = \frac{\theta g^2}{16\pi^2}\tilde{F}^{a\mu\nu}F^a_{\mu\nu}, \quad \tilde{F}^{a\mu\nu} = \frac{1}{2}\epsilon^{\mu\nu\alpha\beta}F^a_{\alpha\beta}. \tag{2.39}$$

A term of the form Eq. (2.39) would violate both parity and time reversal symmetry, in contradiction with the observed properties of the strong interactions. In the context of perturbation theory, this term is innocuous since it can be written as a total divergence:

$$\tilde{F}^{a\mu\nu}F^a_{\mu\nu} = \partial_\mu X^\mu, \quad X^\mu = \epsilon^{\mu\alpha\beta\gamma}\mathrm{Tr}\left[\frac{1}{2}A_\alpha\partial_\beta A_\gamma + \frac{\mathrm{i}}{3}gA_\alpha A_\beta A_\gamma\right]. \tag{2.40}$$

A total divergence contributes only a surface term to the action Eq. (2.31), and can therefore be neglected.

A much more sophisticated analysis [9, 10] shows that $\mathcal{L}_\theta$ can give rise to real physical effects despite the fact that it is a total divergence. The vacuum of QCD can have non-trivial topological structure, and in this case the surface term in the action integral cannot be neglected[10]. Since the operator X^μ is not gauge invariant, it can have singular behaviour at infinity without implying similar behaviour in physical gauge invariant quantities [10]. The existence of this term $\mathcal{L}_\theta$ gives rise to a violation of CP, with a magnitude dictated by the strong interactions. In fact, the limit [9] on the size of the parameter θ, coming from the measurements of the dipole moment of the neutron, is $\theta < 10^{-9}$, and it is plausible to assume that it is exactly zero. The problem of why θ is so small is referred to as the strong CP problem.

Several solutions to the strong CP problem exist in the literature [9]. One of these exploits the fact that the phase which gives rise to physical effects ($\overline{\theta}$) is a sum of a CP-violating phase in the quark mass matrix and the QCD phase θ. If the mass of the up quark were exactly zero, the net physical effect could be rotated away [9]. However, an up quark with zero mass appears not to be acceptable phenomenologically. Another mechanism is to convert θ into a parameter which is dynamically chosen to be small, rather than fixed a priori. This the Peccei-Quinn mechanism, which has the further consequence that it requires the existence of axions. Axions are hypothetical particles which couple to scalar and pseudoscalar fermion currents. However, there is at yet no definitive solution to the strong CP problem.

2.5.2. Chiral symmetry

The Lagrangian of QCD also possesses a number of approximate symmetries. Of the these symmetries, the most important for the study of hadron physics are isospin and chiral symmetry, which are related to the light-quark masses.

Consider the quark sector of the Lagrangian Eq. (2.15) with only the up and down quark fields, which in matrix notation $\psi = (\psi_u, \psi_d)^{\mathrm{T}}$ can be written as

$$\mathcal{L} = \overline{\psi}\left(\mathrm{i}\gamma_\mu D^\mu - M\right)\psi, \tag{2.41}$$

where $M = \mathrm{diag}(m_u, m_d)$ is the quark mass matrix. This Lagrangian Eq. (2.41) is invariant under a separate global phase redefinition of the up and down quark fields, and corresponds to the conservation of baryon number in the real world.

If $m_u - m_d$ is very much less than the hadronic mass scale, the symmetry of the Lagrangian Eq. (2.41) is increased. It is now invariant under a 2×2 unitary global transformation acting on the quark fields:

$$\psi^{'} = \exp\left(\sum_{i=0}^{3} \alpha_i \sigma_i\right)\psi, \tag{2.42}$$

where σ_i $(i = 1, 2, 3)$ are the Pauli matrices, and σ_0 is the unit matrix. This symmetry $U(2)_V$ can be decomposed into the product $U(1)_V \times SU(2)_V$, where $U(1)_V$ is the baryon number symmetry. The approximate $SU(2)_V$ isospin symmetry becomes exact in the limit that the up and down quarks are degenerate in mass. The Noether vector currents associated to the symmetry Eq. (2.42) are

$$J^k_\mu = \overline{\psi}\gamma_\mu\sigma^k\psi \ (k = 1, 2, 3) \quad \text{(isospin current)}, \tag{2.43}$$

$$J_\mu = \overline{\psi}\gamma_\mu\psi \quad \text{(baryonic current)}. \tag{2.44}$$

This approximate flavour current can be further enhanced by considering the strange quark to be degenerate in mass with the up and down quarks. In this case, we obtain the approximate $SU(3)_V$ flavour symmetry which gives rise to the classification of the meson and baryons into flavour octets and decuplets.

If we now take the limit in which the masses of the up and down quarks are negligible $(M = 0)$, the symmetry becomes even larger. To explain this, it is convenient to introduce the left- and right-handed projectors:

$$P_L = \frac{1}{2}\left(1-\gamma_5\right), \quad P_R = \frac{1}{2}\left(1+\gamma_5\right). \tag{2.45}$$

We may decompose the quark fields into left- and right-handed components, $\psi_L = P_L\psi$, $\psi_R = P_R\psi$, respectively. The quark sector of the Lagrangian, Eq. (2.41), becomes

$$\mathcal{L} = \overline{\psi}_L \mathrm{i}\gamma_\mu D^\mu \psi_L + \overline{\psi}_R \mathrm{i}\gamma_\mu D^\mu \psi_R. \tag{2.46}$$

There is now no term which connects left- and right-handed fields, and so independent left and right rotations of the type Eq. (2.42) leave the Lagrangian invariant, yielding a $U(2)_L \times U(2)_R = SU(2)_V \times SU(2)_A \times U(1)_V \times U(1)_A$ chiral symmetry. This implies the additional the Noether axial currents

$$J^k_{5\mu} = \overline{\psi}\gamma_\mu\gamma_5\sigma^k\psi \ (k=1,2,3), \tag{2.47}$$

$$J_{5\mu} = \overline{\psi}\gamma_\mu\gamma_5\psi. \tag{2.48}$$

To the extent that the strange quark can be considered massless, the chiral $SU(2)$ symmetry can be enlarged to chiral $SU(3)$.

However, chiral symmetry is not apparent in the observed spectrum of QCD. If it were, every hadron would be accompanied by a partner of opposite parity with the same mass. Instead, chiral $SU(2)$ is spontaneously broken, leaving only the $U(1)_V \times SU(2)_V$ symmetry of isospin and baryon number conservation. The axial-vector currents are conserved only in the chiral limit, apart from possible anomalies.

If an exact symmetry of the Lagrangian is spontaneously broken, the theory will contain massless spin-zero particles called Goldstone bosons. The Goldstone theorem states that the number of such particles will be equal to the number of spontaneously broken symmetry generators. In the case of chiral $SU(2)$ breaking to $SU(2)_V$, this implies three pseudoscalar bosons, which are identified with the three pions (π^+, π^-, π^0). The $U(1)_V \times U(1)_A$ symmetry is also broken down to $U(1)_V$, but the lost $U(1)_A$ is spoilt by quantum effects, and does not give rise to a Goldstone boson. This is related to the existence of the contribution to the Lagrangian $\mathcal{L}_\theta$, Eq. (2.39).

In the real world, the light quarks are not precisely massless, and therefore the chiral symmetry of the QCD Lagrangian is explicitly broken. Nevertheless, their masses are small on the scale of the strong interaction ($m_u \approx 4\,\mathrm{MeV}, m_d \approx 7\,\mathrm{MeV}$). Correspondingly, the pions are not precisely massless Goldstone bosons, but their masses are much smaller than those of other hadrons.

When the spontaneous symmetry breaking scenario is extended to chiral $SU(3)_A \times SU(3)_V \rightarrow SU(3)_V$, the corresponding eight Goldstone bosons are identified with the members of the lightest pseudoscalar octet: pions, kaons, anti-kaons, and the η meson. The η' meson, on the other hand, falls out of this scheme. The large η' mass reflects the axial $U(1)_A$ anomaly in QCD. Without this anomaly, QCD would actually have $U(3)_L \times U(3)_R$ symmetry, and its spontaneous breakdown would lead to nine rather than eight pseudoscalar Goldstone bosons. The axial anomaly removes the $U(1)_A$ symmetry, keeping $SU(3)_V \times SU(3)_A \times U(1)_V$ intact, which is then spontaneously broken down to $SU(3)_V \times U(1)_V$. The remaining $SU(3)$ flavour symmetry is accompanied by the conserved baryon number which generates $U(1)_V$.

Chiral condensate

Spontaneous chiral symmetry breaking goes in parallel with a qualitative rearrangement of the vacuum [11, 12], an entirely non-perturbative phenomena. The vacuum is now populated by scalar quark-antiquark pairs. The corresponding vacuum expectation value $\langle 0|\overline{\psi}\psi|0\rangle \equiv \langle\overline{\psi}\psi\rangle$ is called the chiral quark condensate. The definition of the chiral condensate is

$$\langle\overline{\psi}\psi\rangle \equiv -\mathrm{iTr} \lim_{y \rightarrow x^+} S_F(x-y), \tag{2.49}$$

with the full quark propagator $S_F(x-y) = -\mathrm{i}\langle 0|T[\psi(x)\overline{\psi}(y)]|0\rangle$. We recall Wick's theorem which states that the time-ordered product $T[\psi(x)\overline{\psi}(y)]$ reduces to the normal product $: \overline{\psi}\psi :$, plus the contraction of two field operators. When considering the perturbative quark propagator, $S_F^0(x-y)$, the time-ordered product is taken with respect to a trivial vacuum, for which the expectation value $: \overline{\psi}\psi :$ vanishes[11, 12]. Long-range, non-perturbative physics is then at the origin of a non-vanishing $: \overline{\psi}\psi :$.

In QCD, it is believed that the light-quark operator $\overline{\psi}\psi$ has a nonzero vacuum expectation value:

$$\langle 0|\overline{\psi}\psi|0\rangle = \langle 0|\left(\overline{u}u + \overline{d}d\right)|0\rangle \approx -(250\,\mathrm{MeV})^3. \tag{2.50}$$

Since the condensate connects left- and right-handed fields,

$$\langle 0|\overline{\psi}\psi|0\rangle = \langle 0|\overline{\psi}_L\psi_L + \overline{\psi}_R\psi_R|0\rangle, \tag{2.51}$$

it breaks chiral symmetry, while remaining invariant under the group $U(1)_V \times SU(2)_V$.

Axial anomaly

If the $U(1)_A$ symmetry was manifested directly, then in the chiral limit all massless hadrons would have a massless partner of opposite chirality. Since this does not happen, we assume that the symmetry is spontaneously broken. But then there should be an isospin singlet $I = 0$ pseudoscalar Goldstone boson, whose physical mass should be about the same mass as the pion. Using chiral perturbation theory, Weinberg [13] estimated the mass to be less than $\sqrt{3}m_\pi$. Among the known hadrons, the only candidates with the right quantum numbers are $\eta(548)$ and $\eta'(958)$. Both violate the Weinberg bound. Furthermore, $\eta(548)$ has already been claimed by the pseudoscalar octet. The $U(1)$ puzzle is: where is the extra Goldstone boson?

In fact, the J_5^μ current is not conserved at the quantum level due to the QCD axial anomaly

$$\partial_\mu J_5^\mu = \frac{g^2}{16\pi^2}\tilde{F}^{a\mu\nu}F^a_{\mu\nu}, \quad \tilde{F}^{a\mu\nu} = \frac{1}{2}\epsilon^{\mu\nu\alpha\beta}F^a_{\alpha\beta}. \tag{2.52}$$

The term $\tilde{F}^{a\mu\nu}F^a_{\mu\nu}$ can be written as a four-divergence, $\tilde{F}^{a\mu\nu}F^a_{\mu\nu} = \partial_\mu X^\mu$, whose integral over all space-time is proportional to the topological charge [10]. We can define a conserved but non-gauge-invariant current

$$\mathcal{J}_5^\mu \equiv J_5^\mu - \frac{g^2}{16\pi^2} X^\mu. \tag{2.53}$$

The generator of the $U(1)_A$ anomaly may now be taken to be

$$Q_5 \equiv \int \mathrm{d}^3x \mathcal{J}_5^0 = \int \mathrm{d}^3x \left[\psi^\dagger \gamma_5 \psi - \frac{g^2}{16\pi^2} X^0\right]. \tag{2.54}$$

In the Abelian case, Q_5 is gauge invariant because of the absence of the topological charge. However, this is not true in the non-Abelian case, and hence Q_5 is not a physical quantity. In fact, Q_5 is not even conserved because of the existence of instantons [10]. To see this, integrate Eq. (2.53) over Euclidean space. The result can be written in the form [10]

$$\int_{-\infty}^{\infty} \mathrm{d}t \frac{\mathrm{d}Q_5}{\mathrm{d}t} = 2q[A], \quad q[A] = \frac{g^2}{32\pi^2} \int \mathrm{d}^4x \tilde{F}^{a\mu\nu} F^a_{\mu\nu}, \tag{2.55}$$

where $q[A]$ is the topological charge, a functional of the gauge field A^a_μ. For A^a_μ corresponding to one instanton, $q[A] = 1$. Therefore, in this case, the boundary values of Q_5 in Euclidean time differ by $\Delta Q_5 = 2q[A]$. This can be attributed to the fact that an instanton interpolates (in Euclidean time) between two gauge field configurations differing by one unit of topological charge. Thus, there is no reason to expect the $U(1)_A$ to have physical manifestations [10].

2.6. Ward-Takahashi identities

The Ward identity, and its generalisation by Takahashi, are exact relations between one-particle irreducible (1PI) vertex functions and propagators, true to all orders in perturbation theory, and indeed non-perturbatively. They follow from the gauge invariance of QED and play an important role in the proof of renormalisability of this theory. Furthermore, this identity is extremely useful when studying the electromagnetic prop-

erties of hadrons in terms of their constituent quarks, as it allows the constructtion of a quark-photon vertex entirely in terms of fully-dressed quark propagators.

We will proceed in this section to derive this identity. The generating functional for QED is

$$\begin{aligned} \mathcal{Z}[J,\overline{\eta},\eta] &= \int \mathcal{D}A\mathcal{D}\overline{\eta}\mathcal{D}\eta \exp\left\{\mathrm{i}\int \mathrm{d}^4x \left(\mathcal{L}_{\text{eff}} + A^a_\mu J^{a\mu} + \overline{\psi}\eta + \overline{\eta}\psi\right)\right\}, \\ \mathcal{L}_{\text{eff}} &= \mathcal{L}_{\text{QED}} - \frac{1}{2\xi}\left(\partial^\mu A_\mu\right)^2 . \end{aligned} \tag{2.56}$$

Recall that without the gauge-fixing and source terms, the action is gauge invariant. This made $\mathcal{Z}$ infinite when integrating over all gauge field configurations, including those connected by a gauge transformation. To find a finite $\mathcal{Z}$, we were forced to introduce a gauge-fixing term[‡]. This, however, means that $\mathcal{L}_{\text{eff}}$, Eq. (2.56), is no longer gauge invariant. The physical consequences of the theory, expressed in terms of Green's functions, however, cannot depend on the gauge, so $\mathcal{Z}$ must be gauge invariant.

On performing an infinitesimal gauge transformation, the source and gauge-fixing terms in $\mathcal{L}_{\text{eff}}$ are not gauge invariant, so the integrand of $\mathcal{Z}$ picks up an extra factor,

$$\exp\left\{\mathrm{i}\int \mathrm{d}^4x \left[-\frac{1}{\xi}(\partial^\mu A_\mu)\partial^2\theta + J^\mu\partial_\mu\theta - \mathrm{i}e\theta(\overline{\eta}\psi - \overline{\psi}\eta)\right]\right\}, \tag{2.57}$$

which, since θ is infinitesimal, can be written as

$$1 + \mathrm{i}\int \mathrm{d}^4x \left[-\frac{1}{\xi}\partial^2(\partial^\mu A_\mu) - \partial_\mu J^\mu - \mathrm{i}e\theta(\overline{\eta}\psi - \overline{\psi}\eta)\right]\theta(x), \tag{2.58}$$

where we have integrated by parts to remove the derivative operator from $\theta(x)$. Invariance of $\mathcal{Z}$ means that the operator Eq. (2.58), when applied to $\mathcal{Z}$, is merely the identity. Since $\theta(x)$ is arbitrary, the operator acting on $\mathcal{Z}$ can be written as the differential equation

[‡]As we have seen, in the Abelian case the Faddeev-Popov determinant is independent of the gauge field and thus can be absorbed into the normalisation of $\mathcal{Z}$.

$$\left[\frac{\mathrm{i}}{\xi}\partial^2\partial^\mu\frac{\delta}{\delta J^\mu}-\partial^\mu J_\mu-e\left(\overline{\eta}\frac{\delta}{\delta\overline{\eta}}-\eta\frac{\delta}{\delta\eta}\right)\right]\mathcal{Z}[J,\eta,\overline{\eta}]=0, \tag{2.59}$$

where we have made the substitutions

$$\psi(x)\to\frac{1}{\mathrm{i}}\frac{\delta}{\overline{\eta}(x)},\quad \overline{\psi}(x)\to\frac{1}{\mathrm{i}}\frac{\delta}{\eta(x)},\quad A_\mu(x)\to\frac{1}{\mathrm{i}}\frac{\delta}{\delta J^\mu}. \tag{2.60}$$

Putting $\mathcal{Z}[J,\eta,\overline{\eta}]=\exp(\mathrm{i}\mathcal{W})$, where $\mathcal{W}[J,\eta,\overline{\eta}]$ is the generating functional for connected Green's functions, we can write Eq. (2.59) in terms of $\mathcal{W}$:

$$\left[\frac{1}{\xi}\partial^2\partial^\mu\frac{\delta\mathcal{W}}{\delta J^\mu}-\mathrm{i}\partial^\mu J_\mu-\mathrm{i}e\left(\overline{\eta}\frac{\delta\mathcal{W}}{\delta\overline{\eta}}-\eta\frac{\delta\mathcal{W}}{\delta\eta}\right)\right]=0. \tag{2.61}$$

Finally, we can convert Eq. (2.61) into an equation for the generating functional for proper vertices, or effective action, $\Gamma[\psi,\overline{\psi},A_\mu]$, defined by the Legendre transformation

$$\Gamma[\psi,\overline{\psi},A_\mu]=\mathcal{W}[\eta,\overline{\eta},J]+\int\mathrm{d}^4x\left(\overline{\eta}\psi+\overline{\psi}\eta+J^\mu A_\mu\right), \tag{2.62}$$

which implies that

$$\frac{\delta\Gamma}{\delta A_\mu(x)}=-J^\mu,\qquad \frac{\delta\mathcal{W}}{\delta J_\mu(x)}=A^\mu(x), \tag{2.63}$$

$$\frac{\delta\Gamma}{\delta\psi(x)}=-\overline{\eta}(x),\qquad \frac{\delta\mathcal{W}}{\delta\overline{\eta}(x)}=\psi(x), \tag{2.64}$$

$$\frac{\delta\Gamma}{\delta\overline{\psi}(x)}=-\eta(x),\qquad \frac{\delta\mathcal{W}}{\delta\eta(x)}=\overline{\psi}(x)=0. \tag{2.65}$$

Eq. (2.61) then becomes

$$-\frac{1}{\xi}\partial^2\partial^\mu A_\mu(x) + \mathrm{i}\partial\frac{\delta\Gamma}{\delta A_\mu(x)} + \mathrm{i}e\psi(x)\frac{\delta\Gamma}{\delta\psi(x)} - \mathrm{i}e\overline{\psi}(x)\frac{\delta\Gamma}{\delta\overline{\psi}(x)} = 0. \tag{2.66}$$

Now, functionally differentiate Eq. (2.66) with respect to $\psi(y_1)$ and $\overline{\psi}(x_1)$, and set $\psi = \overline{\psi} = A_\mu = 0$. The first term vanishes, and the rest give

$$\mathrm{i}\partial^\mu\frac{\delta^3\Gamma[0]}{\delta\overline{\psi}(x_1)\delta\psi(y_1)\delta A^\mu(x)} = \mathrm{i}e\delta(x-x_1)\frac{\delta^2\Gamma[0]}{\delta\overline{\psi}(x_1)\delta\psi(y_1)} - \mathrm{i}e\delta(x-y_1)\frac{\delta^2\Gamma[0]}{\delta\overline{\psi}(x_1)\delta\psi(y_1)}, \tag{2.67}$$

where the ordinary derivative is with respect to x. The left-hand side of Eq. (2.67) is the (ordinary) derivative of the 1PI fermion-photon vertex, and the two terms on the right-hand side are the inverses of exact (fully-dressed) fermion propagators. The content of Eq. (2.67) is clearer in momentum space. Fourier transforming we have

$$q^\mu\Gamma_\mu(p,q,p+q) = S_F^{-1}(p+q) - S^{-1}(q), \tag{2.68}$$

where $\Gamma_\mu(p,q,k)$ is the full fermion-photon vertex, and $S_F(p)$ is the full fermion propagator. Eq. (2.68) is known as the Ward-Takahashi identity. Taking the $q_\mu \to 0$ limit yields the Ward identity

$$\Gamma_\mu(p,0,p) = \frac{\partial S_F^{-1}(p)}{\partial p^\mu}. \tag{2.69}$$

Thus, the principle of gauge invariance not only has given us a procedure to derive interesting Lagrangians, but relations between different (e.g. 2- and 3-) n-point functions in the theory. In fact, Eq. (2.68) is the first of a series involving higher point functions.

Eqs. (2.68,2.69) will be particularly useful when we study electromagnetic interactions of mesons. We will see that in addition to ensuring current conservation, they will allow us to write the longitudinal part of the quark-photon vertex entirely in terms of the (inverse) quark propagator.

2.7. QCD Schwinger-Dyson Equations

The Schwinger-Dyson equations are the equations of motion of the quantum field theory. They are derived from the full generating functional of the quantum theory, Eq. (2.31) for QCD. The starting point for the derivation of the Schwinger-Dyson equations is the observation that the functional integral of a total derivative is zero:

$$\int \mathcal{D}\phi \frac{\delta}{\delta\phi} \equiv 0. \tag{2.70}$$

We are only interested in the explicit derivation of the SDE for the quark propagator. From this equation it will be clear what the set of SDE are. Since quark fields enter additively into the Lagrangian of QCD, we focus on just one flavour, denoted by $\psi(x)$. Furthermore, we will not consider the ghost fields since these do not couple directly to the quarks. The ghosts will enter into the quark SDE through the quark-gluon vertex, and the gluon propagator. The derivation is in fact the same as that for the fermion in QED, the only difference being the colour quantum number. Additionally, cubic and quartic interactions between gauge bosons do not enter explicitly in our derivation. We will consider thus the generating functional of QED.

To derive the SDE for the quark propagator, we apply Eq. (2.70) to the generating functional of QED, with the functional derivative taken with respect to $\overline{\psi}$:

$$\begin{aligned} 0 &= \int \mathcal{D}A\mathcal{D}\overline{\eta}\mathcal{D}\eta \exp\left\{\mathrm{i}\int \mathrm{d}^4x \left(\mathcal{L}_{\mathrm{QED}} + A^a_\mu J^{a\mu} + \overline{\psi}\eta + \overline{\eta}\psi\right)\right\} && (2.71)\\ &= \left[\frac{\delta S_{QED}}{\delta\overline{\psi}(x)}\left(-\mathrm{i}\frac{\delta}{\delta J}, -\mathrm{i}\frac{\delta}{\delta\overline{\eta}}, \mathrm{i}\frac{\delta}{\delta\eta}\right) + \eta(x)\right]\mathcal{Z}[J,\overline{\eta},\eta], && (2.72)\end{aligned}$$

where $S_{QED} = \int \mathrm{d}^4x \mathcal{L}_{\mathrm{QED}}$ with $\mathcal{L}_{\mathrm{QED}}$ given by Eq. (2.1). Performing the functional derivative we have

$$0 = \left[\eta(x) + \left(\mathrm{i}\not{\partial} - m + e\gamma^\mu(-\mathrm{i})\frac{\delta}{\delta J^\mu(x)}\right)(-\mathrm{i})\frac{\delta}{\delta\overline{\eta}(x)}\right]\mathcal{Z}[J,\overline{\eta},\eta]. \tag{2.73}$$

As we are interested in the fermion propagator, we perform and additional functional derivative with respect to $\eta(y)$, and set $\overline{\eta}(x)$ and $\eta(y)$ to zero afterwards. Thus we have, with $\mathcal{Z}[J] \equiv \mathcal{Z}[J,0,0]$,

$$0 = \delta(x-y)\mathcal{Z}[J] - \left(\mathrm{i}\not{\partial} - m + e\gamma^\mu(-\mathrm{i})\frac{\delta}{\delta J^\mu(x)}\right)\mathcal{Z}[J]S_F(x-y;J), \tag{2.74}$$

where $S_F(x-y;J)$ is the fermion propagator in the presence of the source J, as defined in Eq. (2.28). Putting $\mathcal{Z}[J,0,0] = \exp\left(\mathcal{W}[J,0,0]\right)$, Eq. (2.74) can be written as an equation for the generating functional of connected Green's functions, $\mathcal{W}[J] = \mathcal{W}[J,0,0]$:

$$0 = \delta(x-y) - \left(\mathrm{i}\not{\partial} - m + e\gamma^\mu(-\mathrm{i})\frac{\delta\mathcal{W}}{\delta J^\mu(x)}\right)S_F(x-y;J). \tag{2.75}$$

In terms of the effective action, the inverse fermion propagator is given by

$$S_F^{-1}(x-y) = \left.\frac{\delta^2\Gamma}{\delta\overline{\psi}(x)\delta\psi(y)}\right|_{\overline{\psi}=\psi=0}, \tag{2.76}$$

and so we have, setting $\overline{\psi} = \psi = J = 0$ at the end:

$$\begin{aligned}
\frac{\delta}{\delta J^\mu(x)}S_F(x-y;J) &= \int \mathrm{d}^4z \frac{\delta A_\nu(z)}{\delta J^\mu(x)}\frac{\delta}{\delta A_\nu(z)}\left(\frac{\delta^2\Gamma}{\delta\overline{\psi}(x)\delta\psi(y)}\right)^{-1} \\
&= -\int \mathrm{d}^4z\mathrm{d}^4x'\mathrm{d}^4y' \frac{\delta A_\nu(z)}{\delta J^\mu(x)}\frac{\delta^2\Gamma}{\delta\overline{\psi}(x)\psi(x')}\left(\frac{\delta}{\delta A_\nu(z)}\frac{\delta^2\Gamma}{\delta\overline{\psi}(x')\psi(y')}\right)\frac{\delta^2\Gamma}{\delta\overline{\psi}(y')\psi(y)} \\
&= e\int \mathrm{d}^4z\mathrm{d}^4x'\mathrm{d}^4y' D_{\mu\nu}(x-z)S_F(x-x')\Gamma_\nu(x',y';z)S_F(y'-y).
\end{aligned} \tag{2.77}$$

We now multiply Eq. (2.75) with $S_F^{-1}(y-y'')$, integrate with respect to y and relabel to find

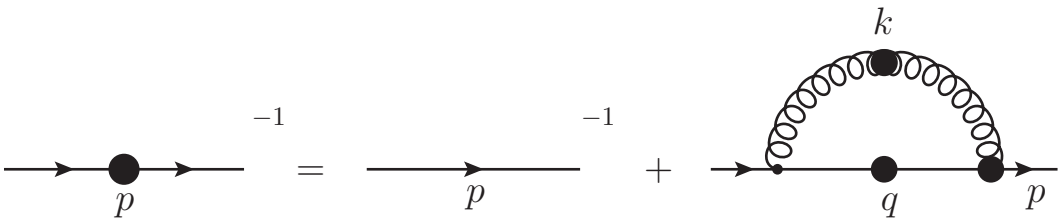

Figure 2.1.: Quark Schwinger-Dyson Equation; filled circles indicate fully dressed objects.

$$S_F^{-1}(x-y) = -(\mathrm{i}\not{\partial} - m)\delta(x-y) - \mathrm{i}e^2 \int \mathrm{d}^4z \mathrm{d}^4x' D^{\mu\nu}(x-z)\gamma_\mu S_F(x-x')\Gamma_\nu(x',y;z), \tag{2.78}$$

where $D^{\mu\nu}(x-z)$ is the photon propagator, and $\Gamma_\nu(x',y;z)$ is the quark-photon vertex. This is the SDE for the fermion propagator in coordinate space. Performing the usual Fourier transform gives the momentum space version of Eq. (2.78):

$$S_F^{-1}(p) = \mathrm{i}\not{p} - m - \mathrm{i}e^2 \int \frac{\mathrm{d}^4k}{(2\pi)^4} D^{\mu\nu}(k)\gamma_\mu S_F(q)\Gamma_\nu(p,q;k). \tag{2.79}$$

The same procedure is applied to the derivation of the SDE for the quark propagator. Here, the photon propagator gets replaced by the gluon propagator, and the quark-photon propagator by the quark-gluon vertex, with the appropriate consideration of the colour matrices. For example $\Gamma_\nu(p,q;k) \to \Gamma^a_\nu(p,q;k)$, where $a = 1,\ldots,8$ since the gluons live in the adjoint representation of $SU(3)$, and similarly $\gamma_\mu \to \gamma^a_\mu$. Furthermore, the quark propagators carry the colour index $i = 1,2,3$, which is left implicit below, because they belong to the fundamental representation of the colour $SU(3)$ group. Thus the SDE for the quark propagator in QCD is

$$S_F^{-1}(p) = \mathrm{i}\not{p} - m - \mathrm{i}g^2 \int \frac{\mathrm{d}^4k}{(2\pi)^4} D^{\mu\nu}(k)\delta^{ab}t^a\gamma_\mu S_F(q)\Gamma^b_\nu(p,q;k), \tag{2.80}$$

where g is the QCD coupling constant, $D^{\mu\nu}(k)\delta^{ab}$ is the gluon propagator, and $\Gamma^a_\nu(p,q;k)$ is the quark-gluon vertex. Both of these quantities satisfy their own SDE, which are

connected to higher n-point functions and so on, thus making an infinite tower of integral equations. The quark SDE is represented pictorially in Figure 2.1.

As we mentioned in Section 2.5.2, chiral symmetry is broken spontaneously. We will see that this effect can be studied with the SDE for the quark propagator. In particular, we will see how the strong interaction in the quark SDE generates (constituent) quark masses of several hundred MeV, even in the limit of zero current quark masses. In addition to this, we will see how the pattern of chiral symmetry breaking emerges when we combine the quark SDE with the meson bound state equation.

2.8. Renormalisation

The gauge coupling and mass parameters in the Lagrangian of QCD are not physical. These quantities need to be brought from their bare values to the their physical values, i.e. quantities that can be experimentally measured. This is achieved through the process of renormalisation, see [14, 15] for a detailed exposition. This process is carried out through the replacements

$$g = Z_g g_R, \quad m = Z_m m_R, \tag{2.81}$$

where Z_g and Z_m are the renormalisation constants for the gauge coupling and mass parameter, respectively, and the subscript R indicates the renormalised quantity. However, the most general objects are the Green's functions, and their renormalisation requires additional renormalisation constants. For the quark and gluon propagators we have

$$S(p) = Z_2 S_R(p), \quad Z_3 D^{ab}_{\mu\nu}(k) = D^{ab}_{R\mu\nu}(k), \tag{2.82}$$

where we note that only the transverse part of the gluon receives radiative corrections. Renormalisation is also required for the interaction vertices. Omitting the Lorentz and colour indices, we can write

$$\Gamma^{\bar{q}gq} = Z_{1F}^{-1}\Gamma_R^{\bar{q}gq}, \quad \Gamma^{3g} = Z_1^{-1}\Gamma_R^{3g}, \quad \Gamma^{4g} = Z_4^{-1}\Gamma_R^{4g}. \tag{2.83}$$

The renormalisability of the theory means that the renormalised quantities, being expressed in terms of renormalised charges and masses, remain finite in the limit when the regularisation is removed.

In covariant gauges, one also needs to renormalise the ghost propagator, the ghost-gluon vertex, and the gauge parameter. The renormalisation constants for the first two Green's functions are $\tilde{Z}_3$ and $\tilde{Z}_1$, respectively. For the gauge parameter, the renormalisation constant is usually taken to be equal to that of the gluon field

$$\xi = Z_3\xi_R. \tag{2.84}$$

The renormalised coupling constant $g = g(\mu)$, where μ is the renormalisation point, can be defined using any of the interaction vertices. Its universality required by gauge invariance means that

$$Z_g^{-1} = Z_3^{1/2}Z_2Z_{1F}^{-1} = Z_3^{3/2}Z_1^{-1} = Z_3Z_4^{-1/2} = Z_3^{1/2}\tilde{Z}_3\tilde{Z}_1^{-1}. \tag{2.85}$$

This means that the renormalisation constants are not independent. The relations

$$\frac{Z_3}{Z_1} = \frac{Z_2}{Z_{1F}} = \frac{Z_3^{1/2}}{Z_4^{1/2}} = \frac{\tilde{Z}_3}{\tilde{Z}_1} \tag{2.86}$$

are fulfilled as a consequence of gauge invariance. These relations are a consequence of the Slavnov-Taylor identities [3], which are the non-Abelian extension of the Ward-Takahashi identities in QED. They guarantee the universality of the coupling constant.

In terms of renormalised quantities, the quark SDE takes the same form as before, the difference being the appearance of the appropriate renormalisation constants:

$$S_F^{-1}(p) = Z_2 \left[S^{\text{bare}}(p)\right]^{-1} - Z_{1F} \mathrm{i} g^2 \int \frac{\mathrm{d}^4 k}{(2\pi)^4} D^{\mu\nu}(k) t^a \gamma_\mu S_F(q) \Gamma^a_\nu(p, q; k), \tag{2.87}$$

where we have suppressed the R subscript.

Up to now we have now developed a considerable part of our machinery for the study of strong QCD. They are the renormalised quark SDE, the Ward-Takahashi identity, and the notions of chiral symmetry breaking. These will be the building blocks for the study of the properties and interactions of the lightest bound states in QCD, e.g. the pion.

Chapter 3.

QCD Bound State Equations

3.1. Introduction

Bound states appear as poles in n-point Green's functions. In perturbative QCD, it is implicitly assumed that we can obtain a reasonable estimate of scattering amplitudes by calculating a few Feynman diagrams of lowest order [**?**]. However, there are many problems [16, 17, 18, 19, 20] for which the calculation of a few Feynman diagrams is inadequate*.

The study of bound states in QCD is one of these problems. A bound state produces a pole in the scattering amplitude in the channel in which it appears. If the bound state is truly composite, no such pole exists in any Feynman diagram, or any finite sum [21]. A pole can only be generated by an infinite sum of diagrams [21].

Ideally, we would like to sum all Feynman diagrams which describe the reaction. If we could do this we assume we have the correct answer. However, such a summation is not possible in general, and we must settle for an infinite sum of a particular class of diagrams we believe particularly important physically (e.g. ladder diagrams). This is achieved by finding an integral equation, the solution of which can be as interpreted as the sum of the class of diagrams under consideration.

*In QCD, the running of the coupling constant introduces further problems, since in the low energy region, appropriate for bound states, QCD is a confining theory and thus the coupling constant becomes strong. In fact, it is divergent [**?**].

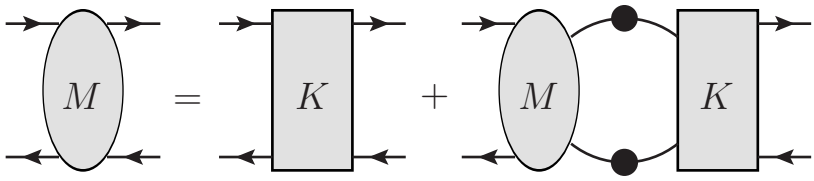

Figure 3.1.: Quark-antiquark scattering matrix SDE: K is the quark-antiquark, fully amputated, two-particle irreducible, scattering kernel; filled dots on the quark lines indicate quark propagators are fully dressed.

3.2. QCD Bound State Equations. Bethe-Salpeter Equation

In QCD, hadrons are bound states of quarks and gluons: mesons corresponds to poles in the 4-point Green's function $\langle 0|q_1 q_1 \bar{q}_2 \bar{q}_2|0\rangle$, and baryons correspond to poles in the 6-point Green's function $\langle 0|qqq\bar{q}\bar{q}\bar{q}|0\rangle$. However, for the purposes of this thesis, we will only treat the bound state equations for mesons, and thus Γ below will represent a quark-meson vertex. Baryons studies can be found in e.g. [22, 23, 24].

As said earlier in the introduction to this chapter, we need an integral equation whose solution can be interpreted as the infinite sum of a particular class of diagrams, or as the infinite sum of all diagrams contributing to the scattering amplitude's bound state pole. We will derive below this integral equation, and in subsequent chapters will solve it for particular classes of diagrams.

In principle, using the functional integral approach developed in the first chapter we can derive all of the equations we need. The quark-antiquark scattering amplitude, M, satisfies the Schwinger-Dyson equation (colour, flavour, and spin indices have been suppressed for brevity)

$$M(p,k;P) = K(p,k;P) + \int_q K(p,q;P)G(q,P)M(q,k;P), \tag{3.1}$$

where M is the 4-point quark-antiquark scattering amplitude, G is a two-body (a quark and an antiquark) dressed-propagator, and K is the fully amputated, two-particle irreducible, quark-antiquark scattering kernel of the equation. $\int_q$ is the integration over the internal loop momenta. Its specific form depends on the equation under consideration, and the appropriate form for the Bethe-Salpeter Equation (BSE) will be given below.

The same applies to the two-body propagator G. The Feynman diagram for Eq. (3.1) is given in Figure 3.1.

If the kernel in Eq. (3.1) is "small", so that perturbation theory converges, the solution of Eq. (3.1) can be obtained formally by iteration. This generates a Born series of the form

$$M = K + \int KGK + \iint KGKGK + \cdots + (\int KG)^n K + \cdots , \tag{3.2}$$

where momentum arguments have been suppressed for notational convenience. Typically, each of the terms in the series is identified with a Feynman diagram[†] (or a part of it), so the sum in Eq. (3.2) is indeed a sum of Feynman diagrams (or parts of Feynman diagrams). Note that successive terms in the sum represent products of the kernel K connected by the propagator G. Any Feynman diagram which can be written in such a form, i.e.

$$M_R = \int M_1 G M_2, \tag{3.3}$$

is said to be reducible with respect to the propagator G[‡], and clearly such a diagram cannot be part of the kernel. The kernel must be built up only of irreducible diagrams.

If we replace the integrals in Eq. (3.2) by sums over a finite set of discrete points in momentum space, so that K and M are matrices and G is a diagonal matrix, then the series in Eq. (3.2) is a geometric series which can be formally summed, giving

$$\begin{aligned} M &= K + KGK + KGKGK + \cdots + (KG)^n K + \cdots \\ &= (1 - KG)^{-1} K. \end{aligned} \tag{3.4}$$

[†]However, in nonperturbative QFT a correspondence between a mathematical expression and a Feynman diagram might not always be possible.

[‡]When M is an n-point Green's function G is an n-body propagator.

For cases when the Born series does not converge, the solution of Eq. (3.1) may still exist, and can be regarded as the analytic continuation of the sum Eq. (3.4), from a region where it converges to a region where is does not converge. This situation is familiar from the theory of complex functions; for example, the complex function

$$f(z) = \frac{z}{1-z} \tag{3.5}$$

is the unique analytic continuation of the series

$$f(z) = \sum_n z^n, \tag{3.6}$$

from the region inside the unit circle $|z| < 1$ to the region outside, $|z| \geq 1$. Note that there is a pole at $z = 1$. If z is a matrix, as in our case, then the generalisation of the existence of a pole at $z = 1$ is that z has eigenvalue equal to one, so that if the corresponding eigenvector is $\mathbf{a}$, then the condition for a pole can be written as

$$\mathbf{a} = z\mathbf{a}. \tag{3.7}$$

The corresponding condition for a pole in the 4-point Green's function M is therefore

$$\Gamma(p;P) = \int_q K(p,q;P)G(q,P)\Gamma(q;P). \tag{3.8}$$

This is the integral equation that we were looking for, the integral equation for the bound state. The function Γ is known as the vertex function. In QCD, Γ is known as the Bethe-Salpeter Amplitude (BSA), and the bound state equation as the Bethe-Salpeter Equation [25, 26]. Writing explicitly the two-body dressed-propagator for a quark and an anti-quark, noting that $G\Gamma = S\Gamma S$, and putting back the relevant indices, the BSE has the form

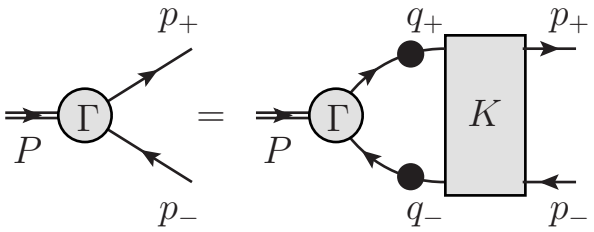

Figure 3.2.: Bethe-Salpeter Equation: Γ is the fully-amputated quark-meson vertex or Bethe-Salpeter Amplitude; K is the quark-antiquark fully-amputated, two-particle irreducible, scattering kernel; filled dots on the quark lines indicate that the propagators are-fully dressed.

$$[\Gamma(p;P)]_{tu} = \int \frac{\mathrm{d}^4 q}{(2\pi)^4} [K(p,q;P)]_{tu;rs} [S(q_+)\Gamma(q;P)S(q_-)]_{sr}, \tag{3.9}$$

where $q_+ - q_- = P$, $P^2 = -m_H^2$ is the meson mass shell, and $s, t, u, \ldots$ represent flavour, colour, and Dirac indices. This equation is depicted in Figure 3.2. The general form of Γ will depend on the quantum numbers (e.g. spin, parity, charge conjugation, etc.) of the meson under consideration [27].

We have shown that the bound state equation Eq. (3.8) is a sufficient condition for a bound state. It is also a necessary condition. The presence of a bound state is associated with a pole at $P^2 = -m_H^2$ in the quark-antiquark scattering matrix M below threshold, so the M matrix near the meson bound state pole would have the form

$$[M(p,k;P)]_{tu;rs} = [\Gamma(p;P)]_{tu} \frac{1}{P^2 + m_H^2} [\overline{\Gamma}(k;P)]_{rs} + [R(p,k;P)]_{tu;rs}, \tag{3.10}$$

pictured in Figure 3.3, where m_H is the bound state mass. In Eq. (3.10), R is a remainder term that has no pole at $P^2 = -m_H^2$. Note that the vertex function is not uniquely defined because the separation into a pole term and a non-pole term is not unique away from the pole. However, this will not be a problem because we will need the vertex function only at the pole. On the other hand, we can circumvent this problem by introducing an eigenvalue $\lambda(P^2)$ into the bound state equation Eq. (3.8) in order to have solutions for all P^2. Eq. (3.9) is thus replaced by

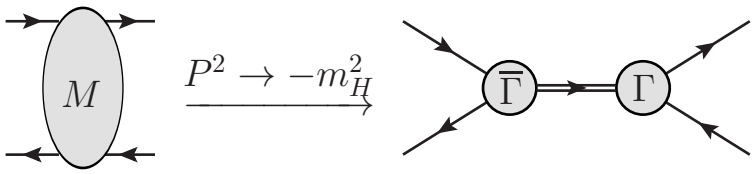

Figure 3.3.: M near the bound state pole: Γ is the fully amputated quark-meson Bethe-Salpeter Amplitude.

$$[\Gamma(p;P)]_{tu} = \lambda(P^2) \int \frac{\mathrm{d}^4 q}{(2\pi)^4} [K(p,q;P)]_{tu;rs} [S(q_+)\Gamma(q;P)S(q_-))]_{sr}, \tag{3.11}$$

with the physical solution corresponding to $\lambda = 1$ at $P^2 = -m_H^2$. The introduction of the eigenvalue $\lambda(P^2)$ will be particularly useful when finding solutions to Eq. (3.8) iteratively, as described in Appendix A.

Assuming the existence of the bound state, and the form taken by the quark-antiquark scattering matrix M near the meson bound state pole[§], Eq. (3.10), an equation for Γ can be derived by using the integral equation for M, Eq. (3.1). Substituting Eq. (3.10) into Eq. (3.1), multiplying by $P^2 + m_H^2$, and then taking the limit $P^2 \to -m_H^2$, eliminates all terms not singular at $P^2 = -m_H^2$. Dropping $\overline{\Gamma}$ from both sides gives Eq. (3.8). Thus, the BSE follows from the pole structure of the quark-antiquark scattering matrix M below threshold.

Note that strictly speaking $\Gamma(p;P)$ is uniquely defined only at the bound state pole, where $P^2 = -m_H^2$. Alternatively, we may say that Eq. (3.8) does not hold everywhere, except at the meson mass shell where $P^2 = -m_H^2$, and hence it is an eigenvalue equation.

3.2.1. Normalisation of the Bethe-Salpeter Amplitude

The bound state equation Eq. (3.8) is an homogeneous eigenvalue equation, and in order for Bethe-Salpeter Amplitude to be completely defined it needs to be normalised. Although the normalisation for the BSA is implicitly given by Eq. (3.10), we need a more practical way for normalising it.

[§]Away from the bound state pole the form Eq. (3.10) is not valid, see the paragraph above Eq. (3.11).

The normalisation condition for the bound state can be obtained directly from Eq. (3.1) and the form of the M-matrix, Eq. (3.10), near the bound state pole. To this end, we note that Eq. (3.1) can be written as

$$M = K + \int MGK, \tag{3.12}$$

where for compactness we have suppressed all momentum arguments in M, K, and G. The equivalence between Eq. (3.1) and Eq. (3.12) follows from the fact that they generate the same Born series Eq. (3.2). In general, K will be real, however, G will be in general complex. Hence, Eq. (3.12) may also be written as

$$\overline{M} = K + \int \overline{MG}K, \tag{3.13}$$

where the bar represents the adjoint, which includes complex conjugation and any additional operations. Writing Eq. (3.13) as

$$K = \overline{M} - \int \overline{MG}K, \tag{3.14}$$

and substituting this equation for K under the integral in Eq. (3.1) gives

$$M = K + \int \overline{M}GM - \iint \overline{MG}KGM. \tag{3.15}$$

Substituting Eq. (3.10), written in shorthand as

$$M = \Gamma \frac{1}{P^2 + m_H^2} \overline{\Gamma} + R, \tag{3.16}$$

into Eq. (3.15), gives terms with a double pole at $P^2 = -m_H^2$, a single pole, and no pole. The double pole terms occur only at the right-hand side, and are

$$\text{double poles} = \left(\frac{1}{P^2 + m_H^2}\right)^2 \left\{\Gamma \int (\overline{\Gamma} G \Gamma)\overline{\Gamma} - \Gamma \iint (\overline{\Gamma} G K G \Gamma)\overline{\Gamma}\right\}. \tag{3.17}$$

The coefficient of the double pole term must be zero at $P^2 = -m_H^2$. Dropping the initial factor of Γ, and the final factor of $\overline{\Gamma}$, gives

$$\begin{aligned} \int \overline{\Gamma} G \Gamma - \iint \overline{\Gamma} K G \Gamma &= \int \overline{\Gamma} G \left[\Gamma - \int K G \Gamma\right] \\ &= \int \left[\overline{\Gamma} - \int \overline{\Gamma} G K\right] G \Gamma \\ &= 0, \end{aligned} \tag{3.18}$$

where the last equality follows because of the bound state equation Eq. (3.8). Alternatively, by equating poles on both sides, Eq. (3.18) is another way to obtain the bound state equation Eq. (3.8), assuming M has the form Eq. (3.10) below threshold.

Next, we look at the single poles. There are terms from the single poles, and terms from the expansion of the coefficients of the double poles, near $P^2 = -m_H^2$, the residue of the double poles. The terms involving R do not contribute because of the bound state equation Eq. (3.8). The expansion of the coefficient of the double pole terms, near $P^2 = -m_H^2$, will generate terms proportional to $\partial\Gamma/\partial P^2$, and $\partial\overline{\Gamma}/\partial P^2$. Again, by using the bound state equation Eq. (3.8), these terms do not contribute either. Finally, the only new result comes from the balancing of the single pole on the left-hand side with the derivatives of G, and GKG, on the right-hand side. Thus we obtain

$$\Gamma\overline{\Gamma} = \Gamma \int \left(\overline{\Gamma} \frac{\partial G}{\partial P^2}\Big|_{P^2=-m_H^2} \Gamma\right) \overline{\Gamma} - \Gamma \iint \left(\overline{\Gamma} \frac{\partial (GKG)}{\partial P^2}\Big|_{P^2=-m_H^2} \Gamma\right) \overline{\Gamma}. \tag{3.19}$$

This can be simplified by dropping the common factor $\Gamma\overline{\Gamma}$, and using the bound state equation, giving

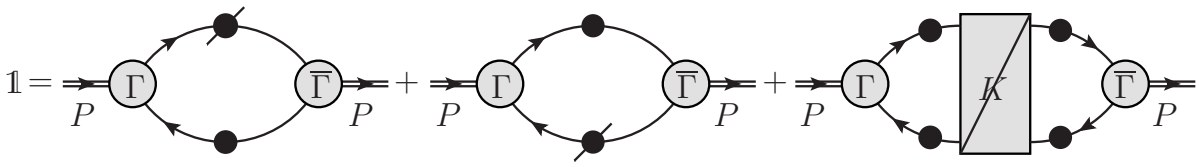

Figure 3.4.: Full normalisation condition for the Bethe-Salpeter amplitude. A slash over a quantity denotes a derivative with respect to the total meson momenta.

$$1 = \int \overline{\Gamma} \frac{\partial G}{\partial P^2}\Big|_{P^2=-m_H^2} \Gamma + \iint \overline{\Gamma} G \frac{\partial K}{\partial P^2}\Big|_{P^2=-m_H^2} G\Gamma, \tag{3.20}$$

depicted in Figure 3.4. Note that the derivation of Eq. (3.20) did not depend on any detail, but only on the structure of the equation. It can therefore be used to obtain the normalisation of any bound state amplitude. For the cases when K is independent of the bound state total momentum P, the normalisation condition reduces to

$$1 = \int \overline{\Gamma} \frac{\partial G}{\partial P^2}\Big|_{P^2=-m_H^2} \Gamma. \tag{3.21}$$

3.2.2. An equivalent normalisation condition for the BSA

In current Bethe-Salpeter equation studies [28, 23, 24, 29], the canonical normalisation condition for the bound state amplitude, Eq. (3.20), is written explicitly as

$$\begin{aligned} 2P_\mu = \int \frac{\mathrm{d}^4 q}{(2\pi)^4} \Bigg\{ & \mathrm{Tr}\left[\overline{\Gamma}(q;-P)\frac{\partial S(q_+)}{\partial P_\mu}\Gamma(q;P)S(q_-)\right] \\ & + \mathrm{Tr}\left[\overline{\Gamma}(q;-P)S(q_+)\Gamma(q;P)\frac{\partial S(q_-)}{\partial P_\mu}\right]\Bigg\} \\ + \iint \frac{\mathrm{d}^4 k}{(2\pi)^4}\frac{\mathrm{d}^4 q}{(2\pi)^4} & \left[\overline{\chi}(q;-P)\right]_{sr} \left[\frac{\partial K(k,q;P)}{\partial P_\mu}\right]_{tu;rs} \left[\chi(k;P)\right]_{ut}, \end{aligned} \tag{3.22}$$

where $\chi(q;P) = S(q_+)\Gamma(q;P)S(q_-)$ is the bound state wave function, and $\overline{\Gamma}(q;-P)^t = C^{-1}\Gamma(-q;-P)C$ with $C = \gamma_2\gamma_4$ the charge conjugation matrix, and X^t denoting the transpose of the matrix X.

An alternative but equivalent normalisation condition to Eq. (3.22) is given by[30, 31]

$$\left(\frac{1}{\lambda}\frac{d\lambda}{dP^2}\right)^{-1} = \int \frac{\mathrm{d}^4q}{(2\pi)^4}\mathrm{Tr}\left[S(q_+)\Gamma(q;P)S(q_-)\overline{\Gamma}(q;-P)\right], \tag{3.23}$$

where λ is the eigenvalue introduced in Eq. (3.11), and $\lambda = 1$ at $P^2 = -m_H^2$. This alternative normalisation condition can be derived in the same way as the bound state equation, by assuming Eq. (3.10) and equating coefficients of poles terms [30, 31]. The advantage of this normalisation condition stems from the fact that it can be applied to any truncation scheme of the Bethe-Salpeter kernel, K, in addition to being a one-loop equation, and so easier to calculate. However, this normalisation condition does not give a hint as to the type of diagrams that need to be considered when calculating electromagnetic form factors, as will be seen in Chapter 5.

3.3. Dynamical Chiral Symmetry Breaking

3.3.1. Chiral symmetry

The QCD Lagrangian Eq. (2.15) with three light quark flavours has a global symmetry

$$SU(3)_V \times SU(3)_A \times U(1)_V \times U(1)_A \tag{3.24}$$

if one neglects the masses of the current up, down, and strange quarks[¶], which are small compared to the typical low-energy scale of QCD, that is, 1 GeV. The $U(1)_V$ symmetry reflects baryon number conservation, and the $U(1)_A$ is not a symmetry at the quantum level because of the axial anomaly[8]. If the $SU(3)_V \times SU(3)_A$ chiral symmetry of the QCD Lagrangian were intact in the vacuum state, we would observe degenerate multiplets in the particle spectrum corresponding to the above symmetry group, and all hadrons made up of these light quarks would have their degenerate partners with opposite parity. Since this degeneracy is not observed in nature, the implication is that

[¶]The mass of the strange quark is much larger than that of the up and down quarks, and thus the $SU(2)_V \times SU(2)_A$ would be a better approximate chiral symmetry when chiral symmetry is explicitly broken.

the chiral symmetry is dynamically broken down to $SU(3)_V$ in the QCD vacuum, i.e. realised in the Nambu-Goldstone mode. The nonzero values of the quark masses break chiral symmetry explicitly, and move the masses of the octet of pseudoscalar mesons from their massless Goldstone boson character to their actual physical masses.

Direct evidence for the spontaneously broken chiral symmetry is a nonzero value of the quark condensate for the light flavours [11, 32, 33]

$$\langle 0|\overline{q}q|0\rangle \approx -(240 - 250 \text{ MeV})^3, \tag{3.25}$$

which represents the order parameter of spontaneously broken chiral symmetry [32, 33]. That this is true we know from various sources: current algebra, QCD sum rules, and lattice QCD [34, 35, 36]. Schwinger-Dyson Equation studies also support this value [37].

There are two important consequences of the spontaneous breaking of chiral symmetry. The first one is the appearance of an octet of pseudoscalar mesons of low mass (π, K, η), which represent the associated Goldstone bosons. The η' decouples from the original nonet because of the $U(1)_A$ anomaly [35, 8]. The second one is that the valence quarks acquire a dynamical or constituent mass through their interaction with the collective excitations of the QCD vacuum– $\bar{q}q$ excitations and the instanton [32, 12].

In the chiral limit ($m_u = m_d = m_s = 0$), all members of the pseudoscalar octet (π, K, η) would have zero mass, which is clearly seen in the Gell-Mann–Oakes-Renner relations [35] that relate the pseudoscalar meson masses to the quark condensates and current quark masses. Therefore, the nonzero mass of the pseudoscalar mesons is determined by the nonzero value of the quark condensate, a signal of DCSB, and the nonzero values of the current quark masses.

As we will see in the next section, and following chapters, the phenomenological consequences of chiral symmetry breaking, spontaneous or otherwise explicit, and its breaking pattern, can be studied in the Schwinger-Dyson–Bethe-Salpeter approach to low energy QCD, namely, hadron physics.

3.3.2. Axial-Vector Ward-Takahashi identity

The above phenomenological features of chiral symmetry, and its dynamical breaking, can be systematically studied in the functional integral approach to QCD, by means of the renormalised axial-vector Ward-Takahashi identity (axWTI)

$$-\mathrm{i}P_\mu\Gamma^H_{5\mu}(k;P) = S^{-1}(k_+)\gamma_5 T^H + \gamma_5 T^H S^{-1}(k_-) - \{\Gamma^H_5(k;P), M_H\}, \tag{3.26}$$

where $M_H = \mathrm{diag}(m_u, m_d, m_s)$ is the current quarks mass matrix, $P = k_+ - k_-$, and T^H gives the flavour structure of the meson under consideration, e.g. $T^{K^+} = \frac{1}{2}(\lambda^4 + \mathrm{i}\lambda^5)$, $T^{\pi^+} = \frac{1}{2}(\lambda^1 + \mathrm{i}\lambda^2)$ with $\{\lambda^i, i = 1, \ldots, 8\}$ the $SU(3)$-flavour Gell-Mann matrices.

As can be seen from Eq. (3.26), the axWTI relates the axial-vector vertex $\Gamma^H_{5\mu}$, the pseudoscalar vertex Γ^H_5, and the quark propagator S. This in turn implies a relationship between the kernel in the BSE and that in the quark SDE. This will be made explicit below, and must be preserved by any viable truncation scheme of the SDE-BSE complex. It is the preservation of this identity which will prove useful in obtaining the defining characteristics of the octet of pseudoscalar mesons mentioned above, namely, their low mass, and their masslessness in the chiral limit.

The renormalised axial-vector vertex satisfies its own SDE, namely,

$$\Gamma^H_{5\mu}(k;P) = Z_2\gamma_5\gamma_\mu T^H + \int \frac{\mathrm{d}^4q}{(2\pi)^4} K(k,q;P) S(q_+)\Gamma^H_{5\mu}(q;P)S(q_-), \tag{3.27}$$

with the appropriate indices contracted. The renormalised pseudoscalar vertex similarly satisfies

$$\Gamma^H_5(k;P) = Z_4\gamma_5 T^H + \int \frac{\mathrm{d}^4q}{(2\pi)^4} K(k,q;P) S(q_+)\Gamma^H_5(q;P)S(q_-), \tag{3.28}$$

where in both equations, Eq. (3.27) and Eq. (3.28), $K(k,q;P)$ is the Bethe-Salpeter kernel that appears in the bound state equation Eq. (3.8); Z_2 and Z_4 are the renormalisation constants that appear in the quark SDE, Eq. (2.87).

In order to reveal the connection between the kernel in the BSE and the kernel in the quark SDE, rewrite the axWTI, Eq. (3.26), as

$$-\mathrm{i}P_\mu\Gamma^H_{5\mu}(k;P) + \{\Gamma^H_5(k;P), M_H\} = S^{-1}(k_+)\gamma_5 T^H + \gamma_5 T^H S^{-1}(k_-) \tag{3.29}$$

and rewrite the right-hand side using the general form of the renormalised dressed-quark propagator, $S^{-1}(p) = Z_2\mathrm{i}\not{p} + Z_4 M_H + \Sigma(p)$ with $\Sigma(p) = \mathrm{diag}(\Sigma_u(p), \Sigma_d(p), \Sigma_s(p))$, as

$$\begin{aligned} S^{-1}(k_+)\gamma_5 T^H + \gamma_5 T^H S^{-1}(k_-) = \; & Z_2\mathrm{i}\not{P}\gamma_5 T^H + Z_4\{\gamma_5 T^H, M_H\} \\ & + \Sigma(k_+)\gamma_5 T^H + \gamma_5 T^H \Sigma(k_-), \end{aligned} \tag{3.30}$$

where $\{\gamma_5, \gamma_\mu\} = 0$, and $P = k_+ - k_-$ have been used.

By using the SDE, Eqs. (3.27,3.28), for $\Gamma^H_{5\mu}$ and Γ^H_5, respectively, the left-hand side of Eq. (3.29) can be rewritten as

$$\begin{aligned} -\mathrm{i}P_\mu\Gamma^H_{5\mu}(k;P) + \{\Gamma^H_5(k;P), M_H\} = \; & Z_2\mathrm{i}\not{P}\gamma_5 T^H + Z_4\{\gamma_5 T^H, M_H\} \\ & + \int_q K(k,q;P) S(q_+) \left[-\mathrm{i}P_\mu\Gamma^H_{5\mu} + \{\Gamma^H_5, M_H\}\right] S(q_-). \end{aligned} \tag{3.31}$$

Now, the term between square brackets can be rewritten by using Eq. (3.29), to obtain

$$\begin{aligned} -\mathrm{i}P_\mu\Gamma^H_{5\mu}(k;P) + \{\Gamma^H_5(k;P), M_H\} = \; & Z_2\mathrm{i}\not{P}\gamma_5 T^H + Z_4\{\gamma_5 T^H, M_H\} \\ & + \int_q K(k,q;P) S(q_+) \\ & \times \left[S^{-1}(q_+)\gamma_5 T^H + \gamma_5 T^H S^{-1}(q_-)\right] S(q_-). \end{aligned} \tag{3.32}$$

Finally, by equating both sides, Eq. (3.32) and Eq. (3.30), and cancelling identical terms, we obtain

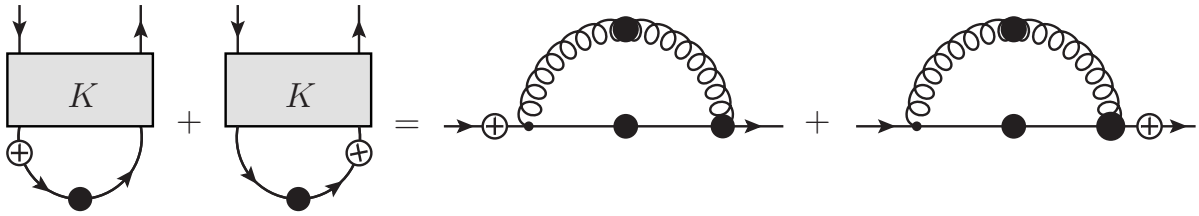

Figure 3.5.: The axial-vector Ward-Takahashi identity Eq. (3.33): It relates the quark self-energy to the quark-antiquark scattering kernel. Filled dots denote fully dressed objects, while cross circles denote a γ_5 insertion.

$$\int \frac{\mathrm{d}^4 q}{(2\pi)^4} K_{tu;rs}(k,q;P)\left[\gamma_5 T^H S(q_-) + S(q_+)\gamma_5 T^H\right]_{sr} = \left[\Sigma(k_+)\gamma_5 T^H + \gamma_5 T^H \Sigma(k_-)\right]_{tu}, \quad (3.33)$$

which clearly makes evident the relationship between the kernel in the BSE and that in the the quark SDE, through the quark self-energy, as advertised. This identity is depicted in Figure 3.5. It is a crucial identity that ensures the correct implementation of chiral symmetry and its breaking pattern. A quark-antiquark scattering kernel K that preserves this identity in the chiral limit will ensure the appearance of the pion as the Goldstone boson of chiral symmetry breaking. In addition, for nonzero current quark masses, it will lead to a generalisation of the Gell-Mann–Oakes–Renner relation, see Eq. (3.42).

We will use this expression, Eq. (3.33), in future chapters to construct the Bethe-Salpeter kernel. Any truncation or approximation to the kernel of these equation must preserve this relation in order to capture an essential symmetry of the strong interactions and its breaking pattern, as emphasised in [28, 23, 24, 29].

3.3.3. Axial-Vector Ward-Takahashi identity II

Independent of the assumptions about the form of the quark-antiquark scattering kernel K, we derive an explicit relation between the pseudoscalar BSA and the quark propagator in the chiral limit, by using the axWTI, Eq. (3.26). For any value of the current quark masses, we also obtain an exact expression for the pseudoscalar decay constant, and a relation between the pseudoscalar mass, decay constant, quark condensate, and current quark masses.

Consider first the chiral limit, $M_H = \mathrm{diag}(0,0,0)$, of the axial-vector Ward-Takahashi identity, Eq. (3.26):

$$-iP_\mu \Gamma^H_{5\mu}(k;P) = S^{-1}(k_+)\gamma_5 T^H + \gamma_5 T^H S^{-1}(k_-). \tag{3.34}$$

The axial-vector vertex has the general form [27]

$$\begin{aligned}\Gamma^H_{5\mu}(k;P) = \; & T^H \gamma_5 \left[\gamma_\mu F_R(k;P) + \not{k} k_\mu G_R(k;P) - \sigma_{\mu\nu} k_\nu H_R(k;P)\right] \\ & + \tilde{\Gamma}^H_{5\mu}(k;P) + \frac{r_A P_\mu}{P^2 + m_H^2}\Gamma^H(k;P),\end{aligned} \tag{3.35}$$

where $F_R, \ldots, H_R$, and $\tilde{\Gamma}^H_{5\mu}$, are regular as $P^2 \to -m_H^2$, $P_\mu \tilde{\Gamma}^H_{5\mu} \sim O(P^2)$, and $\Gamma^H(k;P)$ is the solution of the homogeneous BSE for a pseudoscalar bound state, whose general form is given by [27]

$$\Gamma_H(p;P) = T^H \gamma_5 \left[\mathrm{i}E_H(p;P) + \not{P} F_H(p;P) + \not{p}(p\cdot P) G_H(p;P) + \sigma_{\mu\nu} p_\mu P_\nu H_H(p;P)\right], \tag{3.36}$$

where the functions $E_H, \ldots, H_H$ are Lorentz-scalar dressing functions that characterise $\Gamma^H(k;P)$, e.g. $E_H(k;P) = E_H(k^2, k\cdot P; P^2)$, with $P^2 = -m_H^2$ the pseudoscalar meson mass shell.

By substituting Eq. (3.35) into Eq. (3.34), it is clear that, if present, Γ^H satisfies Eq. (3.9). Hence, if Γ^H is nonzero then the pseudoscalar mass pole in Eq. (3.35) must be at $P^2 = -m_H^2$, since Eq. (3.9) admits nonzero solutions only for $P^2 = -m_H^2$. Therefore, if $K(k,q;P)$ supports such a bound state, then the axial-vector vertex, Eq. (3.35), contains a pseudoscalar pole contribution. However, the residue r_A is not fixed by the homogeneous Bethe-Salpeter equation [38].

Assuming $m_H^2 = 0$ above, substituting Eqs. (3.35,3.36,2.87) into Eq. (3.34), and equating poles we find [38] the chiral limit relations

$$
\begin{aligned}
r_A E_H(k;0) &= B(k^2) && (3.37)\\
F_R + 2r_A F_H(k;0) &= A(k^2) && (3.38)\\
G_R + 2r_A G_H(k;0) &= 2A'(k^2) && (3.39)\\
H_R + 2r_A H_H(k;0) &= 0 && (3.40)
\end{aligned}
$$

where $A(k^2)$ and $B(k^2)$ are the dressing functions of the quark propagator in the chiral limit, and the prime denotes a derivative of $A(k^2)$ with respect to its argument.

It is important to note at this point that to any order in perturbative QCD, $B(k^2) = 0$ in the chiral limit[39, 40, **?**, 33]. The appearance of a nonzero $B(k^2)$ solution of the quark SDE in the chiral limit indicates that chiral symmetry is dynamically broken. Eq. (3.35) and Eqs. (3.37-3.40) show that when chiral symmetry is dynamically broken: (1) the homogeneous, flavour-non-singlet, pseudoscalar BSE, has a massless solution; (2) the BSA for the massless pseudoscalar bound state has a term proportional to γ_5 alone, with the momentum dependence of $E_H(k;0)$ completely determined by the scalar part of the quark propagator in the chiral limit, in addition to other structures that are not zero in general; and (3) the axial-vector vertex is dominated by the pseudoscalar bound state pole at $P^2 = 0$.

For $M_H \neq 0$, the axial-vector Ward-Takahashi identity is given in Eq. (3.26). The pseudoscalar vertex satisfies the inhomogeneous SDE, Eq. (3.28), and has the general form

$$
\begin{aligned}
\mathrm{i}\Gamma_5^H(k;P) = T^H\gamma_5\big[\mathrm{i}E_R^P + \not{P}F_R^P(k;P) + \not{k}(k\cdot P)G_R^P(k;P)\\
+ \sigma_{\mu\nu}k_\nu P_\mu H_R^P(k;P)\big] + \frac{r_P}{P^2+m_H^2}\Gamma^H(k;P),
\end{aligned}
\qquad (3.41)
$$

where $E_R^P, \ldots, H_R^P$ are regular as $P^2 \to -m_H^2$, that is, the pseudoscalar vertex also receives a contribution from the pseudoscalar bound state pole. In this case, after equating poles on both sides of Eq. (3.26), we obtain

$$
r_A m_H^2 = r_P \mathcal{M}_H, \qquad (3.42)
$$

where $\mathcal{M}_H \equiv \mathrm{Tr}_{\mathrm{Flavour}}[M_H\{T^H,(T^H)^t\}]$.

By using similar arguments, i.e. by equating pole structures, we can obtain explicit expressions for the residues r_A and r_P. In particular, we will see that r_A is equal to the pseudoscalar leptonic decay constant, as defined below. To see this, note that Eq. (3.27) can be written as

$$\frac{1}{Z_2}\Gamma^H_{5\mu}(k;P) = \gamma_5\gamma_\mu T^H + \int \frac{\mathrm{d}^4q}{(2\pi)^4} M(k,q;P)S(q_+)\gamma_5\gamma_\mu T^H S(q_-), \tag{3.43}$$

where M is the quark-antiquark scattering amplitude introduced in Eq. (3.1). Substituting the general form of $\Gamma^H_{5\mu}$, Eq. (3.35), and the form of M below threshold, Eq. (3.10), into Eq. (3.43), and equating residues on both sides of this equation at the pseudoscalar pole, we obtain

$$r_A P_\mu = Z_2 \int \frac{\mathrm{d}^4q}{(2\pi)^4} \mathrm{Tr}\left[(T^H)^t\gamma_5\gamma_\mu S(q_+)\Gamma^H(q;P)S(q_-)\right], \tag{3.44}$$

where the trace is over Dirac, colour, and flavour indices. The appearance of the renormalisation constant Z_2 on the right-hand side of this equation, Eq. (3.44), is necessary to ensure that r_A is independent of the renormalisation point, regularisation mass-scale, and gauge parameter [41].

Furthermore, we can give a physical meaning to r_A by considering the renormalised axial-vector vacuum polarisation, and its relation to the pseudoscalar leptonic decay constant f_H at the pseudoscalar bound state pole.

The renormalised axial-vector vacuum polarisation is given by

$$\Pi^H_{\mathrm{W}\mu\nu}(P) = \left(Z_3^{\mathrm{W}} - 1\right)\left(\delta_{\mu\nu}P^2 - P_\mu P_\nu\right) - Z_2 g_{\mathrm{W}}^2 \int \frac{\mathrm{d}^4q}{(2\pi)^4} \mathrm{Tr}\left[T^H\gamma_5\gamma_\mu\chi^H_{5\nu}(q;P)\right], \tag{3.45}$$

where Z_3^{W} is the weak-boson wave-function renormalisation constant, and g_{W} is the electroweak coupling. The pseudoscalar leptonic decay constant f_H appears with the pseudoscalar bound state pole contribution to this vacuum polarisation [41] as

$$\Pi^H_{\mathrm{W}\mu\nu}(P) = \left(\delta_{\mu\nu}P^2 - P_\mu P_\nu\right)\left[\Pi(P^2) + g_{\mathrm{W}}^2 f_H^2 \frac{1}{P^2 + m_H^2}\right], \tag{3.46}$$

where $\Pi(P^2)$ is regular as $P^2 \to -m_H^2$. As before, after substituting the general form for the axial-vector vertex, Eq. (3.35), and Eq. (3.46) into Eq. (3.45), and equating poles on both sides we find

$$r_A = f_H, \tag{3.47}$$

that is, the residue of the pseudoscalar bound state pole in the axial-vector vertex is the pseudoscalar leptonic decay constant.

By an identical procedure, but this time using the general form of the pseudoscalar vertex, Eq. (3.41), and its SDE, Eq. (3.28), we find the following explicit expression for the residue of the pseudoscalar bound state pole in the pseudoscalar vertex

$$r_P = Z_4 \int \frac{\mathrm{d}^4 q}{(2\pi)^4} \mathrm{Tr}\left[(T^H)^t \gamma_5 S(q_+)\Gamma^H(q;P)S(q_-)\right]. \tag{3.48}$$

Recall that the renormalisation constant Z_4, appearing on the right-hand side of Eq. (3.48), depends on the gauge parameter, the regularisation mass-scale, and the renormalisation point. This dependence is what is required to ensure that r_P is finite and gauge-parameter independent[38]. Its renormalisation point dependence is just what is required to ensure that Eq. (3.42) is independent of the renormalisation point [41].

Using the general form for the pseudoscalar bound state Γ^H, Eq. (3.36), and the chiral limit relations Eqs. (3.37-3.40) we find

$$r_H^\chi = -\frac{1}{f_H^\chi}\langle 0|\bar{q}q|0\rangle^\chi, \tag{3.49}$$

where the superscript χ indicates that the quantity is calculated in the chiral limit, and $\langle 0|\bar{q}q|0\rangle^\chi$ is the chiral vacuum quark condensate. The chiral vacuum quark condensate, as defined here, is given by

$$-\langle 0|\bar{q}q|0\rangle^\chi \equiv Z_4 \int \frac{\mathrm{d}^4 q}{(2\pi)^4} \mathrm{Tr}\left[S^\chi(q)\right], \tag{3.50}$$

where the trace is over colour and Dirac indices. It is renormalisation-point dependent, but independent of the gauge parameter and regularisation mass-scale[41]. As a corollary of Eq. (3.42) we find

$$f_\pi^2 m_\pi^2 = -\left[m_u + m_d\right]\langle 0|\bar{q}q|0\rangle + 0(\hat{m}_q^2) \tag{3.51}$$

$$f_K^2 m_K^2 = -\left[m_u + m_s\right]\langle 0|\bar{q}q|0\rangle + 0(\hat{m}_q^2), \tag{3.52}$$

where m_u, m_d, and m_s are the renormalisation-point dependent current-quark masses, and $\hat{m}$ is the renormalisation-group independent current-quark mass. The above relations, Eqs. (3.51,3.52), are what are commonly known as the Gell-Mann–Oakes–Renner relations. They are a consequence of chiral symmetry and its breaking pattern, as implemented by the axial-vector Ward-Takahashi identity.

3.4. Summary

By assuming a pole structure for the quark-antiquark scattering matrix, Eq. (3.10), we have defined the Bethe-Salpeter amplitude and derived its bound state equation Eq. (3.8). This is an homogeneous eigenvalue equation that admits solutions only for discrete values of the meson momenta squared $P^2 = -m_H^2$. In order to have solutions for all values of $P^2 = -m_H^2$ we have introduced a fictitious eigenvalue to it, see Eq. (3.11). Being the solution of a homogeneous eigenvalue equation, the normalisation of the BSA

has to be defined by a separate equation. Again, by assuming the pole structure of the quark-antiquark scattering matrix, Eq. (3.10), and balancing poles, we have obtained a normalisation condition for the BSA. An alternative, but equivalent, normalisation condition that includes the fictitious eigenvalue was also derived.

In principle, the only input quantities to the bound state equation are the quark-antiquark scattering kernel and the constituent dressed-quark propagators. Both of these quantities satisfy their own SDE. However, e.g. the quark propagator itself depends on the full gluon propagator, and the full quark-gluon vertex through the quark SDE. In turn, these 2- and 3-point functions depend on other higher n-point functions, and so on. This dependence illustrates the major drawback of the Schwinger-Dyson equations approach to quantum field theory: It is an infinite tower of coupled n-point functions which has to be truncated in order to define a tractable problem. That is, we have to make an ansatz for the n-point functions whose SDE are not explicitly solved for.

Irrespective of the complexity of the truncation scheme designed, it has to respect some qualitative features of the strong interactions, such as chiral symmetry and its breaking pattern, in order to be a viable truncation scheme. This is the content of Eq. (3.33) and the way in which chiral chiral symmetry breaking is *implemented* in the SDE-BSE approach. Any truncation scheme employed on the quark SDE kernel must be related, via Eq. (3.33), to that employed in the quark-antiquark scattering kernel, in order to preserve an essential symmetry of the strong interactions, namely chiral symmetry and its breaking pattern. This relation is satisfied by ensuring the preservation of the axial-vector Ward-Takahashi identity Eq. (3.26). In a more practical way, Eq. (3.33) can be used to construct the kernel for the BSE given an expression for the quark self-energy.

Independent of the form of the quark-antiquark scattering kernel, we derived a number of explicit relations involving the BSA and the quark propagator. In the chiral limit, and when chiral symmetry is dynamically broken through a nonzero value of the quark mass dressing function: the homogeneous, flavour-non-singlet, BSE has a massless pseudoscalar bound state solution, with a term proportional to γ_5 alone, and whose momentum dependence is given completely in terms of the scalar part of the quark propagator, Eq. (3.37), which in turn is nonzero due to chiral symmetry being spontaneously broken. An expression for the chiral quark condensate has also been given. Away from the chiral limit, we obtained an explicit expression for the residue of the pseudoscalar bound state pole in the axial-vector vertex, and that in the pseudoscalar vertex, respectively; a relation between these, via the pseudoscalar bound state mass

squared and the renormalised current quark masses, a generalisation of the Gell-Mann–Oakes–Rener relation, has also been obtained. Finally, by considering the axial-vector vacuum polarisation, and its form near the pseudoscalar bound state pole, we derived an explicit relation for the pseudoscalar leptonic decay constant, and related this to the residue of the pseudoscalar bound state pole in the axial-vector vertex.

Because of the nature of the infinite nesting of the system of SDE-BSE, it will inevitably be necessary to introduce a truncation scheme. The results discussed above will provide important guidance in determining the structure of the BSE kernel, and be a useful test for further approximations made.

Chapter 4.

Rainbow-Ladder truncation of SDE-BSE

4.1. Introduction

The complex nature of the SDE-BSE system of equations requires the introduction of a truncation scheme in order to define a tractable problem. In this chapter we introduce the rainbow-ladder [38, 42] truncation scheme of this system of equations, and provide a phenomenologically-motivated model for the effective quark-quark interaction. We then systematically study its phenomenological consequences for the static properties of the pion and kaon, by calculating their masses and decay constants. This is achieved after solving numerically the corresponding equations for the quark propagators and meson Bethe-Salpeter amplitudes. The results presented will allow the verification of the general results based on chiral symmetry and its dynamical breaking, as presented in the previous chapter. This will give us the confidence to take this truncation scheme as a foundation for future improvement.

4.2. The quark SDE

The starting point for the study of mesons, as bound states of dressed quarks and gluons, is the SDE for the dressed-quark propagator in QCD. It is one of the main inputs to the meson BSE, as seen in the previous chapter. The SDE for the dressed-quark propagator describes how the propagation of a quark is modified as it travels through the interacting vacuum of QCD. In propagating through this medium, the quark and gluon

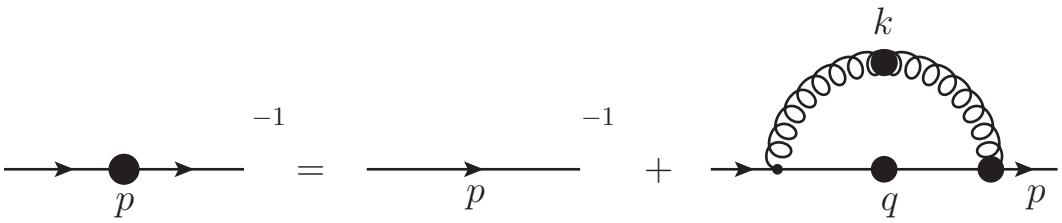

Figure 4.1.: Quark Schwinger-Dyson Equation; filled circles indicate fully dressed objects.

propagators acquire momentum-dependent modifications that fundamentally alter their spectral properties. It is therefore important for us to understand such modifications in order to study meson bound states as composed of dressed quarks and gluons. We start this section with some general features of the renormalised quark SDE as obtained from general Quantum Field Theory in Euclidean space. More detailed presentations can be found in [28, 23, 24, 43].

In QCD, the renormalised Schwinger-Dyson equation for the dressed-quark propagator for a particular quark flavour, as derived in Chapter 2, is

$$S^{-1}(p) = Z_2(\mathrm{i}\not{p} + m_{\mathrm{bare}}) + Z_1 \int \frac{\mathrm{d}^4 q}{(2\pi)^4} g^2 D_{\mu\nu}(k) \frac{\lambda^a}{2} \gamma_\mu S(q) \Gamma^a_\nu(k,p), \tag{4.1}$$

where $k = p - q$ is the momentum of the gluon, g is the renormalisation-point-dependent coupling constant, $D_{\mu\nu}(k)$ is the renormalised dressed-gluon propagator, $\Gamma^a_\nu(k,p)$ is the renormalised dressed-quark-gluon vertex, and m_{bare} is the bare current-quark mass that appears in the Lagrangian Eq. (2.27); $Z_1(\mu,\Lambda)$ and $Z_2(\mu,\Lambda)$ are the quark-gluon-vertex and the quark wave-function renormalisation constants, respectively, which depend on the renormalisation point μ and the regularisation mass scale Λ. This equation is depicted in Figure 4.1. The dressed-quark propagator, as well as the dressed-gluon propagator, and the dressed-quark-gluon vertex, depend on the renormalisation point at which they are defined; however, observables do not depend on this.

The quark SDE explicitly shows what we mentioned at the end of the previous chapter: The SDE are a coupled infinite set of nonlinear integral equations. The kernel in Eq. (4.1) involves the dressed-gluon propagator $D_{\mu\nu}(k)$ and the dressed-quark-gluon-vertex $\Gamma^a_\nu(k,p)$, which in turn satisfy their own SDE and therefore the quark SDE is coupled to them. These equations in turn are coupled to higher n-point functions ... *ad infinitum*, and hence the SDE are an infinite tower of coupled nonlinear integral equa-

tions, with a tractable problem being defined once a truncation scheme has been specified. The problem is further complicated once we want to study meson bound states as composed of dressed quarks and gluons. However, independent of these complexities, general results can be derived as demonstrated in the previous chapter.

The general form of the renormalised dressed-quark propagator, obtained as the solution of Eq. (4.1), is given in terms of two Lorentz-scalar dressing functions, written in various forms as

$$\begin{aligned} S^{-1}(p) &= \mathrm{i}\not{p}A(p^2,\mu^2) + B(p^2,\mu^2) \\ &= Z^{-1}(p^2,\mu^2)\left[\mathrm{i}\not{p} + M(p^2)\right], \end{aligned} \tag{4.2}$$

which are equivalent. In the last form, $Z(p^2,\mu^2)$ is known as the wave-function renormalisation, and $M(p^2)$ is the dressed-quark mass function, which is independent of the renormalisation point if the quark propagator is renormalised multiplicatively.

The solution of the quark SDE, Eq. (4.2), is subject to the renormalisation condition, for μ large and spacelike [38],

$$S^{-1}(p)\Big|_{p^2=\mu^2} = \mathrm{i}\not{p} + m(\mu), \tag{4.3}$$

where $m(\mu)$ is the flavour-dependent renormalised current-quark mass, and

$$m(\mu) = Z_m^{-1}(\mu,\Lambda)m_{\mathrm{bare}}(\Lambda), \quad Z_m(\mu,\Lambda) = Z_2^{-1}(\mu,\Lambda)Z_4(\mu,\Lambda), \tag{4.4}$$

hold, with $Z_m(\mu,\Lambda)$ being the mass renormalisation constant. In this thesis we will take the renormalisation point to be $\mu = 19\,\mathrm{GeV}$, as we want to compare our results to those of others.

The renormalisation constants Z_2 and Z_4 are determined by imposing the renormalisation condition, Eq. (4.3), on the solutions of the quark SDE, Eq. (4.1). These in turn

imply the following renormalisation conditions for the quark dressing functions given in Eq. (4.2):

$$A(\mu^2,\mu^2) = 1 \tag{4.5}$$
$$B(\mu^2,\mu^2) = m(\mu). \tag{4.6}$$

Equations for the quark propagator dressing functions $A(p^2)$ and $B(p^2)$ can be derived by taking appropriate Dirac traces of Eq. (4.1) with the projectors $P_A(p) = -(\mathrm{i}/4p^2)\not{p}$ and $P_B(p) = (1/4)\mathbb{1}$, respectively, resulting in

$$A(p^2) = Z_2 + Z_1 C_F \int \frac{\mathrm{d}^4q}{(2\pi)^4} g^2 D_{\mu\nu}(k) \mathrm{Tr_D}\left[P_A(p)\gamma_\mu S(q), \Gamma_\nu(k,p)\right] \tag{4.7}$$
$$B(p^2) = Z_4 m(\mu) + Z_1 C_F \int \frac{\mathrm{d}^4q}{(2\pi)^4} g^2 D_{\mu\nu}(k) \mathrm{Tr_D}\left[P_B(p)\gamma_\mu S(q)\Gamma_\nu(k,p)\right], \tag{4.8}$$

where we have written $\Gamma^a_\nu(k,p) = (\lambda^a/2)\Gamma_\nu(k,p)$, and $C_F = 4/3$ is the quadratic Casimir operator for colour SU(3). At this point we could perform the Dirac traces and contractions appearing in Eqs. (4.7,4.8), by using the general form of $D_{\mu\nu}(k)$, $S(q)$, and $\Gamma_\nu(k,p)$, but we leave this for a later section when we introduce a truncation scheme.

As we will be particularly interested in the phenomenon of dynamical breaking of chiral symmetry, we formally introduce at this point the chiral limit. In QCD, the chiral limit is unambiguously defined by [28, 23, 24]

$$Z_2(\mu,\Lambda) m_{\mathrm{bare}}(\Lambda) \equiv 0, \quad \forall \Lambda \gg \mu, \tag{4.9}$$

which is equivalent to the renormalisation-point-invariant current-quark mass being zero, i.e. $\hat{m} = 0$ [28, 23, 24].

The best known truncation scheme of the SDE is the weak coupling expansion, which reproduces every diagram in perturbation theory. It is a systematic-improvable truncation scheme, and a essential tool for the investigation of large momentum transfer

phenomena because QCD is asymptotically free [44, **?**, 35, 45]. However, it excludes the possibility of obtaining information about the low-energy regime relevant for the hadron structure and reactions, and the phenomena of dynamical chiral symmetry breaking (DCSB), which are all essentially nonperturbative*.

As a demonstration of the nonperturbative nature of the phenomena of chiral symmetry breaking, consider the chiral limit in perturbative QCD, as defined in Eq. (4.9). In this case, the theory is chirally symmetric, and a perturbative evaluation of the quark propagator dressing functions, Eq. (4.2), gives [39, 40, **?**, 33]

$$B(p^2) = m \left[1 - \frac{\alpha}{\pi} \ln \left(\frac{p^2}{m^2} \right) + \cdots \right], \tag{4.10}$$

where the ellipsis denote higher order terms in α. However, it is always true that at any order in perturbation theory

$$\lim_{m \to 0} B(p^2) = 0, \tag{4.11}$$

and hence dynamical chiral symmetry breaking is impossible in perturbation theory, and the quark SDE cannot generate a mass gap.

The question is whether the above situation can ever be avoided. That is, are there circumstances (e.g. a truncation scheme) under which it is possible to obtain dynamical chiral symmetry breaking†? In this case the interactions between the propagating quark and the collective excitations of the QCD vacuum would have nonperturbatively generated a mass gap, whose appearance breaks chiral symmetry dynamically.

We will see in the next section that it is indeed possible to construct a truncation scheme in which DCSB is possible. There are additional models in which this is also possible, e.g. [46, 29], however all of these share the property of an infrared enhancement in the effective quark SDE kernel [47, 48, 49, 50], namely for energy scales ≈ 1 GeV^2.

*From the hadron spectrum we know that chiral symmetry has to be spontaneously broken in the nontrivial QCD vacuum, which is a nonperturbative effect.

†We insist in DCSB since this effect is responsible for the large mass difference between parity partners in the hadron spectrum, amongst other things such as the pion being light, and the rho and nucleon being heavy.

4.3. Rainbow truncation of the quark SDE

The kernel in the quark SDE, Eq. (4.1), is formed from the product of the dressed-gluon propagator and the dressed-quark-gluon-vertex, and therefore the structure of these quantities is largely responsible for the spectral properties of the dressed-quark propagator. However, in developing a truncation scheme for the quark SDE it is insufficient to concentrate only on these, as the SDE system forms an infinite tower. In the low-energy region of the strong interactions, dynamical chiral symmetry breaking is the dominant nonperturbative effect characterising the light hadron spectrum, in particular that of the octet of pseudoscalar mesons[11]. It is thus imperative that the implemented truncation scheme does not break chiral symmetry, and the pattern by which it is broken, if it is to be a viable approach.

In QCD, the accepted theory of the strong interactions [44], chiral symmetry and its breaking pattern are expressed through the axial-vector Ward-Takahashi identity, Eq. (3.26). This identity entails a relation between the kernel in the BSE and that in the quark SDE, Eq. (3.33). Thus, in order to preserve an essential symmetry of the strong interactions and its breaking pattern, any truncation scheme, or approximation made to these quantities, must preserve that relation.

Both, the dressed-gluon propagator and the dressed-quark-gluon-vertex satisfy their own SDE, and in order to define a self-consistent solution we must study their SDE too, which is a difficult problem. However, such a task is outside the scope of this thesis, and therefore we concentrate only on the quark SDE, Eq. (4.1). Despite their complexity, recent progress has been made in unveiling their nonperturbative structure using their SDE [51, 52, 53, 54, 55], as well the lattice formulation of QCD [56, 57, 58, 59, 60]. Ultimately, the detailed infrared behaviour of these quantities should not materially affect the observable consequences of the quark SDE and meson BSE, as long as the infrared enhancement in the quark SDE implements the appropriate amount of dynamical chiral symmetry breaking, and explains the (pseudo)Goldstone character of the pion [50].

4.3.1. Gluon propagator and quark-gluon-vertex

Gluon propagator

The dressed-gluon propagator satisfies its own SDE, and the general solution to this equation has the form

$$D_{\mu\nu}(k) = \frac{G(k^2,\mu^2)}{k^2}\Big(\delta_{\mu\nu} - \frac{k_\mu k_\nu}{k^2}\Big), \tag{4.12}$$

in Euclidean space and Landau gauge, where $G(k^2,\mu^2)$ is gluon dressing function, related to the vacuum polarisation by $G(k^2,\mu^2) = 1/(1+\Pi(k^2,\mu^2))$. In Eq. (4.12), we have made explicit the dependence of the dressed-gluon propagator on the renormalisation point μ through $G(k^2,\mu^2)$. The dressed-gluon propagator is calculable in a perturbative expansion in the coupling constant, and the free gluon propagator, used in QCD perturbation theory, is simply given by setting $G(k^2,\mu^2) = 1$ in Eq. (4.12).

Quark-gluon-vertex

The dressed-quark-gluon-vertex also satisfies its own SDE, and its general form can be characterised by 12 Lorentz-scalar dressing functions. Its Lorentz-Dirac basis can be constructed from the linear combinations of the three vectors γ_μ, k_μ, and p_μ, each multiplied by one of the four independent matrices $\mathbb{1}$, $\not{k}$, $\not{p}$, and $\sigma_{\mu\nu}k_\mu p_\nu$. The choice of the Lorentz-Dirac basis is constrained by the required properties under Lorentz and CPT transformations, but it is not unique, see e.g. [56]. The general form of the dressed-quark-gluon-vertex is thus given by

$$\Gamma_\mu(k,p) = \sum_{i=1}^{12} F^i(k,p,\mu) V^i_\mu(k,p), \tag{4.13}$$

where μ indicates the renormalisation-point dependence of the quark-gluon vertex, F^i ($i = 1,\ldots,12$) are the Lorentz-scalar dressing functions characterising $\Gamma_\mu(k,p)$, and $V^i_\mu(k,p)$ ($i = 1,\ldots,12$) is the Lorentz-Dirac basis being employed. For our purposes it

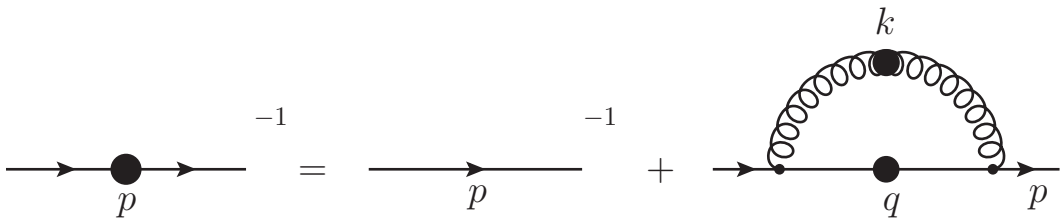

Figure 4.2.: Rainbow truncation of the quark SDE. The resulting equation consists of an effectively dressed gluon exchange Eq. (4.14).

will be sufficient to note that $V_\mu^1(k,p) = \gamma_\mu$ [56] since the other structures will not be taken into account explicitly.

4.3.2. A phenomenological model for the effective interaction

In modelling the quark SDE kernel we follow [38, 42], and make the following approximation in the quark self-energy Eq. (4.1), the so-called rainbow approximation,

$$Z_1 \int \frac{\mathrm{d}^4q}{(2\pi)^4} g^2 D_{\mu\nu}(k) \frac{\lambda^a}{2} \gamma_\mu S(q) \Gamma^a_\nu(k,p) \to \int \frac{\mathrm{d}^4q}{(2\pi)^4} \mathcal{G}(k^2) D^{\mathrm{free}}_{\mu\nu}(k) \frac{\lambda^a}{2} \gamma_\mu S(q) \frac{\lambda^a}{2} \gamma_\nu, \quad (4.14)$$

where the phenomenological "effective" coupling $\mathcal{G}(k^2)$ contains information about the behaviour of the product $G(k^2,\mu^2)F^1(k,p,\mu)$, and the model is completely defined once a form for $\mathcal{G}(k^2)$ has been specified. Note that we have actually made the replacement $\Gamma^a_\nu(k,p) \to (\lambda^a/2)\gamma_\nu$, and absorbed $Z_1 g^2$ into the effective coupling $\mathcal{G}(k^2)$. The function $\mathcal{G}(k^2)$ can be interpreted as an effective gluon dressing function. The resulting diagrammatic expression is presented in Figure 4.2, and it is clear from this figure that the solution to this equation resums an effectively-dressed gluon rainbow.

In principle, constraints on the form of $\mathcal{G}(k^2)$ come from the SDE satisfied by the dressed-gluon propagator and the dressed-quark-gluon vertex. However, we know that the behaviour of the QCD running coupling $\alpha(k^2)$ in the ultraviolet, i.e. $k^2 >$ 2-3 GeV^2, is well described by perturbation theory [61], and therefore the model dependence is restricted to the infrared region. On the other hand, the effective interaction in the quark SDE should exhibit sufficient infrared enhancement capable of triggering dynamical chiral symmetry breaking, through a nonzero quark condensate, and the generation of a

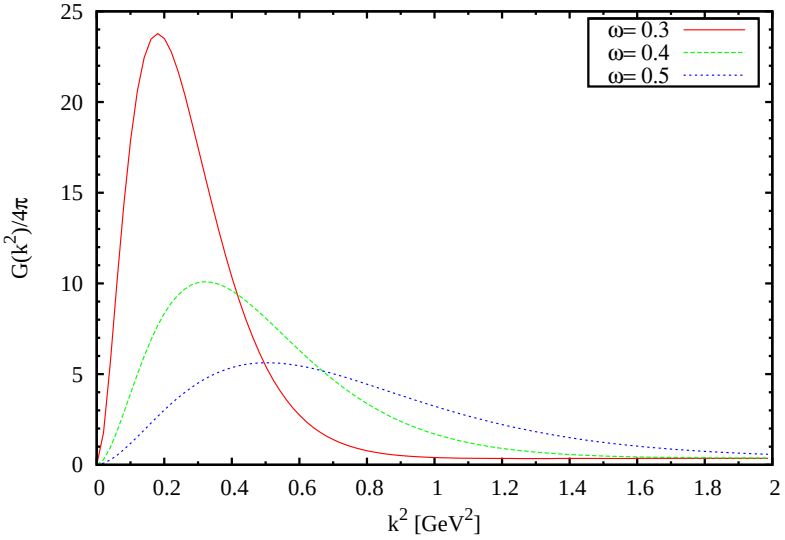

Figure 4.3.: Effective coupling for the quark SDE, Eq. (4.15), for various values of ω, with $(\omega D)^{1/3} = 0.72$ GeV. For $k^2 > 2$ GeV^2 $\mathcal{G}(k^2) \approx 4\pi\alpha(k^2)$.

momentum-dependent quark mass dressing function[29] that connects the current-quark mass to a constituent-like quark mass.

Various models for the effective interaction $\mathcal{G}(k^2)$ combining the ultraviolet behaviour known from perturbative QCD and an ansatz for the infrared part have been designed in the past. These have been applied to different detailed studies of dynamical chiral symmetry breaking, hadron structure and reactions [38, 42, 62, 63, 64, 65, 66].

In choosing a form for the effective coupling we follow reference [38, 42], and write the effective gluon dressing function $\mathcal{G}(k^2)$ as

$$\frac{\mathcal{G}(k^2)}{k^2} = 4\pi^2 \frac{D}{\omega^6} k^2 \exp\left(-\frac{k^2}{\omega^2}\right) + 4\pi \frac{\gamma_m \pi}{\frac{1}{2}\ln\left[\tau + \left(1 + \frac{k^2}{\Lambda_{\rm QCD}}\right)^2\right]} \mathcal{F}(k^2), \tag{4.15}$$

where $\mathcal{F}(k^2) = \left(1 - \exp\left(-\frac{k^2}{4m_t^2}\right)\right)/k^2$, and fixed parameters $m_t = 0.5$ GeV, $\tau = e^2 - 1$, $N_f = 4$, $\gamma_m = 12/(33 - 2N_f)$, $\Lambda_{\rm QCD}^{N_f} = 0.234$ GeV. The remaining parameters, ω and D, are phenomenological parameters fitted, together with the renormalised quark masses $m_u = m_d$ and m_s, to pion and kaon observables. The effective gluon dressing function $\mathcal{G}(k^2)$ is plotted in Figure 4.3 for various values of ω and D.

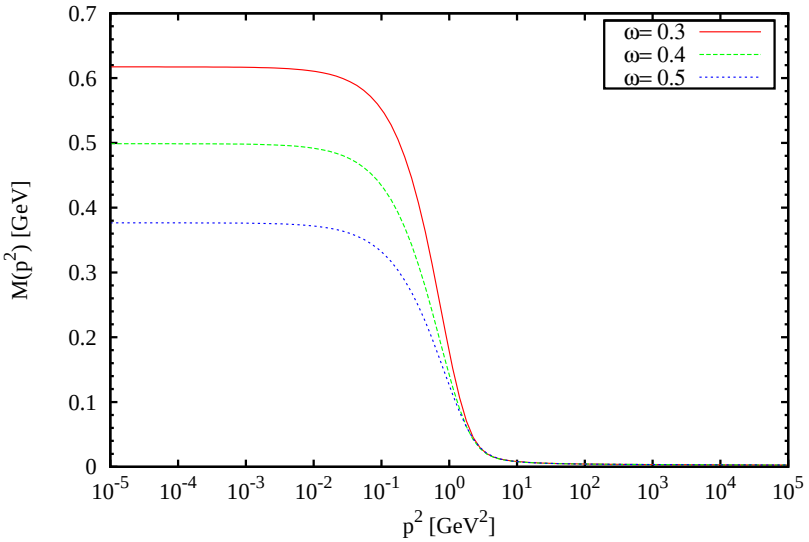

Figure 4.4.: Quark mass function for different values values of the model parameters. The renormalised current quark mass $m_u = 3.7$ MeV is given at the renormalisation point $\mu = 19$ GeV.

From the expression for $\mathcal{G}(k^2)$, Eq. (4.15), we see that the first term describes the infrared properties of the effective interaction through the parameters ω and D[‡]. For ω fixed, D controls the amplitude of $\mathcal{G}(k^2)$. On the other hand, ω not only controls the amplitude of $\mathcal{G}(k^2)$, but also its width. The first term thus provides the phenomenologically required infrared enhancement of the quark SDE kernel, necessary for the dynamical generation of a constituent-like quark mass and a chiral vacuum quark condensate. The second term accounts for the ultraviolet behaviour known from perturbative QCD, and ensures the preservation of one-loop results [38, 42].

The detailed study of [42] found that pseudoscalar and vector meson ground state properties are practically insensitive to variations in the model parameters, with $\omega =$ 0.3-0.5 GeV and $(\omega D)^{1/3} = 0.72$ GeV, as long as the integrated strength of the effective interaction is strong enough to generate an acceptable amount of chiral symmetry breaking, as required by the chiral quark condensate. However, this is not true for excited states made up of light quarks, where the long range part of the effective quark-quark interaction plays a significant role [67, 68, 69, 70].

[‡]The parameters ω and m_t are not freely varied, they are fixed mainly to ensure that $\mathcal{G}(k^2) \approx 4\pi\alpha(k^2)$ for $k^2 > 2$ GeV^2 [38].

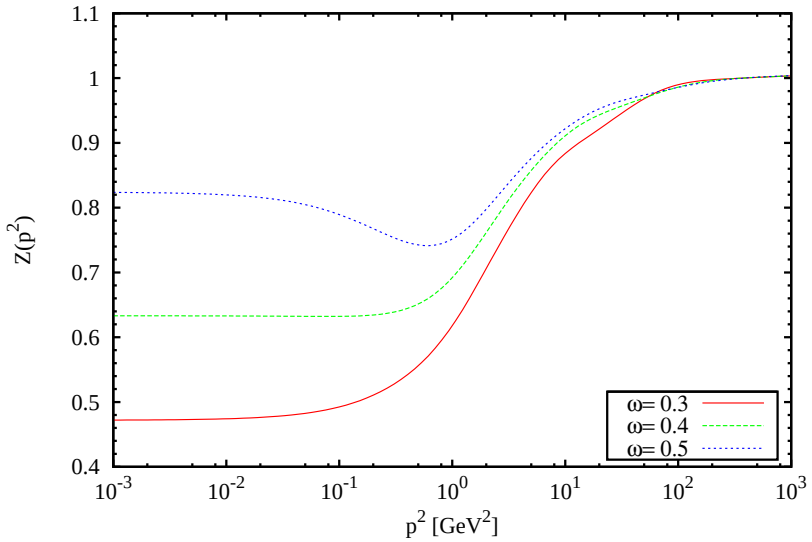

Figure 4.5.: Quark wave function renormalisation for different values of the model parameters. The renormalised current quark mass $m_u = 3.7$ MeV is given at the renormalisation point $\mu = 19$ GeV.

	Experiment (estimates) [MeV]	$\omega = 0.4$ [GeV] $D = 0.93$ [GeV^2]
$m_{u/d}$	5-10	5.54
m_s	100-300	125
m_π	138.5	138
m_K	496	497
f_π	130.7	131

Table 4.1.: Parameters in Eq. (4.15), fitted to pion and kaon static properties [42]. Renormalised current-quark masses have been evolved to the renormalisation point $\mu = 1$ GeV using one-loop equations. ω is fixed a priori such that $\mathcal{G}(k^2) \approx 4\pi\alpha(k^2)$ for $k^2 > 2$ GeV^2 [38, 42].

4.3.3. Numerical results for the rainbow-truncated quark SDE

The true phenomenological parameters in the rainbow quark SDE are D and the renormalised current-quark masses of the u/d- and s-quarks, $m_{u/d}(\mu)$ and $m_s(\mu)$, respectively. The parameters ω and m_t are chosen so as to ensure that $\mathcal{G}(k^2) \approx 4\pi\alpha(k^2)$ for $k^2 > 2$ GeV^2 [38, 42]. The current quark masses $m_{u/d} = 3.7$ MeV and $m_s = 83.8$ MeV, renormalised at $\mu = 19$ GeV, were fitted to the pion and kaon masses, respectively [42].

Using the one-loop expression [39, 40, **?**, 33] to evolve these masses down to $\mu = 1$ GeV results in the values for $m_{u/d}$ and m_s presented in the third column of Table 4.1. With the parameters fixed with static pion and kaon observables, subsequent calculated meson properties are predictions. Using this model, good agreement with the experimental values for the light pseudoscalar and vector meson masses and decay constants is achieved [42, 71]. Not only the meson masses and leptonic decay constants agree with experiment without parameter readjustment but also a wide range of other observables, see e.g. [24] and references therein.

Given the values of these phenomenological parameters, we can now solve numerically the quark SDE for the dressing functions $A(p^2)$ and $B(p^2)$ in Eqs. (4.7,4.8), renormalised according to Eqs. (4.5,4.6). Performing the traces and contractions appearing in Eqs. (4.7,4.8), we obtain the following coupled nonlinear integral equations for the quark dressing functions

$$A(p^2) = Z_2 + \frac{C_F}{p^2}\int \frac{\mathrm{d}^4q}{(2\pi)^4}\frac{\mathcal{G}(k^2)}{k^2}\left\{-\frac{2}{k^2}\left[p^2q^2-(p\cdot q)^2\right]+3(p\cdot q)\right\}\sigma_V(q^2) \quad (4.16)$$

$$B(p^2) = Z_4 m(\mu) + 3C_F\int \frac{\mathrm{d}^4q}{(2\pi)^4}\frac{\mathcal{G}(k^2)}{k^2}\sigma_S(q^2), \quad (4.17)$$

where

$$\sigma_V(q^2) = \frac{A(q^2)}{q^2A^2(q^2)+B^2(q^2)}, \quad (4.18)$$

$$\sigma_S(q^2) = \frac{B(q^2)}{q^2A^2(q^2)+B^2(q^2)}. \quad (4.19)$$

We present numerical solutions to Eqs. (4.16,4.17) for the wave-function renormalisation $Z(p^2) = 1/A(p^2)$ and mass dressing function $M(p^2) = B(p^2)/A(p^2)$ in Figures 4.6,4.7, renormalised at $\mu = 19$ GeV. In Figures 4.6,4.7, various values of the renormalised current-quark mass are considered, while $\omega = 0.4$ GeV and $D = 0.93$ GeV^2 are kept fixed. On the other hand, in Figures 4.4,4.5 the current-quark mass of the quark to $m_u = 3.7\,\mathrm{MeV}$, and vary ω and D.

Figure 4.6 makes evident that DCSB is a reality, i.e. can be implemented, in the rainbow truncation with the effective coupling given by Eq. (4.15). At ultraviolet momenta,

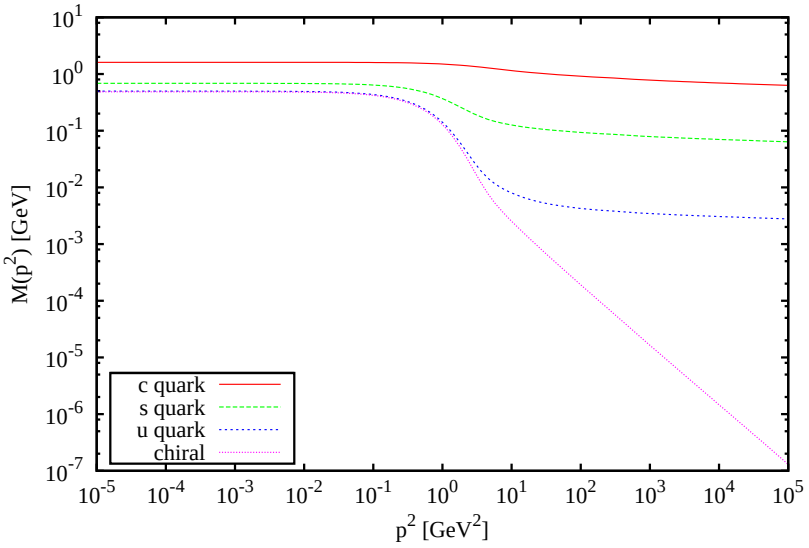

Figure 4.6.: Quark mass function in the rainbow-ladder truncation with the Maris-Tandy dressing function for various values of the renormalised current-quark mass, with $\omega = 0.4$ GeV and $D = 0.93$ GeV^2.

the magnitude of the mass function is determined by the renormalised current-quark mass. In the infrared, however, and specially for light-quarks, $M(p^2)$ is significantly enhanced. For light quarks, this enhancement is orders of magnitude larger than the mass present in the Lagrangian. Figure 4.6 also shows that the evolution from the current-quark mass to a constituent-like quark mass occurs at the scale of ≈ 1 GeV^2, as required from hadron phenomenology.

To get a quantitative idea of the effects of dynamical chiral symmetry breaking on the propagation characteristics of quarks, we define[§] [38] the Euclidean constituent-quark mass M^E as the solution of $p^2 = M^2(p^2)$. Table 4.2 presents the Euclidean constituent-quark mass for various values of the renormalised current-quark mass. The ratio $M_f^E/m_f(\mu)$ is a quantitative measure of the nonperturbative effects of DCSB on a particular quark flavour. As can be seen from the third column of Table 4.2 and Figures 4.6,4.7, this effect is particularly important for light quarks, i.e. the evolution and magnitude of their mass function in the infrared is dominated by the nonperturbative effect of DCSB. The domain in which the effect of DCSB is relevant decreases as the renormalised current-quark mass increases.

[§]Quark confinement implies that there is no pole mass. This definition is therefore arbitrary since we could have defined $M(p^2 = 0)$ as our quantitative measure.

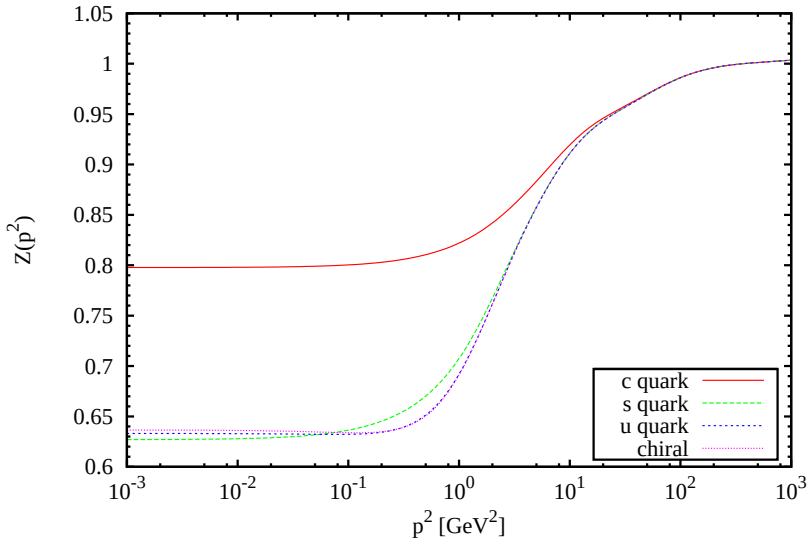

Figure 4.7.: Wave function renormalisation in the rainbow-ladder truncation with the Maris-Tandy dressing function for various values of the renormalised current-quark mass, with $\omega = 0.4$ GeV and $D = 0.93$ GeV^2.

$m_f(\mu)$ [MeV]	M^E [GeV]	$M^E/m_f(\mu)$
0.0	0.391	∞
3.7	0.400	108.12
83.8	0.555	6.62
827	1.416	1.71

Table 4.2.: Euclidean constituent-quark mass for various quark flavours as the solution of $p^2 = M^2(p^2)$. The renormalised current-quark masses are defined at the renormalisation point $\mu = 19$ GeV.

Because the truncation preserves the one-loop renormalisation group properties of QCD, the ultraviolet behaviour of the solutions of the quark SDE is that of perturbative QCD, in the chiral limit and in the presence of explicit chiral symmetry breaking, see Figures 4.6,4.7. In the presence of explicit chiral symmetry breaking, the mass function is described by [72, 73]

$$M(p^2) \overset{p^2 \gg \Lambda_{\rm QCD}^2}{=} \frac{\hat{m}}{\left[\frac{1}{2}\ln\left(p^2/\Lambda_{\rm QCD}^2\right)\right]^{\gamma_m}}, \tag{4.20}$$

where $\hat{m}$ is the renormalisation-group-invariant current-quark mass, while when dynamical chiral symmetry breaking occurs, the ultraviolet behaviour is given by [72, 73]

$$M(p^2) \overset{p^2\gg\Lambda_{\rm QCD}^2}{=} \frac{2\pi^2\gamma_m}{3}\frac{1}{p^2}\frac{-\langle\overline{q}q\rangle^0}{\left[\frac{1}{2}\ln\left(p^2/\Lambda_{\rm QCD}^2\right)\right]^{1-\gamma_m}}, \tag{4.21}$$

where $\langle\overline{q}q\rangle^0$ is the renormalisation-point-independent chiral vacuum quark condensate. Fitting Eq. (4.21) to the ultraviolet tail of our chiral limit numerical solutions in Figure 4.6 we find

$$-\langle\overline{q}q\rangle^0 = (0.228\ \text{GeV})^3. \tag{4.22}$$

The behaviour of the quark mass function and wave function renormalisation of Figures 4.6,4.7 has also been confirmed semi-quantitatively in lattice simulations of QCD [74, 75, 76]. Agreement for a range of quark masses requires the effective interaction to be flavour dependent, and dressing the quark-gluon-vertex ensures this dependence, as pointed out in [49].

4.4. Ladder truncation of the meson BSE

We now turn our study to meson bound states. Meson bound states, whose flavour structure is given by a dressed quark-antiquark $(a\bar{b})$ pair¶, are described by the Bethe-Salpeter equation (BSE), depicted in Figure 4.8,

$$[\Gamma_H(p;P)]_{tu} = \int\frac{\mathrm{d}^4q}{(2\pi)^4}\,[K(p,q;P)]_{tu;rs}\left[S^a(q_+)\Gamma_H(q;P)S^b(q_-)\right]_{sr}, \tag{4.23}$$

where $H = (a\bar{b})$ indicates the flavour structure. Here, $\Gamma_H(p;P)$ is the meson Bethe-Salpeter amplitude (BSA) describing the bound state, $S^f(q_\pm)$ is the propagator for a dressed quark, and $K(p,q;P)_{tu;rs}$ is the quark-antiquark scattering kernel. Latin indices

¶In the rainbow truncation, quark propagators, obtained as the solution of the quark SDE, are distinguished only by the renormalised current quark mass.

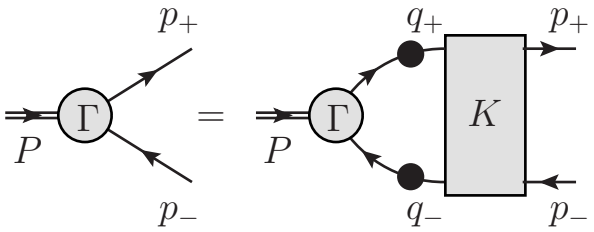

Figure 4.8.: Bethe-Salpeter Equation: Γ is the fully-amputated quark-meson vertex or Bethe-Salpeter Amplitude; K is the fully-amputated, two-particle irreducible, scattering kernel; filled dots on the quark lines indicate quark propagators are fully dressed.

indicate the colour, flavour, and Dirac structure. Poincaré covariance and momentum conservation entail $q_+ = q+\eta P$, $q_+ = q-(1-\eta)P$, and similarly for $p_\pm$, with $P = p_+ - p_-$. The parameter $\eta \in [0,1]$ describes the meson momentum sharing between the quark-antiquark pair. Observables, however, do not depend on this, see Tables 4.3,4.4.

The Bethe-Salpeter equation, Eq. (4.23), is a homogeneous eigenvalue equation that admits solutions only for discrete values of the meson momenta $P^2 = -m_H^2$, where m_H is the mass of the meson under consideration. In a particular channel, the lowest mass solution corresponds to the physical ground state.

In Eq. (4.23), $K(p,q;P)_{tu;rs}$ is the fully-amputated, two-particle irreducible, quark-antiquark scattering kernel. It is a four-point Schwinger function, obtained formally as the sum of a countable infinity of skeleton diagrams[77]. The complexity of $K(p,q;P)_{tu;rs}$ is one of the reasons why quantitative SDE and BSE studies employ modelling of $D_{\mu\nu}(k)$ and $\Gamma^a_\nu(k,p)$ [38], because $K(p,q;P)_{tu;rs}$ also appears in the SDE satisfied by $\Gamma^a_\nu(k,p)$. However, as illustrated in the previous chapter, the lack of a full understanding of the interaction between quarks, through the complete knowledge of $K(p,q;P)_{tu;rs}$, does not prevent us from obtaining general results in hadron physics. If explicit calculations of the static and dynamics properties of mesons are intended, an explicit expression for $K(p,q;P)_{tu;rs}$ must be at hand however.

4.4.1. Axial-Vector Ward-Takahashi identity and ladder Bethe-Salpeter Kernel

In the low-energy region of the strong interaction, dynamical chiral symmetry breaking is the main effect characterising the octet of pseudoscalar mesons [11]. In QCD, chiral symmetry and its breaking pattern are expressed through the axial-vector Ward-

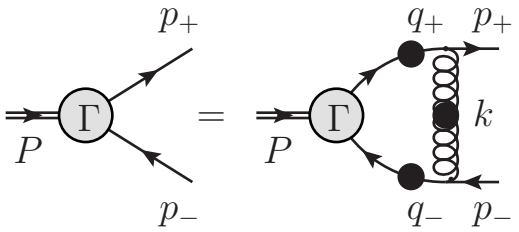

Figure 4.9.: Bethe-Salpeter equation in the ladder truncation. This truncation is consistent with the rainbow truncation of the quark SDE in the sense that they satisfy the axWTI, Eq. (4.24).

Takahashi identity Eq. (3.26). This identity provides a relation between the kernel in the quark SDE and that in the BSE,

$$\int \frac{\mathrm{d}^4 q}{(2\pi)^4} K_{tu;rs}(k,q;P) \left[\gamma_5 T^H S(q_-) + S(q_+)\gamma_5 T^H\right]_{sr} = \left[\Sigma(k_+)\gamma_5 T^H + \gamma_5 T^H \Sigma(k_-)\right]_{tu}, \quad (4.24)$$

thus constraining the content of the quark-antiquark scattering kernel $K(p,q;P)_{tu;rs}$ if an essential symmetry of the strong interactions, and its breaking pattern, is to be preserved.

From a practical point of view, Eq. (4.24) provides a way of obtaining the quark-antiquark scattering kernel if we can solve this constraint, given an expression for the quark self-energy. However, this is not always possible, see e.g. [78], and we must find an alternative way of preserving the chiral symmetry properties of the strong interactions. In principle, one may construct a quark-antiquark scattering kernel satisfying Eq. (4.24) from a functional derivative of the quark self-energy with respect to the quark propagator [79], within the framework of the effective action formalism for composite operators developed in [80].

Fortunately, for the rainbow truncation of the quark self-energy, Eq. (4.14), the axial-vector Ward-Takahashi identity can be easily satisfied. The quark-antiquark scattering kernel that is consistent with the rainbow truncation of the quark self-energy, in the sense that the axial-vector Ward-Takahashi identity, Eq. (4.24), is satisfied, is given by

$$K(p,q;P)_{tu;rs} = -\mathcal{G}(k^2)D^{\text{free}}_{\mu\nu}(k)\left[\frac{\lambda^a}{2}\gamma_\mu\right]_{ts}\left[\frac{\lambda^a}{2}\gamma_\nu\right]_{ru}, \tag{4.25}$$

where $k = p - q$, and $\mathcal{G}(k^2)$ is the effective coupling of Eq. (4.15). This is the so-called ladder truncation of the BSE. In this approximation, the Bethe-Salpeter equation takes the form

$$\Gamma_H(p;P) = -C_F\int\frac{\mathrm{d}^4q}{(2\pi)^4}\mathcal{G}(k^2)D^{\text{free}}_{\mu\nu}(k)\gamma_\mu S^a(q_+)\Gamma_H(q;P)S^b(q_-)\gamma_\nu, \tag{4.26}$$

where the $s, t, \ldots$ indices have been suppressed. This equation is represented diagrammatically in Figure 4.9. As can be seen from Figure 4.9, this equation corresponds to a single effective dressed-gluon exchange, and its solution corresponds to resumming this gluon rung, thus providing the (infinite) ladder.

Note from the Bethe-Salpeter kernel, Eq. (4.25), that

$$\frac{\partial K(p,q;P)_{tu;rs}}{\partial P_\mu} = 0, \tag{4.27}$$

and thus the normalisation condition Eq. (3.22) for the Bethe-Salpeter amplitude greatly simplifies to

$$\begin{aligned} 2P_\mu = \int\frac{\mathrm{d}^4q}{(2\pi)^4}\Bigg\{&\mathrm{Tr}\left[\overline{\Gamma}_H(q;-P)\frac{\partial S^a(q_+)}{\partial P_\mu}\Gamma_H(q;P)S^b(q_-)\right] \\ &+\mathrm{Tr}\left[\overline{\Gamma}_H(q;-P)S^a(q_+)\Gamma_H(q;P)\frac{\partial S^b(q_-)}{\partial P_\mu}\right]\Bigg\}, \end{aligned} \tag{4.28}$$

which is a one loop expression.

4.4.2. Numerical solution to the ladder-truncated meson BSE

As stated earlier, the Bethe-Salpeter equation is a homogeneous eigenvalue equation that admits solutions only for discrete values of the meson momenta $P^2 = -m_H^2$, where m_H is the mass of the meson under consideration. In order to facilitate the numerical solution of this equation, we modify it by introducing a fictitious eigenvalue $\lambda(P^2)$ into Eq. (4.23),

$$[\Gamma_H(p;P)]_{tu} = \lambda(P^2) \int \frac{\mathrm{d}^4 q}{(2\pi)^4} \left[K(p,q;P)\right]_{tu;rs} \left[S^a(q_+)\Gamma_H(q;P)S^b(q_-)\right]_{sr}, \qquad (4.29)$$

with the physical solution obtained when $\lambda(P^2 = -m_H^2) = 1$. The general structure of the meson under consideration will depend on its quantum numbers, such as flavour, Dirac, and CPT transformations [27]. Scalar and pseudoscalar mesons are characterised by four Lorentz-scalar dressing functions, see Eq. (4.32), while vector mesons are characterised by eight. These are denoted generically by $F_H^i(p;P)$. In this thesis we will be interested mainly in pseudoscalar mesons, however the general method described below can be applied to any meson, with slight variations. The equations for pseudoscalar mesons in the rainbow-ladder truncation of the SDE-BSE complex are given explicitly in Appendix A.

We solve the BSE for the Bethe-Salpeter amplitude $\Gamma_H(p;P)$ using matrix methods as follows. We project the BSE onto the Lorentz-scalar dressing functions $F_H^i(p;P)$ using appropriate projectors, see Appendix A for the pseudoscalar case. This results in a system of either four or eight coupled integral equations for the dressing functions $F_H^i(p;P)$. This system can be solved directly for the scalar dressing functions $F_H^i(p;P)$ depending on two variables, p^2 and $p\cdot P$, and labelled by P^2 as an integral eigenvalue equation. This makes a high demand on computer memory. However, in order to elucidate the angular dependence of the Lorentz-scalar dressing functions $F_H^i(p;P)$, and save on computer memory, we expand these in a Chebyshev polynomials decomposition in the angle[‖] $\widehat{p\cdot P} = p\cdot P/|pP|$ as

[‖]In the meson rest frame we have $P_\mu = (\mathrm{i}m_H, 0, 0, 0)$, and therefore $\widehat{p\cdot P} \in [-1, 1]$.

$$F_H^i(p;P) = \sum_k F_{H,k}^i(p^2;P^2) T_k\left(\widehat{p\cdot P}\right), \quad \text{with} \quad P^2 = -m_H^2. \tag{4.30}$$

The functions $F_{H,k}^i(p^2;P^2)$ can be further projected out using the orthonormal properties of the Chebyshev polynomials T_k. With the angular dependence made explicit, we can evaluate the non-trivial angular integrals appearing in Eq. (4.29) numerically. We then arrange the remaining radial integral in the form of a matrix equation for the Chebyshev moments, by matching the radial, external and internal, momenta at the integration nodes p_j^2. Thus, the amplitude of our BSE is effectively projected out onto the decomposition $F_{H,k}^i(p_j^2;P^2)$. Schematically we are solving

$$\mathbf{F} = \lambda \mathbf{K}\mathbf{F}, \tag{4.31}$$

for the eigenvector $\mathbf{F}$, made up of Chebyshev moments, as a parametric equation of $P^2 = -m_H^2$, with m_H the mass of the meson. The physical solution corresponds to $\lambda = 1$, where the lowest mass solution with $\lambda = 1$ corresponds to the ground state in any particular channel. Equivalently, we can set $\lambda = 1$ from the beginning, with the solution obtained once $\det[\mathbb{1} - \mathbf{K}] = 0$, for $P^2 = -m_H^2$. However, the eigenvalue method gives the mass and BSA of the meson at the same time.

4.5. Static properties of pseudoscalar mesons from RL SDE-BSE

The procedure described above is employed iteratively to determine the smallest m_H satisfying $\lambda(P^2 = -m_H^2) = 1$, and its respective eigenvector $\Gamma_H(p;P)$, as discussed in Appendix A. This corresponds to the ground state solution in any particular channel. Excited states can also be found in this way, with a slight modification to this procedure. This involves the subtraction of the ground state contribution from the kernel, as detailed in [81, 22].

In the pseudoscalar channel ($J^P = 0^-$), the lowest mass solutions are the pion and kaon mesons, with flavour structure $u\overline{d}$ and $u\overline{s}$, respectively. The general form of the BSA in this channel is given by

$$\Gamma_H(p;P) = T^H\gamma_5\left[\mathrm{i}E_H(p;P) + \not{P}F_H(p;P) + \not{p}(p\cdot P)G_H(p;P) + \sigma_{\mu\nu}p_\mu P_\nu H_H(p;P)\right], \tag{4.32}$$

with $H = \pi$, K. For mesons that are eigenstates of the charge conjugation operation C, such as the π^0, there is an additional constraint on the Bethe-Salpeter amplitude to obtain a specified C-parity**. In Eq. (4.32), all the elements of the Lorentz-Dirac basis employed are even under C, and thus the only remaining quantity that can produce a definite C-parity is $p\cdot P$, which is odd under C. Therefore, a $C = +1\,(-1)$ solution will have dressing functions $F_H^i(p;P)$ that are even (odd) in $p\cdot P$. For mesons that are not eigenstates of C, each dressing function will contain both even an odd terms in $p\cdot P$. Since the ladder truncation of the BSE is invariant under C if equal momentum partition is used, the observation above of the definite parity on $p\cdot P$ of the dressing functions can be used as a test of numerical accuracy. For the Chebyshev expansion Eq. (4.30), this means that for $C = +1\,(-1)$ we will only require even (odd) Chebyshev polynomials, and thus the odd (even) Chebyshev coefficients will vanish.

The pseudoscalar leptonic decay constant is calculated using

$$f_H P_\mu = Z_2\int\frac{\mathrm{d}^4q}{(2\pi)^4}\mathrm{Tr}\left[\frac{(T^H)^t}{2}\gamma_5\gamma_\mu S^a(q_+)\Gamma_H(q;P)S^b(q_-)\right], \text{ at } P^2 = -m_H^2, \tag{4.33}$$

where $H = \pi$, K, and the trace is over Dirac, colour, and flavour indices. In Eq. (4.33), $\Gamma_H(q;P)$ is the normalised BSA. In the present truncation scheme, it is equivalently normalised according to either Eq. (4.28) or Eq. (3.23).

The residue of the pseudoscalar vertex is similarly calculated using

**In the isospin symmetric limit ($m_u = m_d$) we are working in, the mass and dressing functions of $\pi^\pm$ mesons will be equal to those of π^0.

	$\eta = 0.0$			$\eta = 0.25$			$\eta = 0.5$		
N	m_π	f_π	R_π	m_π	f_π	R_π	m_π	f_π	R_π
1	0.1849	0.1210	1.8435	0.1958	0.1292	2.0552	0.1999	0.1325	2.1371
2	0.2102	0.1307	2.3535	0.2022	0.1320	2.1855	0.1999	0.1325	2.1371
3	0.1363	0.1305	0.9858	0.1376	0.1323	1.0048	0.1380	0.1329	1.0112
4	0.1375	0.1318	1.0037	0.1379	0.1326	1.0093	0.1380	0.1329	1.0112
5	0.1385	0.1329	1.0111	0.1384	0.1328	1.0107	0.1384	0.1328	1.0106
6	0.1384	0.1329	1.0112	0.1384	0.1328	1.0108	0.1384	0.1328	1.0106
7	0.1384	0.1328	1.0111	0.1384	0.1328	1.0108	0.1384	0.1328	1.0106
8	0.1384	0.1328	1.0111	0.1384	0.1328	1.0108	0.1384	0.1328	1.0107

Table 4.3.: Dependence on the momentum sharing parameter η_π and the number of Chebyshev polynomials of the mass and decay constant of the pion. All four dressing functions are taken into account. A $R_\pi = 1$ means that the axWTI is satisfied. The renormalised current quark mass $m_u = 3.7$ MeV is given at the renormalisation point $\mu = 19$ GeV. The parameter D and the renormalized mass of the current up quark $m_{u/d}$ were fitted to m_π and f_π in [38, 42].

$$r_H = Z_4 \int \frac{\mathrm{d}^4 q}{(2\pi)^4} \mathrm{Tr}\left[\frac{(T^H)^t}{2}\gamma_5 S^a(q_+)\Gamma_H(q;P)S^b(q_-)\right], \quad \text{at} \quad P^2 = -m_H^2. \tag{4.34}$$

From the previous chapter, we know that the axial-vector Ward-Takahashi imposes a relationship between f_H and r_H, known as the generalised Gell-Mann–Oakes-Renner relation,

$$f_H m_H^2 = r_H(m_a + m_b), \tag{4.35}$$

where m_a and m_b are the renormalised masses of the quark and the antiquark, respectively. This relation must be satisfied at and beyond the chiral limit by any truncation scheme. Confirming this relation serves both as a check of our numerical procedure and how well the kernel satisfies the axWTI.

In Table 4.3 we present results for the mass and leptonic decay constant of the pion, as a function of the momentum sharing parameter η and the number of Chebyshev

	$\eta = 0.0$			$\eta = 0.25$			$\eta = 0.5$		
N	m_K	f_K	R_K	m_K	f_K	R_K	m_K	f_K	R_K
1	0.5140	0.1330	1.0064	0.5395	0.1487	1.1741	0.5397	0.1568	1.2664
2	0.5598	0.1439	1.2404	0.5402	0.1520	1.1971	0.5457	0.1565	1.2486
3	0.4980	0.1496	0.9593	0.5001	0.1526	1.0094	0.4981	0.1570	1.0332
4	0.4984	0.1677	1.0008	0.4963	0.1551	1.0086	0.4953	0.1568	1.0148
5	0.5001	0.1613	1.0062	0.4974	0.1533	1.0091	0.4969	0.1568	1.0141
6	0.4974	0.1558	1.0143	0.4967	0.1553	1.0118	0.4967	0.1565	1.0117
7	0.4974	0.1556	1.0142	0.4967	0.1553	1.0118	0.4967	0.1564	1.0117
8	0.4974	0.1556	1.0142	0.4967	0.1553	1.0117	0.4967	0.1564	1.0117

Table 4.4.: Dependence on the momentum sharing parameter η_K and the number of Chebyshev polynomials of the mass and decay constant of the kaon. All four dressing functions are taken into account. A $R_K = 1$ means that the AxWTI is satisfied. The renormalised current quark masses $m_u = 3.7$ MeV $m_s = 82$ MeV are given at the renormalisation point $\mu = 19$ GeV. The parameter D and the renormalized mass of the current up and strange quarks, $m_{u/d}$ and m_s, were fitted to m_π, f_π, and m_K in [38, 42]. The decay constant of the kaon is a prediction of the approach.

polynomials used in Eq. (4.30). We also present results for $R_\pi \equiv f_\pi m_\pi^2 / [r_\pi(m_u + m_d)]$. A value of $R_\pi = 1$ means that the axial-vector Ward-Takahashi identity is satisfied. From Table 4.3, we observe that when the $p \cdot P$ dependence of the dressing functions in the BSA is appropriately included, through a sufficiently large number of Chebyshev polynomials, physical observables are independent of the momentum sharing parameter η appearing in the BSE, Eq. (4.23), as required. All four dressing functions in the BSA must be included to ensure this, and to obtain the correct value for the static properties m_π and f_π, and for $R_\pi = 1$.

Although the number of Chebyshev polynomials reported in Table 4.3 is considerable, accurate results can be produced with a low number of Chebyshev polynomials, e.g. 4, especially for $\eta = 1/2$, where odd Chebyshev coefficients vanish. The same observations with respect to the angular dependence in the BSA apply to the kaon, whose results we present in Table 4.4. In this case, however, we need to include both even and odd Chebyshev polynomials, since the kaon is not a charge conjugation eigenstate.

In Figure 4.10 we present some nonzero Chebyshev moments of the BSA dressing functions of Eq. (4.32). From this figure and from Table 4.3, we see that the zeroth

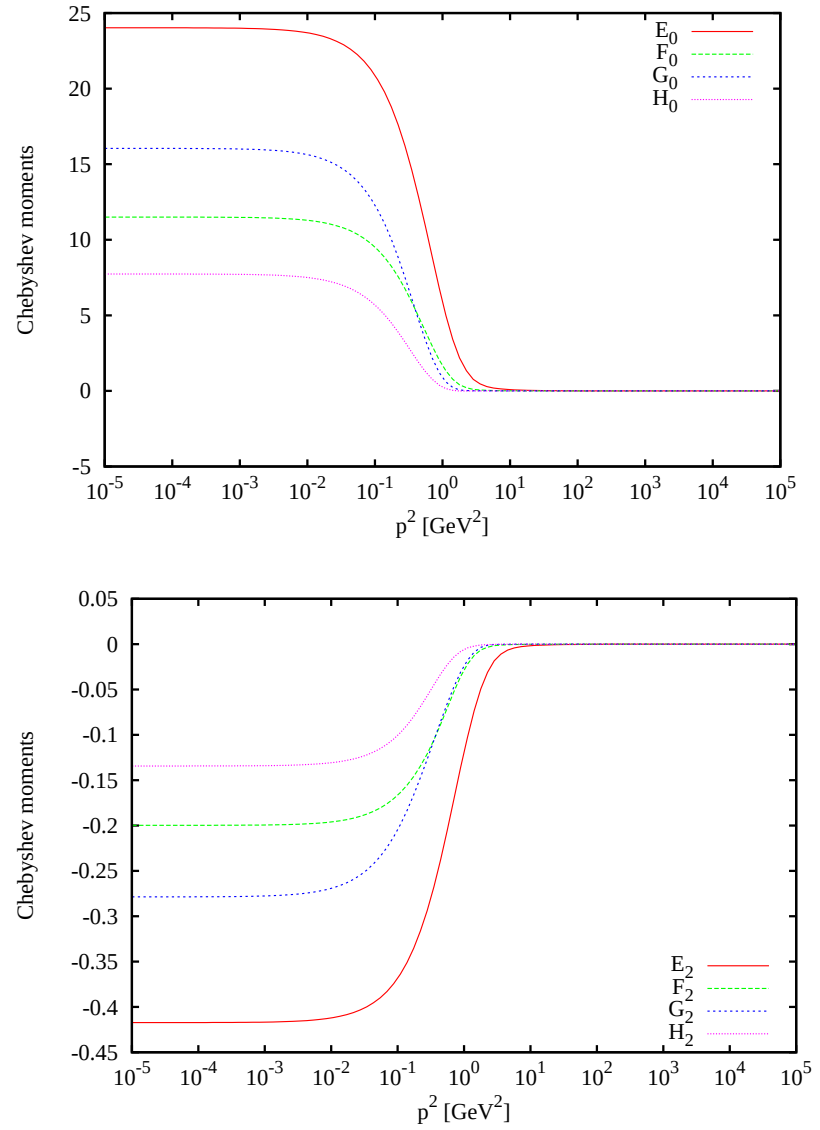

Figure 4.10.: Chebyshev moments for the various dressing functions of the pion BSA, Eq. (4.32). Top: zeroth order; Bottom: second order. Odd Chebyshev moments vanish.

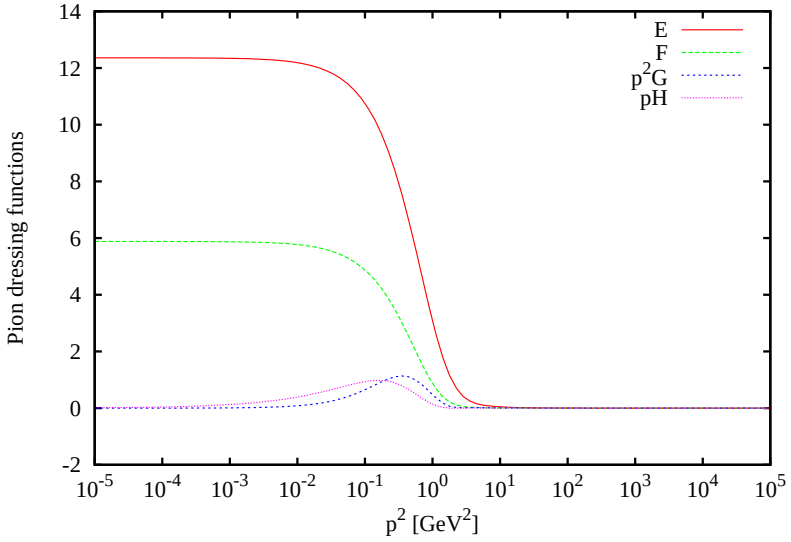

Figure 4.11.: Momentum dependence of the various dressing functions of the pion BSA, Eq. (4.32). The angular dependence in negligible, and chosen here such that $p \cdot P = 0$; the Chebyshev sum in Eq. (4.30) is performed using the Clenshaw's recurrence formula [82].

order Chebyshev moment contributes the most to the BSA and to the static properties of the pion. However, for an accurate description of the mass and decay constant of the pion, Chebyshev moments beyond the zeroth order need to be included, as seen from Tables 4.3,4.4.

In Figure 4.11 we plot the relative-momentum dependence of the various terms in the BSA, Eq. (4.32), namely $E_\pi(p;P)$, $F_\pi(p;P)$, $p^2G_\pi(p;P)$, and $pH_\pi(p;P)$, at the meson mass shell, for the angular point $p \cdot P = 0$. As can be seen from this figure, the first two terms in the pion BSA are the most significant, nevertheless, all four are necessary to ensure the η independence of static properties of the pion, as well as their correct value. These observations apply to the kaon as well.

4.6. Summary

In this chapter we have introduced the rainbow-ladder truncation scheme of the SDE-BSE system of equations, complemented with a successful phenomenological dressing function [42]. First, we have defined the rainbow truncation of the quark SDE, and presented numerical solutions to the resulting equations for various quark flavours, from the chiral limit to the strange quark mass. We have shown that chiral symmetry breaking

is a nonperturbative phenomenon, and that such an effect is indeed possible in the rainbow truncation scheme with a phenomenologically motivated effective quark-quark interaction. Additionally, we have presented evidence that the phenomenon of dynamical chiral symmetry breaking is specially important in the light quark sector, and that it is largely responsible for the existence of a constituent-like quark mass that is significantly bigger than the mass scale present in the QCD Lagrangian. Indeed, this dynamically generated mass is proportional to Λ_{QCD}. In the second part of this chapter we have obtained the Bethe-Salpeter (ladder) kernel by solving the axial-vector Ward-Takahashi identity, ensuring the preservation of the generalised Gell-Mann–Oakes-Renner relation. Once we have obtained the ladder Bethe-Salpeter kernel, we have solved the Bethe-Salpeter integral eigenvalue equation numerically for the pion and kaon, systematically calculating their static properties. This demonstrates that the rainbow-ladder truncation scheme is a good starting point for the investigation of the static properties of ground state pseudoscalar mesons, and that it can be used as a firm foundation for future improvements, as well as the investigation of the dynamic properties of the pion.

Chapter 5.

Pion form factor in the impulse approximation

5.1. Introduction

The fact that the strongly interacting particles, the hadrons, do have a substructure was realised more than 50 years ago at SLAC, where deep inelastic scattering experiments [1, 83] were performed. The interpretation of these large momentum transfer experiments revealed the presence of point-like free Dirac particles inside the hadrons, and lead to the parton model. Further investigations, and the property of asymptotic freedom of Non-Abelian gauge field theories, lead to the identification of these partons with the quarks and gluons of Quantum Chromodynamics.

The picture that emerged from these large momentum transfer experiments was that of a proton being a bound state of weakly interacting quarks and gluons. In this way, the inelastic electron-proton scattering, through photon exchange, was viewed simply as the elastic scattering of the electron on a free quark within the proton.

The property of asymptotic freedom of QCD allows perturbation theory techniques to be used for the calculation of hadronic observables at large momentum transfer. Favourable comparisons [44, 61] of QCD predictions to high energy experimental data allowed QCD to emerge as the theory of the strong interactions. For small momentum transfers, the proton does not break up, and the elastic scattering can be interpreted in terms of electric and magnetic form factors that can be measured experimentally.

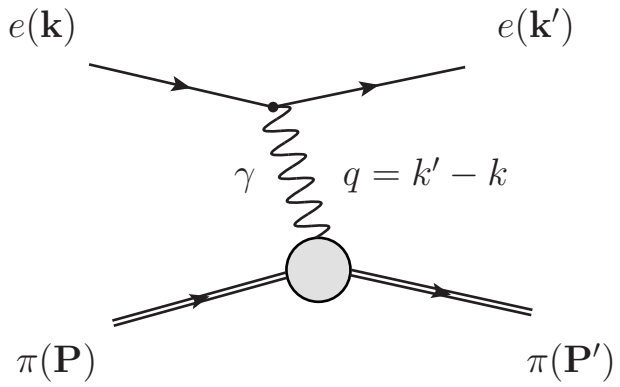

Figure 5.1.: Investigation of pion substructure by means of electron scattering. Simplified one-photon exchange elastic scattering.

The above picture of hadrons is not complete, however, since quarks and gluons are not observed as the free particles that hit the detector, but are confined inside the hadrons. Although not proven theoretically yet from QCD, the confinement property of the strong interactions forbids single quarks and gluons to propagate as free particles over large distances. Due to the running of the strong coupling constant, in propagating over these distances, quarks and gluons interact with the nontrivial vacuum of QCD and eventually hadronise into the colourless particles that hit the detectors.

At large distances or low momentum transfer, the QCD coupling constant is large so that perturbation theory techniques cannot be employed, and the high energy picture of hadrons, as being composed of weakly interacting quarks and gluons, cannot be extrapolated to these scales. It is at these momentum scales where the nonperturbative aspects of QCD are important in understanding the complex bound state structure and dynamics of hadrons.

5.2. Electromagnetic form factors

The investigation of the structure of matter through electron scattering experiments is a well-proved technique in physics since the electromagnetic probe is well known. Suppose that we want to study the charge distribution of a hadron, e.g. the pion of Figure 5.1. The experimental procedure is to measure the angular distribution of the scattered electrons and compare it to the known cross section for scattering electrons from a point charge, in the form

$$\frac{d\sigma}{d\Omega} = \left(\frac{d\sigma}{d\Omega}\right)_{\text{point}} |F(q)|^2 , \tag{5.1}$$

where $q = k' - k$ is the momentum transfer between the incident electron and the hadron target, and F is the hadron electromagnetic form factor. We then attempt to deduce the structure (and its dynamics) of the target from the measured electromagnetic form factor $F(q)$, which only depends on the probe's resolution.

It is important to note, however, that the above discussion cannot be applied directly to the experimental investigation of the pion structure. First, although Eq. (5.1) is given for a spinless charge distribution, it only applies to a static charge, and the pion will usually recoil under electron scattering. Second, free pion targets are not available. Nevertheless, Eq. (5.1) can be applied to study of elastic scattering of high energy pions from atomic electrons[84, 85], where low momentum transfers are involved, and therefore it can be useful in the determination of the "size" of the pion. For higher momentum transfer, other experimental techniques need to be implemented, as described below.

We can still gain insight into the pion structure and dynamics using low momentum transfer experiments. For a static target, it is found [77, 83] that the form factor in Eq. (5.1) is just the Fourier transform of the normalised charge distribution $\rho(\mathbf{x})$,

$$F(\mathbf{q}) = \int \mathrm{d}^3x \rho(\mathbf{x}) \exp(\mathrm{i}\mathbf{q}\cdot\mathbf{x}). \tag{5.2}$$

If the momentum transfer is small, and we assume a spherically symmetric charge distribution, we can expand the exponential in Eq. (5.2), obtaining

$$F(\mathbf{q}) = 1 - \frac{1}{6}\langle r^2\rangle |\mathbf{q}|^2 + \cdots , \tag{5.3}$$

so that the mean square radius of the pion charge distribution is given by

$$\langle r^2 \rangle = -6 \left. \frac{\mathrm{d}F(Q^2)}{\mathrm{d}Q^2} \right|_{Q^2=0}. \tag{5.4}$$

That is, the low-momentum transfer scattering only measures the mean square radius of the pion charge cloud, and nothing else. This is because in the small momentum transfer limit the photon is soft, and with its long wavelength it can resolve only the size of the pion charge distribution, but is not sensitive to the details of its substructure.

We are not only interested in understanding the overall structure of the bound state pion by calculating its static properties, but we are also interested in the nonperturbative dynamics of its substructure that is responsible for its form factor. In order to achieve this, it is necessary to study electron-pion scattering at larger momentum transfers, where the photon probe has more resolution power, and can therefore tell us something about the pion's detailed structure.

The Feynman diagram for the elastic electron scattering off pions is shown in Figure 5.1. Using the momentum labelling of Figure 5.1, the one-photon exchange amplitude for electron-pion elastic scattering is given by

$$T_{fi} = (-\mathrm{i}e)^2 \overline{u}(k')\gamma_\mu u(k) \frac{-\mathrm{i}}{q^2} \langle \pi^+(P')|J_\mu|\pi^+(P)\rangle, \tag{5.5}$$

where u and $\overline{u}$ are electron spinors, $q = k' - k$ is the momentum transfer carried by the virtual photon, $|\pi^+(P)\rangle$ is the full pion bound state, and J_μ is the pion's electromagnetic current.

In the quark model [86], the pion electromagnetic current is given in terms of the electromagnetic current of its constituent quarks

$$J_\mu(x) = \frac{2}{3}\overline{u}(x)\gamma_\mu u(x) - \frac{1}{3}\overline{d}(x)\gamma_\mu d(x), \tag{5.6}$$

where u and d are the free Dirac spinors for the up and down quarks, respectively; 2/3 and 1/3 are their electromagnetic charges, respectively. Note that this current cannot be used for our purposes since it ignores the effects of quark confinement, the nonperturbative

QCD dynamics, the bound state structure of the pion, and the nonperturbative structure of the quark-photon vertex, see section 5.4.

The quantity $\langle \pi^+(P')|J_\mu|\pi^+(P)\rangle$ is the pion-photon vertex, whose structure we do not know and would like to understand in terms of the nonperturbative interactions between quarks, gluons, and photons, either by their underlying theories or by some modelling of them. This is particularly important for QCD since in the nonperturbative regime there is a lack of a systematic approach to hadronic observables*. Although we do not know the details about the pion-photon vertex in terms of QCD and QED dynamics, we know that J_μ must be a Lorentz four-vector, and therefore the electromagnetic interaction of a spinless particle, like the pion, can be described by a single form factor, so that we can write

$$\langle \pi^+(P')|J_\mu|\pi^+(P)\rangle = (P' + P)_\mu F_\pi(Q^2), \tag{5.7}$$

where F_π is the form factor that appears in Eq. (5.1). For electron scattering q^2 is negative, and it is common to define the positive quantity Q^2 by $Q^2 \equiv -q^2$.

The form factor $F_\pi(Q^2)$ parametrises our ignorance about the detailed structure of the pion and the dynamics of its substructure, represented by the blob in Figure 5.1. In principle, it can be calculated unambiguously from QCD for large momentum transfers because QCD is asymptotically free, see section 5.2.1. However, it is not clear whether presently accessible momentum transfers are large enough to test predictions based on a perturbative analysis in QCD, see Figure 5.4. For low-to-present-day momentum transfers, the contributions coming from the dynamics of strong QCD play an important, if non-dominant, role. In this regime, perturbative QCD is inapplicable and other methods that incorporate these effects must be developed.

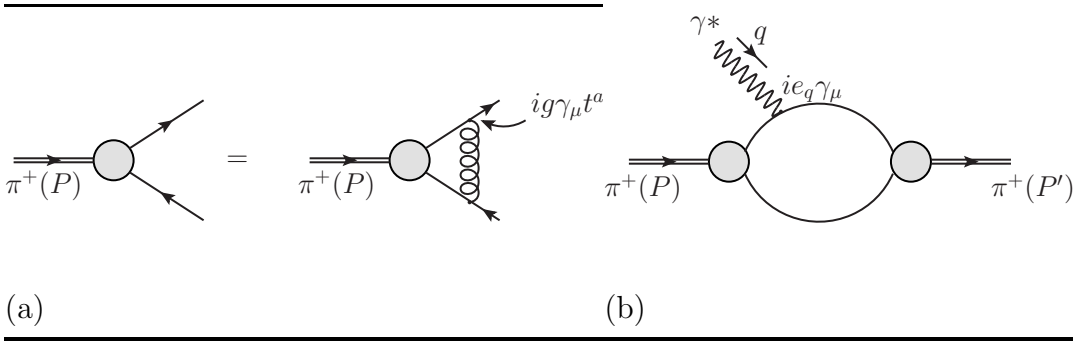

Figure 5.2.: Perturbative evaluation of the pion form factor: (a) Perturbative one-gluon exchange approximation to the pion Bethe-Salpeter equation; (b) The photon interacts perturbatively with both the up quark or the down antiquark.

5.2.1. Perturbative QCD prediction for F_π

According to Brodsky and Lepage[87, 88], the large Q^2 limit of lepton-hadron scattering processes can be separated into a soft part containing the longe-range dynamics and a hard part due to the scattering kernel T_H for the high-momentum exchange between the lepton and the valence quarks in the hadron. In this case [87, 88], the pion form factor can thus be written as a sum of contributions from the purely soft part, which vanishes as $\mathcal{O}(1/Q^4)$ or faster, and the dominating overlaping integral over the hard contributions

$$F_\pi(Q^2) = \iint \mathrm{d}x\mathrm{d}y\phi_\pi^*(x)T_H(x,y;Q^2)\phi_\pi(y), \tag{5.8}$$

where ϕ_π is the pion distribution amplitude, and x (y) is the fraction of the pion momentum P (P') carried by the individual valence quarks in the initial (final) state, with $0 < x, y < 1$, see Figure 5.2. The hard scattering kernel T_H is a sum over contributions from one-gluon exchange, two-gluon exchange, and so on. Due to the asymptotic freedom of QCD, in the $Q^2 \to \infty$ limit Eq. (5.8) is dominated by the one-gluon exchange term, and thus F_π is written as

*Chiral perturbation theory (ChPT) and Lattice QCD are the only two ab-initio approaches to the confined phase of QCD. Chiral perturbation theory is restricted to small values of momenta. Moreover, if extended to higher orders in the perturbation series, ChPT loses any predictive power because the number of unknown low energy constants increases. Lattice QCD, on the other hand, is still limited to the use of unphysical large quark masses.

$$F_\pi(Q^2) \overset{Q^2\to\infty}{=} \iint \mathrm{d}x\mathrm{d}y \frac{2\pi}{3}\left(\frac{\alpha_s(Q^2)}{Q^2}\right)\left(\frac{1}{xy}\right)\phi_\pi^*(x)\phi_\pi(y), \tag{5.9}$$

where α_s is the strong coupling constant, and xyQ^2 is the "virtuality" of the exchanged gluon. The gluon virtuality sets the scale for the QCD running coupling constant $\alpha_s(Q^2)$, and can be understood generally as the measure of the applicability of perturbative QCD to the interaction.

In the asymptotic limit $Q^2 \to \infty$ the pion distribution amplitude evolves into the form [87, 88]

$$\phi_\pi(x) \overset{Q^2\to\infty}{\longrightarrow} \phi_\pi^{\mathrm{as}}(x) = 6 f_\pi x(1-x), \tag{5.10}$$

where f_π is the pion decay constant. Using Eqs. (5.9,5.10) one gets the perturbative QCD prediction for the pion form factor

$$\lim_{Q^2\to\infty} F_\pi(Q^2) = \frac{8\pi\alpha_s(Q^2) f_\pi^2}{Q^2}. \tag{5.11}$$

The pQCD prediction accounts for the high momentum components of the pion's wave function, but cannot describe the lower momentum part [87, 88, 89, 90, 91]. Because the pion is very light, it is expected that the transition from "soft" to "hard" degrees of freedom will occur at a relative low momentum transfer, and thus be more likely to be experimentally testable.

It has to be stressed that the transverse momenta carried by the quark has been neglected in Eq. (5.9). Isgur and Llewellyn-Smith [89, 90, 91] raised the issue that at momentum transfers of a few GeV the contribution from the end point regions of the pion distribution amplitude where x or $(1-x)$ are close to zero cannot be calculated consistently in perturbative QCD, since at low values of xyQ^2 the coupling constant α_s becomes too big. The picture is modified when the transverse degrees of freedom of the quark are included into the perturbative calculation, as discussed in [89, 90, 91].

For the highest Q^2 data available, see Figure 5.4, there is a very weak suggestion that the condition $Q^2 F_\pi =$ constant is being approached. Since these data are several times larger than the perturbative QCD prediction, the conclusion is that nonperturbative effects are still dominant.

The issue then is down to which finite values of Q^2 Eq. (5.11) is valid, and the transition from the soft regime, governed by all kinds of nonperturbative quark-gluon correlations at low Q^2, to the perturbative regime at high Q^2, dominated by one-gluon exchange, starts to take place.

5.3. Experimental data on F_π

The experimental measurement of the electromagnetic form factor of the pion, F_π, is a nontrivial task. To date, reliable experimental data for $F_\pi(Q^2)$ exist in the timelike (negative) Q^2 region [84, 92, 93, 94], for small (positive) spacelike values of Q^2, where F_π is dominated by the ρ meson, and up to $Q^2 = 2.45$ GeV. In this thesis we are interested only in the form factor in the spacelike region, therefore we concetrate on this region below.

At low values of the momentum transfer squared Q^2, the pion form factor has been determined experimentally to a high precision in a model-independent way up to $Q^2 = 0.28\,\mathrm{GeV}^2$ at CERN [84, 85]. In these experiments, F_π has been extracted from the total cross section for elastic scattering of high-energy pions off atomic electrons. From this data the charge radius of the pion, r_π, has also been extracted [95].

For higher values of Q^2, high-energy electroproduction of pions[†] on a proton target has to be used [96, 97, 17]. For selected kinematics, near the pion pole $t = m_\pi^2$, this process can be described as quasi-elastic scattering of the high-energy electron off a virtual pion associated with the proton's pion cloud [96, 97]. The physical region for the Mandelstam variable $t = (p_\pi - q)^2$, where p_π is the pion four-moment, in pion electroproduction is negative, so measurements should be performed at the smallest reachable values of $-t$. The longitudinal component, σ_L, of the total cross section for pion electroproduction contains the pion exchange (t-pole) process in which the virtual photon couples to the virtual pion. This process is expected to dominate at small values

[†]The price paid for the higher values of Q^2 is that the initial state pion is off-shell before the interaction with the photon, and this needs to be taken into account in the experimental extraction of F_π.

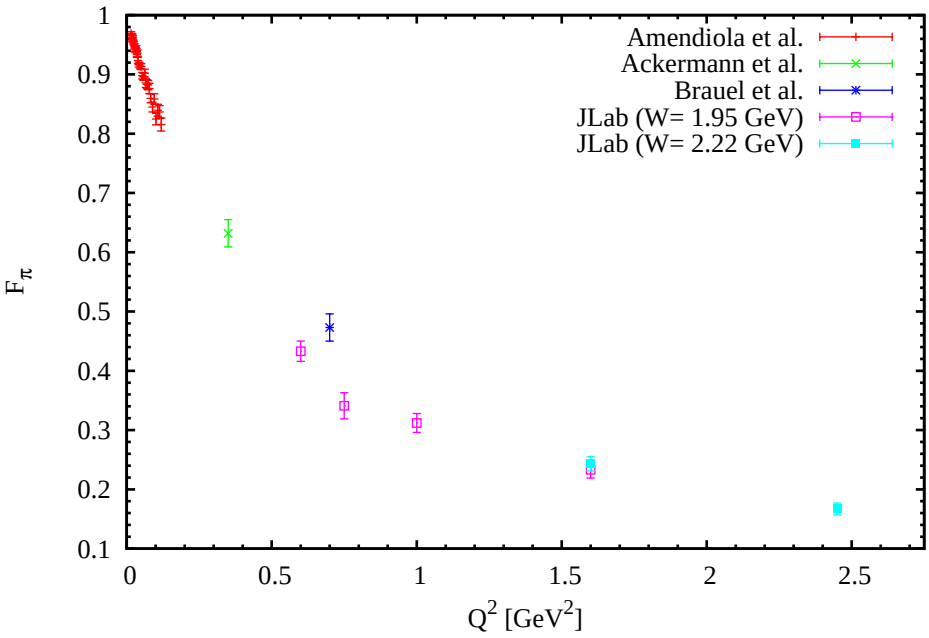

Figure 5.3.: Pion form factor data

of $-t$, and since it contains F_π, it therefore allows, in principle, the extraction[‡] of F_π from the data [96, 97]. Hence, the longitudinal cross section needs to be separated from the measured total cross section. This is done using the so-called Rosenbluth separation method [97], for which measurements at different electron energies, but for constant values of Q^2 and invariant mass W of the photon-nucleon system, are necessary.

The extraction of F_π from the separated pion electroproduction data is done using a theoretical model for the electroproduction cross section at small values of $-t$, wherein F_π is a free parameter that is fitted to the experimental data [96, 99, 100, 101]. There are a number of approaches [102, 103] for the extraction of the pion form factor from these cross sections, each with their associated uncertainties [96]. This way of extracting F_π from the experimental data means that the result depends on the theoretical model used in the analysis. Nevertheless, it is anticipated that this dependence can be reduced at sufficiently small -t [104, 98].

In this way, data on F_π has been extracted from experiments at DESY [105, 106], Cambridge Electron Accelerator (CEA), and Cornell [107, 108, 109]. In the DESY ex-

[‡]The separated cross sections versus t over some range of Q^2 and invariant mass of the photon-nucleon system $W = (p_p + q)^2$, where p_p is the proton mass, are the actual observables measured by the experiment, and the extraction of the pion form factor from these data needs theoretical input and therefore it is unavoidable model dependent [98].

periments, pion electroproduction data for $Q^2 = 0.35$ GeV^2, $W = 2.10$ GeV [110], and $Q^2 = 0.7$ GeV^2, $W = 2.19$ GeV [105, 106] were taken. The longitudinal cross sections were determined using a Rosenbluth separation, and the Born term model of [111] was used to extract the values for F_π from these data on σ_L.

The experiments performed at CEA and Cornell covered the Q^2 range of 0.28-9.77 GeV^2. A Rosenbluth separation was performed for some data points, but the results suffered from large uncertainties [109, 96]. Due to this, σ_L was calculated for each measurement by subtracting a simple model for the transverse cross section, σ_T, from the measured total cross section. A Born term model was used[112] to extract values for F_π from these data. However, the results are still inconsistent, and because of their large systematic and statistical uncertainties have in fact no power to constrain theoretical models for F_π [96, 109].

Clearly, reliable experimental data for F_π are needed for values of Q^2 above 0.7 GeV^2. Over the past decade, the F_π-collaboration [113] has measured the total cross section for the pion electroproduction reaction, at the Hall C of the Thomas Jefferson National Accelerator Facility (JLab), in order to study the pion form factor at intermediate Q^2. Because of the excellent capabilities of the JLab electron beam and experimental setup, separated, longitudinal and transverse, cross sections were determined with high accuracy. Two experiments have been completed, and plans[114, 115, 116, 117] for a 12 GeV upgrade have been made. In the first of these experiments [99, 100], data were taken for $Q^2 \in [0.6, 1.6]$ GeV^2, at $W = 1.95$ GeV, using a 4 GeV electron beam. In the second one [101], these measurements were extended to the highest Q^2 possible with a 6 GeV electron beam. This second experiment allowed new $Q^2 = 1.6$ GeV^2 data to be obtained 30 % closer to the $t = m_\pi^2$ pole, significantly reducing the model uncertainties in F_π, as well as new data at $Q^2 = 2.45$ GeV^2 to be extracted. In both of these experiments the use of the Regge model[§] of [102, 118] has emerged as a reliable tool [96, 97, 101] for the extraction of F_π from the σ_L data.

Further improvements are awaiting the 12 GeV upgrade to be completed at the JLab's Continuous Electron Beam Accelerator Facility (CEBAF), in order to extend the above measurements up to $Q^2 = 6$ GeV^2. The higher energy of the upgraded JLab electron beam is essential not only for obtaining higher momentum transfers Q^2, but also to allow data to be taken closer to the pion pole, in order to maximise its contribution

[§]This model incorporates the π^+ production mechanism and spectator neutron effects. The exchange of high-spin, high-mass particles is taken into account by replacing the pole-like Feynman propagators of Born term models with Regge propagators

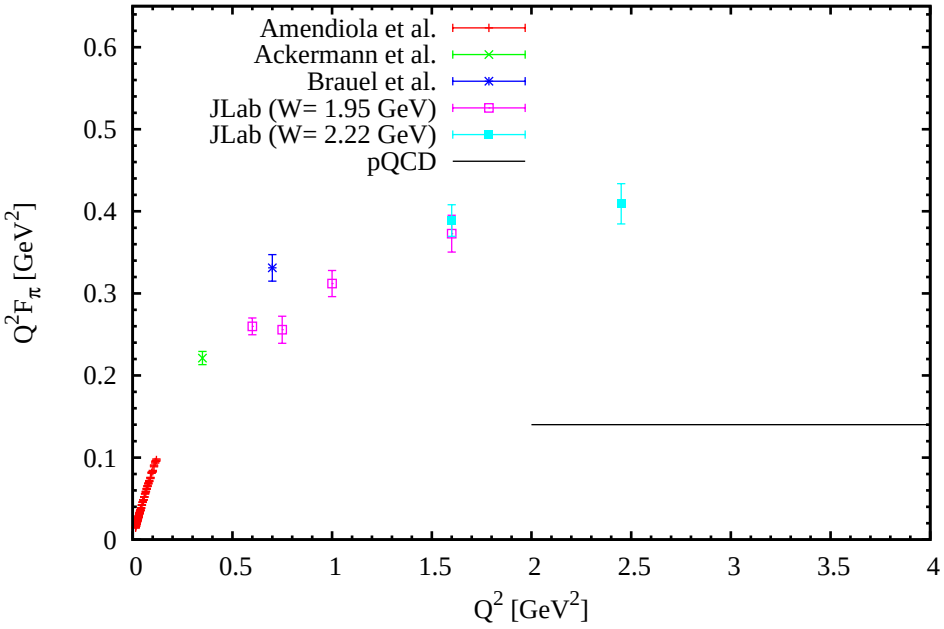

Figure 5.4.: Pion form factor data versus perturbative QCD prediction. As a result of the running of the strong coupling constant α_s, the pQCD prediction for F_π should also so "run" with the momentum scale Q^2. This pQCD result is valid for large asymptotic Q^2 however. The value used for α_s in the perturbative QCD prediction Eq. (5.11) is $\alpha_s = 0.32$, which corresponds roughly to the momentum scale Q^2 of 1 GeV^2. Here, its running is not taken into account. However, this running is logarithmic and the precise value of Q^2 should not matter. This comparison is only qualitative, however it illustrates the dominance of nonperturbative physics.

to the cross section [114, 98]. These recent data is plotted together with the previous reliable one in Figures 5.3,5.4. In Figure 5.4, the perturbative prediction, Eq. (5.11), for F_π is compared to these data. As can be seen from Figure 5.4, for the highest Q^2 data available, there is a very weak suggestion that the condition Q^2F_π = constant is being approached. Since these data are several times larger than the perturbative QCD prediction, nonperturbative effects are still dominant.

5.4. The nonperturbative quark-photon vertex

The aim of the SDE-BSE approach to hadron physics is to understand the bound state structure and reactions of hadrons in terms of the nonperturbative interactions between quarks, gluons, and photons, directly from the underlying theory. In this way, we would like to understand the electromagnetic interaction of the pion with a virtual photon in

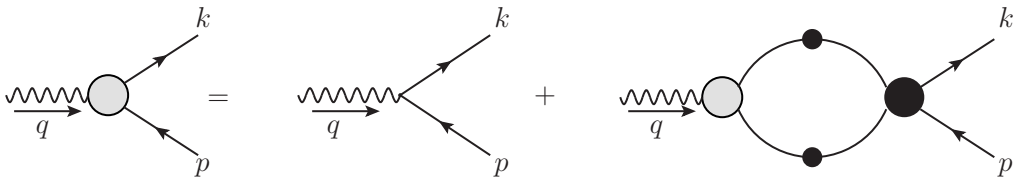

Figure 5.5.: The SDE for the quark-photon vertex. Note the appearance of the four-point quark-antiquark scattering kernel that incorporates both strong and electromagnetic dressing.

terms of the nonperturbative interaction of the virtual photon with the pion's charged constituents, that is the quarks, which is described by the gauge theory of Quantum Electrodynamics (QED).

The quark-photon vertex $\Gamma_\mu(p,k;q)$ satisfies its own SDE that describes both strong and electromagnetic dressing of the vertex

$$\Gamma^a_\mu(p,k;q) = Z_2\gamma_\mu + \int \frac{\mathrm{d}^4\ell}{(2\pi)^4} K(p,k,\tilde{p},\tilde{k}) S^a(\tilde{p}) \Gamma^a_\mu(\tilde{p},\tilde{k};q) S^a(\tilde{k}), \tag{5.12}$$

given in Figure 5.5, where Z_2 is the renormalisation constant that appears in the quark SDE, S^a is a dressed-quark propagator, and $K(p,k,\tilde{p},\tilde{k})$ is the four-point quark-antiquark scattering kernel. The solution of this equation is a difficult problem. Nevertheless, some progress has been achieved by solving it in the rainbow-ladder truncation for various forms of the dressed-gluon two-point function [119, 120]. Solutions to the homogeneous version of Eq. (5.12), at discrete timelike momenta Q^2, define vector meson bound states with masses $Q^2 = -m^2$. In fact, $\Gamma_\mu(p,k;q)$ has poles at these locations [42, 120]. Despite this, information about its form can be gained by resorting to gauge invariance of the electromagnetic interactions and Lorentz symmetry, in addition to other key constraints such as being free of kinematic singularities, have the correct perturbative limit in the ultraviolet, and transform as the bare vertex under charge conjugation and Lorentz transformations [121].

The requirement of gauge invariance is implemented through the well-known Ward-Takahashi identity (WTI) of Quantum Electrodynamics [122, 1]

$$\mathrm{i}q_\mu \Gamma_\mu(p,k;q) = S^{-1}(p) - S^{-1}(k), \tag{5.13}$$

where $q = p - k$ is the incoming photon momenta, and $S(p)$ is the fully-dressed quark propagator. It is clear that the bare vertex does not satisfy this constraint if dressed quark propagators are employed, however, this identity is satisfied order by order in perturbation theory.

Being free of kinematic singularities, the quark-photon vertex must satisfy the $q \to 0$ limit of the WTI, namely the Ward identity (WI) [123]

$$\mathrm{i}\Gamma_\mu(p,p;0) = \frac{\partial S^{-1}(p)}{\partial p_\mu}. \tag{5.14}$$

Furthermore, the full quark-photon vector vertex can be decomposed into a longitudinal and a transverse part

$$\Gamma_\mu(p,k;q) = \Gamma^L_\mu(p,k;q) + \Gamma^T_\mu(p,k;q), \tag{5.15}$$

where

$$q_\mu \Gamma^T_\mu(p,k;q) = 0. \tag{5.16}$$

From Eqs. (5.15,5.16), it follows that the WTI only constrains the longitudinal part of the vertex, relating it to the full quark propagator, while the transverse part Γ_T is not constrained by gauge invariance.

Being a Lorentz vector, the general form of the quark-photon vertex Γ_μ can be decomposed into 12 Lorentz-scalar dressing functions. Its Lorentz-Dirac basis can be constructed from the linear combinations of the three vectors γ_μ, k_μ, and p_μ, each multiplied by one of the four independent matrices $\mathbb{1}$, $\not{k}$, $\not{p}$, and $\sigma_{\mu\nu}k_\mu p_\nu$. The choice of the Lorentz-Dirac basis is constrained by the required properties under Lorentz and CPT transformations, but it is not unique, see e.g. [56]. Four of these covariants represent the longitudinal part of the vertex, which is completely specified by the WTI in terms of the full quark propagator. The transverse part can be expanded in eight covariants

T^i_μ, $i = 1, \ldots, 8$, see e.g. [56]. Furthermore, multiplicative renormalisability of the fermion SDE can be used [124, 125] to put constraints on $\Gamma^T_\mu(p,k;q)$.

The vertex that satisfies the Ward-Takahashi identity, Eq. (5.13), and is free of kinematic singularities, by satisfying Eq. (5.14), is given by

$$\begin{aligned}\Gamma^L_\mu(p,k;q) = &\frac{1}{2}\left[A(p^2)+A(k^2)\right]\gamma_\mu \\ &+\frac{1}{2}\left[\frac{A(p^2)-A(k^2)}{p^2-k^2}\right](\not{p}+\not{k})\,(p+k)_\mu \\ &-\left[\frac{B(p^2)-B(k^2)}{p^2-k^2}\right]\mathrm{i}\,(p+k)_\mu\,,\end{aligned} \tag{5.17}$$

which is the well-known Ball-Chiu (BC) ansatz [126].

Writing the longitudinal part in terms of the basis L^i_μ, $i = 1, \ldots, 4$,

$$\Gamma^L_\mu(p,k;q) = \sum_{i=1}^{4} \lambda^i(p,k;q) L^i_\mu(p,k;q), \tag{5.18}$$

we can identify from Eq. (5.17) the following basis for the longitudinal part, as well as their corresponding dressing functions,

$$\lambda^1(p,k;q) = \frac{1}{2}\left[A(p^2)+A(k^2)\right], \qquad L^1_\mu(p,k,q) = \gamma_\mu, \tag{5.19}$$

$$\lambda^2(p,k;q) = \frac{1}{2}\left[\frac{A(p^2)-A(k^2)}{p^2-k^2}\right], \qquad L^2_\mu(p,k,q) = (\not{p}+\not{k})\,(p+k)_\mu\,, \tag{5.20}$$

$$\lambda^3(p,k;q) = \frac{B(p^2)-B(k^2)}{p^2-k^2}, \qquad L^3_\mu(p,k,q) = -\mathrm{i}\,(p+k)_\mu\,, \tag{5.21}$$

$$\lambda^4(p,k;q) = 0, \qquad L^4_\mu(p,k,q) = \sigma_{\mu\nu}\,(p+k)_\nu\,, \tag{5.22}$$

where we note that the dressing function $\lambda^4(p,k;q)$ identically vanishes due to the Ward-Takahashi identity. Taking the $k \to p$ limit of Eq. (5.17) we can identify a further constraint on the transverse part, that is

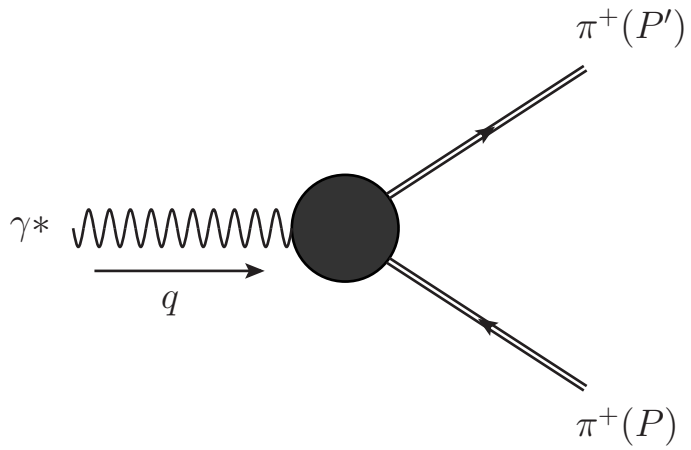

Figure 5.6.: Full pion-photon vertex. The pion is a bound state of a constituent dressed quark-antiquark pair.

$$\Gamma^T_\mu(p,p;0) = 0, \tag{5.23}$$

which makes the full vertex free of kinematic singularities and satisfies Eqs. (5.13,5.14).

In summary, the Ball-Chiu ansatz, Eq. (5.17), satisfies the constraints from the WTI and the WI, transforms under CPT as a vector should, has the correct perturbative limit in the ultraviolet, and is free of kinematic singularities. The longitudinal part is exact, i.e. completely determined by the WTI and WT, while the transverse part is exact only at $q = 0$, where $\Gamma^T_\mu(p,k;q\to 0) = 0$, and in the ultraviolet limit, where $\Gamma^T_\mu(p,k;q\to\infty) = 0$.

5.5. Impulse approximation to F_π

The dynamics of the internal structure of hadrons affects their observable properties, and the electromagnetic form factor of hadrons is an example of such an observable. The interaction of a virtual photon with a meson probes its internal structure and dynamics through the meson form factor. The study of their form factors will thus allow us to extract information about the nonperturbative dynamics of its constituents.

The theoretical prediction of F_π, defined in Eq. (5.7), at experimentally accessible Q^2, below say 10 GeV^2, is a nontrivial task since the complex nonperturbative physics of

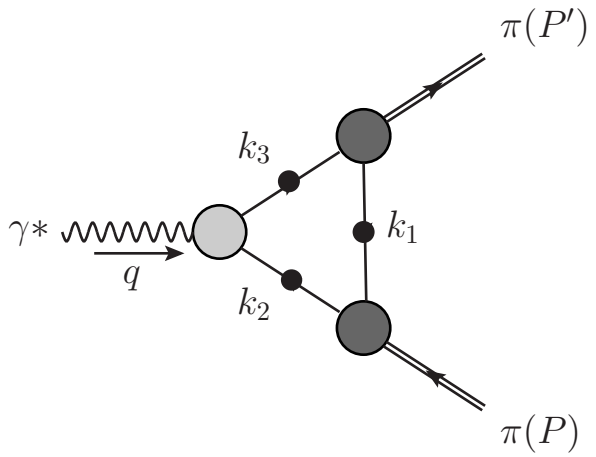

Figure 5.7.: Impulse approximation to the pion-photon vertex. All quantities have built in nonperturbative dressing effects.

confinement, dynamical chiral symmetry breaking, and bound state structure are highly dependent on the modelling of the strong coupling regime that is not reachable using pQCD.

5.5.1. Impulse approximation general setting

In this section we present the impulse approximation to the meson-photon vertex, using the continuum modelling of strong QCD we have developed so far. That is, we want to incorporate the nonperturbative effects of dynamical chiral symmetry breaking, and bound state structure in our calculation for F_π at moderate values of Q^2.

In the SDE-BSE approach to bound state structure and dynamics we have taken, a meson is a bound state of a nonperturbatively dressed constituent quark-antiquark pair, whose flavour structure is denoted by $H = a\overline{b}$. The meson bound state is described by the meson Bethe-Salpeter amplitude (BSA), and governed by the meson BSE, Eq. (4.23); the constituent quark (a) and antiquark ($\overline{b}$) are described by their propagators, and are dressed nonperturbatively through the solution of the the quark SDE, Eq. (4.1).

The impulse approximation to the meson-photon vertex of Figure 5.6 is illustrated in Figure 5.7 for the case of the pion, and makes evident the main elements of this approach. In physical terms, in the impulse approximation the photon probe interacts nonperturbatively with either the dressed quark or the dressed antiquark that make up the meson bound state, as can be seen from Figure 5.7.

In what follows, we refer only to pseudoscalar mesons since these are described by just one form factor, but the general setting can be easily extended to vector mesons [71, 127].

We denote the general meson-photon vertex by $\Lambda_\mu^H(P,P';q)$, where P and P' are, respectively, the initial and final meson momenta, and q is the momentum transfer carried by the virtual photon. The full meson-photon vertex is thus given by

$$\begin{aligned}\Lambda_\mu^H(P,P';q) &\equiv \langle H(P')|J_\mu|H(P)\rangle \\ &= (P+P')_\mu F^H(Q^2), \end{aligned} \tag{5.24}$$

where $|H(P)\rangle$ is the full bound state meson, e.g. $H=\pi$, K, and J_μ its electromagnetic current. This vertex is depicted in Figure 5.6 for the pion.

The building blocks of the impulse approximation, Figure 5.7, are: the nonperturbative quark-photon vertex $\Gamma_\mu^f(p,k;q)$; the dressed quark and antiquark propagators $S^f(p)$; and the meson bound state Bethe-Salpeter amplitude $\Gamma^H(p;P)$. The propagators for the quark and antiquark are dressed by nonperturbative gluon exchange, and are obtained by solving the quark SDE in the rainbow approximation; the meson BSA are obtained by solving the BSE in the rainbow-ladder truncation, as discussed in the previous chapter.

In the impulse approximation, the meson-photon vertex is written as the sum of two terms,

$$\Lambda_\mu^H(P,P';q) = \hat{Q}^a\Lambda_\mu^{H,a}(P,P';q) + \hat{Q}^{\overline{b}}\Lambda_\mu^{H,\overline{b}}(P,P';q), \tag{5.25}$$

where $\Lambda_\mu^{H,a}(P,P';q)$ is the contribution to the meson-photon vertex from the diagram where the photon couples to the quark, and $\Lambda_\mu^{H,\overline{b}}(P,P';q)$ that where the photon couples to the antiquark; $\hat{Q}^a$ and $\hat{Q}^{\overline{b}}$ are the electromagnetic charges of the quark and the antiquark, respectively. Using appropriate momentum labelling, see Figure 5.7, $\Lambda_\mu^{H,\overline{b}}(P,P';q)$ is given by

$$\Lambda_\mu^{H,\overline{b}}(P,P';q) = N_c \int \frac{\mathrm{d}^4\ell}{(2\pi)^4} \mathrm{Tr}\left[S^a(k_1)\Gamma^H(k_1,k_2;P)S^b(k_2) \right. \\ \left. \mathrm{i}\Gamma^b(k_2,k_3;q)S^b(k_3)\overline{\Gamma}^H(\hat{k};-P')\right], \tag{5.26}$$

where N_c is the number of colours, the trace is performed over Dirac indices, and ℓ is an appropriate loop integration variable. In $\Gamma^H(k_1,k_2;P)$, k_1 is the momentum of the quark, and k_2 that of the antiquark, such that $k_1 - k_2 = P$, $P^2 = -m_H^2$. A similar expression for $\Lambda_\mu^{H,a}(P,P';q)$ can be written down.

Similarly to Eqs. (5.24,5.25), we can identify the contributions to the meson form factor from $\Lambda_\mu^{H,a}(P,P';q)$ and $\Lambda_\mu^{H,\overline{b}}(P,P';q)$. When the photon couples to the antiquark we have

$$\Lambda_\mu^{H,\overline{b}}(P,P';q) = (P'+P)_\mu F^{H,\overline{b}}(Q^2), \tag{5.27}$$

where $F^{H,\overline{b}}(Q^2)$ is the form factor associated to $\Lambda_\mu^{H,\overline{b}}(P,P';q)$, and similarly for $F^{H,a}(Q^2)$. In the impulse approximation the meson form factor F^H is thus given by

$$F^H(Q^2) = \hat{Q}^a F^{H,a}(Q^2) + \hat{Q}^{\overline{b}} F^{H,\overline{b}}(Q^2). \tag{5.28}$$

5.5.2. Isospin symmetry

From Eq. (5.28), the pion form factor is given by

$$F^\pi(Q^2) = \frac{2}{3}F^{\pi,u}(Q^2) + \frac{1}{3}F^{\pi,\overline{d}}(Q^2). \tag{5.29}$$

In the rainbow truncation of the quark SDE, quark propagators for different flavours are distinguished only by their current mass, and therefore in the isospin symmetric limit ($m^u = m^{\overline{d}}$) we are working in the dressed quark propagators for the up and down quark are equal. It thus follows that

$$\Lambda_\mu^{\pi,u}(P,P';q) = \Lambda_\mu^{\pi,\overline{d}}(P,P';q), \tag{5.30}$$

and therefore there is only one independent form factor to calculate in Eq. (5.29)

5.5.3. Current conservation

Electromagnetic current conservation poses constraints on the form of the meson-photon vertex and its form factor. It requires that

$$F^H(Q^2=0) = \hat{Q}^a + \hat{Q}^{\overline{b}} \quad \text{and} \quad q_\mu \Lambda_\mu^H(P,P';q) = 0 \tag{5.31}$$

are satisfied. This in turn requires for the quark and antiquark contributions, Eqs. (5.25,5.28), that

$$F^{H,a}(Q^2=0) = 1, \quad F^{H,\overline{b}}(Q^2=0) = 1, \tag{5.32}$$

$$q_\mu \Lambda_\mu^{H,a}(P,P';q) = 0, \quad q_\mu \Lambda_\mu^{H,\overline{b}}(P,P';q) = 0. \tag{5.33}$$

It is an easy exercise to show that the impulse approximation preserves the electromagnetic current automatically, provided that: (a) the kernel in the Bethe-Salpeter equation, Eq. (4.23), is independent of the meson momenta; (b) the quark-photon vertex satisfies the Ward-Takahashi identity, Eq. (5.13); and (c) the quark-photon vertex is free of kinematic singularities by satisfying the Ward identity, Eq. (5.14).

Consider for example the $\Lambda_\mu^{H,\overline{b}}(P,P';q)$ vertex. At $q=0$ we have, after using the Ward identity, Eq. (5.14),

$$\begin{aligned}\Lambda_\mu^{H,\overline{b}}(P,P;0) &= 2P_\mu F^{H,\overline{b}}(Q^2=0) \\ &= N_c \int \frac{\mathrm{d}^4\ell}{(2\pi)^4} \mathrm{Tr}\left[S^a(k_1)\Gamma^H(k_1,k_2;P)S^b(k_2)\overline{\Gamma}^H(k_2,k_1;-P)\right],\end{aligned} \tag{5.34}$$

where $\ell = k_1$ is chosen to be the loop integration variable in Figure 5.7, and $k_2 = \ell - P$. Comparing this equation to the canonical normalisation condition, Eq. (4.28), we see that if the Bethe-Salpeter kernel is independent of the meson momenta P then the canonical normalisation condition for Γ^H ensures that $F^{H,\overline{b}}(0) = 1$. The same procedure applies to $\Lambda^{H,a}(P, P'; q)$. The second constraint, Eq. (5.33), can be satisfied if the quark-photon vertex satisfies the Ward-Takahashi identity, Eq. (5.13). Using Eq. (5.13) in Eq. (5.26) we obtain

$$\begin{aligned} q \cdot \Lambda^{H,\overline{b}}(P, P'; q) = N_c \int \frac{\mathrm{d}^4\ell}{(2\pi)^4} \mathrm{Tr}\left[S^a(k_1)\Gamma^H(k_1, k_2; P)S^b(k_3)\overline{\Gamma}^H(k_3, k_1; P')\right] \\ - N_c \int \frac{\mathrm{d}^4\ell}{(2\pi)^4} \mathrm{Tr}\left[S^a(k_1)\Gamma^H(k_1, k_2; P)S^b(k_2)\overline{\Gamma}^H(k_3, k_1; P')\right], \end{aligned} \tag{5.35}$$

which identically vanishes. The same occurs for $q \cdot \Lambda^{H,a}$.

If one goes beyond the rainbow-ladder truncation for the quark SDE and pion BSE, then one has to go beyond the impulse approximation in order to ensure current conservation [128, 129], since this consistency between the different truncations is crucial for the preservation electromagnetic charge, as demonstrated above. In this case, the last term in the full canonical normalisation condition, Eq. (3.22), will not vanish in general, and further structure to the meson-photon vertex will need to be added. It is not clear, however, whether a nonperturbative diagrammatic representation for Λ^H_μ exists for an arbitrary, P-dependent, Bethe-Salpeter kernel.

The diagrammatic expression for the impulse approximation is similar to the perturbative one, Figure 5.2. The difference lies in the fact that here we are taking into account the nonperturbative effects of gluon dressing in the quark-gluon vertex, quark-photon vertex, quark propagators, and pion Bethe-Salpeter amplitude, by modelling the infrared part of the effective coupling. In this approximation, the photon interacts nonperturbatively with either the dressed up quark or the dressed down antiquark. Since the rainbow-ladder truncation preserves the ultraviolet behaviour of QCD, we are guaranteed to recover the leading power-law of F_π. An explicit verification of this is difficult since numerical accuracy at such Q^2 is problematic [130].

5.5.4. Momentum routing and frame independence

We have solved the BSE in the rest frame $P_\mu = (\mathrm{i}m_H, 0, 0, 0)$ of the meson, and calculated static properties for the pion and kaon in the previous chapter. However, when calculating dynamic properties of mesons, like electromagnetic form factors, at least one of the mesons is moving. This occurs in any reference frame, and requires the solution of the meson BSE to be calculated in this particular frame.

Since the SDE-BSE approach to hadron physics is Poincaré covariant, it is guaranteed that meson observables will be independent of the reference frame in which these are calculated. This has been explicitly demonstrated in [131, 71], where the masses and decay constants of the pion and rho meson have been calculated for a nonzero three-momentum of the meson under consideration.

The solution of the homogeneous BSE in a frame that implies a nonzero three-momentum of the meson is a numerically-intensive task, since the Lorentz-scalar dressing functions characterising the meson BSA will be now functions of three variables, one radial and two angular. In the case of the Chebyshev decomposition of the previous chapter, the Chebyshev coefficients will now be functions of two variables, since we perform only one angular decomposition.

In evaluating the loop integral in the meson-photon vertex numerically in the impulse approximation, Eq. (5.26) and Figure 5.7, if we choose the momentum routing and integration variables appropriately in both the meson BSA and the loop integral in the meson-photon vertex, we can arrange the integration nodes in such a way that we do not need any interpolation or extrapolation. The price paid for this is that we have to solve the meson BSE for every value of the photon momenta Q^2, a numerically demanding task.

Overall momentum conservation implies that only two momenta are independent, since $P_i - P_f + Q = 0$, where we have relabelled the initial and final momenta of the meson to be P_i and P_f, respectively, see Figure 5.7. We choose the independent momenta to be the incoming photon momenta Q, and some other momenta, say P. We then write the initial and final meson momenta in terms of Q and P as $P_i = P - \frac{1}{2}Q$ and $P_f = P + \frac{1}{2}Q$, respectively. The condition of elastic scattering imposes constraints on P and Q, in such a way that only one remains independent. The on-shell conditions, $P_i^2 = P_f^2 = -m_H^2$, require $P^2 + \frac{1}{4}Q^2 = 0$ and $P \cdot Q = 0$. That is, the magnitude and direction of say P are determined by those of Q. Our momentum routing is given by

$$\begin{aligned}
&\text{Momentum conservation:} \quad P_i - P_f + Q = 0, \\
&\qquad k_1 - k_2 = P_i, \qquad k_2 - k_3 = Q, \qquad k_3 - k_1 = -P_f, \qquad (5.36) \\
&\text{Initial state meson:} \qquad P_i = P - \tfrac{1}{2}Q, \\
&\qquad k_1 = \tilde{k} - \frac{1}{2}P_i, \qquad k_2 = \tilde{k} + \tfrac{1}{2}P_i, \qquad \tilde{k} \equiv k + \frac{1}{4}Q, \qquad (5.37) \\
&\text{Quark-photon vertex:} \\
&\qquad k_2 = \bar{k} + \frac{1}{2}Q, \qquad k_3 = \bar{k} - \tfrac{1}{2}Q, \qquad \bar{k} \equiv k - \frac{1}{2}P, \qquad (5.38) \\
&\text{Final state meson:} \qquad P_f = P + \tfrac{1}{2}Q, \\
&\qquad k_3 = \hat{k} + \frac{1}{2}(-P_f), \quad k_1 = \hat{k} - \tfrac{1}{2}(-P_f), \quad \hat{k} \equiv k - \frac{1}{4}Q, \qquad (5.39)
\end{aligned}$$

where $k = \ell$ is the loop integration variable in the meson-photon triangle diagram, see Figure 5.7; $\tilde{k}$, $\bar{k}$, and $\hat{k}$ are the relative momenta in the initial state meson BSA, quark-photon vertex, and final state meson BSA, respectively. We use the specific momentum frame

$$Q_\mu = (0, Q, 0, 0) \qquad (5.40)$$

$$P_\mu = (P_0, 0, 0, 0), \qquad (5.41)$$

with $P_0^2 = -\frac{1}{4}Q^2 - m_H^2$. Depending on the value of Q^2, P, Q, or both are imaginary. The possible cases for spacelike or timelike photon momenta are

$$\begin{aligned}
&Q^2 \geq 0: \\
&\qquad Q = (Q^2)^{1/2} \qquad (5.42) \\
&\qquad P_0 = \mathrm{i}\left(m_H^2 + \frac{1}{4}Q^2\right)^{1/2} \qquad (5.43) \\
&Q^2 < 0: \\
&\qquad Q = \mathrm{i}\left(\left|Q^2\right|\right)^{1/2} \qquad (5.44) \\
&\qquad P_0 = \begin{cases} \mathrm{i}\left(m_H^2 - \frac{1}{4}\left|Q^2\right|\right)^{1/2}, & -4m_H^2 < Q^2 < 0 \\ \left(\frac{1}{4}\left|Q^2\right| - m_H^2\right)^{1/2}, & -\infty < Q^2 < -4m_H^2, \end{cases} \qquad (5.45)
\end{aligned}$$

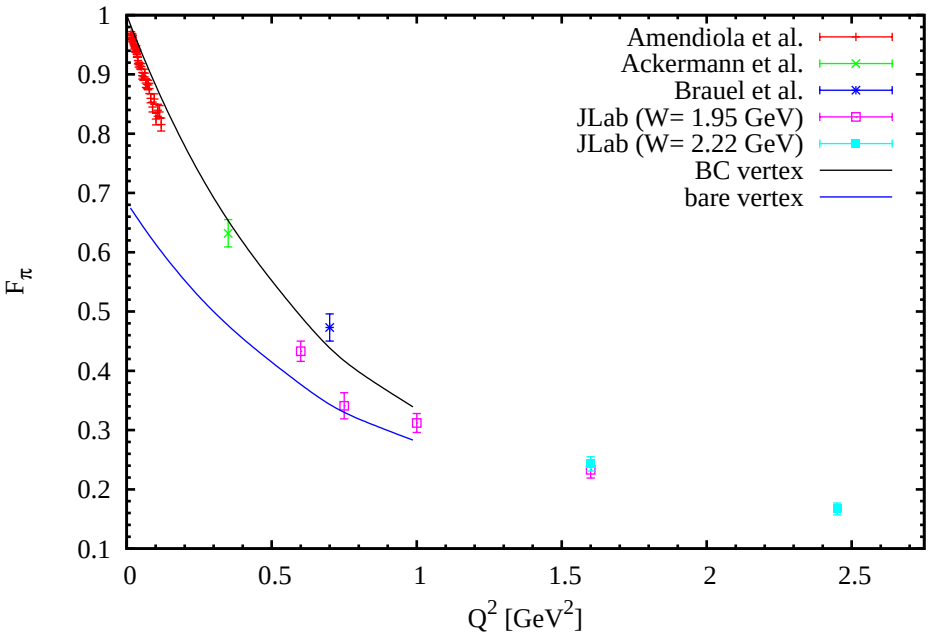

Figure 5.8.: Predicted F_π versus experimental data. The upper curve represents the calculation of F_π using the Ball-Chiu vertex; the lower curve employs the bare vertex.

however, we are only interested in the calculation of the form factor for spacelike photon momenta. For timelike momenta, F_π is dominated by the ρ meson resonance contribution [132], which is contained in the transverse part of the quark-photon vertex, but we neglected this altogether, see Section 5.4.

5.6. Numerical results for F_π

In Figure 5.8 we present numerical results for our calculation of the pion form factor F_π in the impulse approximation using the Ball-Chiu and bare vertices.

As can be seen from Figure 5.8, the bare quark-quark photon vertex, $\Gamma_\mu(p,k;q) = \gamma_\mu$, is inappropriate since it does not satisfy current conservation, which requires $F_\pi(0) = 1$. That this would be the case could have been anticipated from Eq. (5.13), because the bare vertex violates the Ward-Takahashi identity, Eq. (5.13), if dressed quark propagators are used. This identity is satisfied by the bare vertex only if quark propagators are not dressed, but the dressing of the quark propagator is an essential property of the dy-

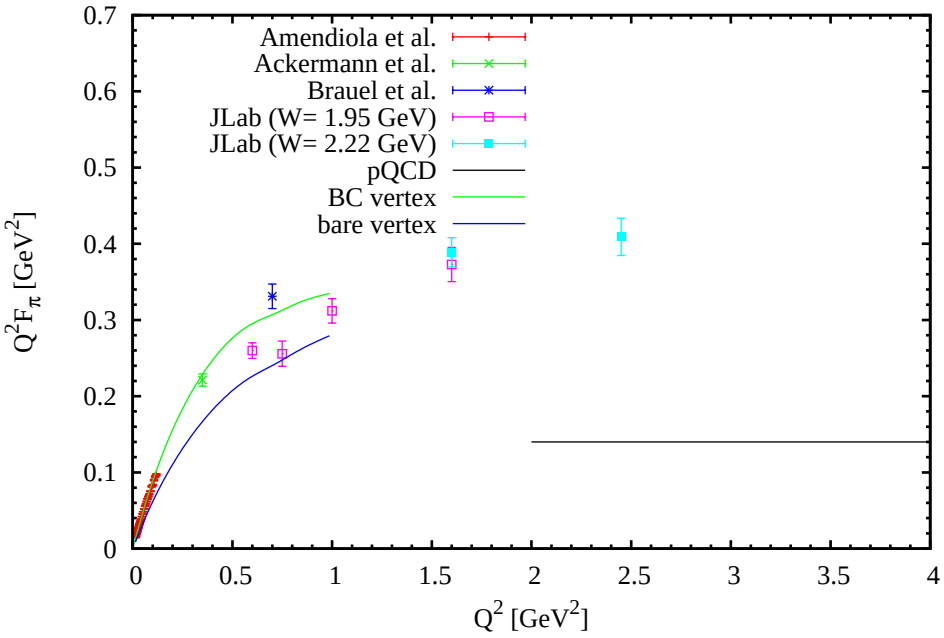

Figure 5.9.: Predicted F_π versus experimental data. The upper curve represents the calculation of F_π using the Ball-Chiu vertex; the lower curve employs the bare vertex.

namical breaking of chiral symmetry in QCD. Furthermore, this property is fundamental in the description of low energy hadron physics and therefore cannot be ignored.

On the other hand, use of the Ball-Chiu vertex conserves electromagnetic current because it satisfies, by construction, the vector Ward-Takahashi identity, Eq. (5.13). However, the calculated form factor misses the data. One reason for this is that we have completely neglected the transverse piece of the vertex, and this could have sizable contributions in the Q^2 region studied. The incorporation of vector meson bound states from the transverse piece could also be an important element for improvement[130, 120].

For the pion charge radius, r_π, which is essentially the slope of F_π at $Q^2 = 0$, the Ball-Chiu vertex produces the value $r_\pi^2 = 0.182\,\mathrm{fm}^2$, a value that is less than half the experimental one, $r_\pi^2 = 0.44\,\mathrm{fm}^2$. This is mainly because the Ball-Chiu vertex does not incorporate vector meson poles, which are contained in the transverse part of the quark-photon vertex, and therefore the Q^2 slope of F_π is poorly represented by this vertex.

Current conservation constrains the pion form factor at $Q^2 = 0$ to be $F_\pi = 1$. This is satisfied if the quark-photon vertex satisfies Eqs. (5.13,5.14) and the pion BSA is properly

Chebyshev polynomials used	6	5	4	3	2	1
$E_\pi, F_\pi, G_\pi, H_\pi$	1.000	1.000	1.000	1.000	0.998	0.998
E_π, F_π, G_π	0.920	0.920	0.921	0.921	0.921	0.921
E_π, F_π	0.957	0.957	0.958	0.958	0.963	0.963
E_π	1.312	1.312	1.317	1.317	1.264	1.264

Table 5.1.: Contributions to the pion form factor $F_\pi(Q^2)$ at zero momentum transfer from the different dressing functions and Chebyshev coefficients. The pion BSA is properly normalised, with $m_\pi = 0.1385$. The Ball-Chiu vertex is employed.

normalised, according to Eq. (3.22) or Eq. (3.23) in the rainbow-ladder truncation. In Table 5.1 we present the contributions to $F_\pi(Q^2 = 0)$ coming from the different dressing functions in the pion BSA, Eq. (4.32), and the different Chebyshev coefficients used in the Chebyshev expansion of Eq. (4.30). The BSA amplitude Γ_π is properly normalised by satisfying Eq. (3.22) or Eq. (3.23). We produce this data as follows. Once the homogeneous BSE is solved using all four dressing functions E_π, F_π, G_π, and H_π for $Q^2 = 0$, and the BSA is properly normalised, we then assess the different contributions coming from these dressing functions and the different Chebyshev coefficients. That is, we solve the BSE once, canonically normalise Γ_π using all four dressing functions, and then put to zero the Chebyshev coefficients we want to study their impact on $F_\pi(0)$. This guarantees that the mass and decay constant of the pion are correctly produced to be $m_\pi = 0.1385\,\text{GeV}$ and $f_\pi = 0.132\,\text{GeV}$, respectively.

From Table 5.1 we can see that the major part of $F_\pi(0)$ comes from the E_π dressing function, with little contribution from high order Chebyshev polynomials. At $Q^2 = 0$, Γ_π is only a function of two variables, one radial and one angular, and the odd order Chebyshev coefficients do not contribute since these vanish for a symmetric partitioning of the meson momenta, that is $\eta = 1/2$ in the BSE. Nevertheless, the rest of the dressing functions are required to ensure that the normalisation condition, Eq. (3.22) or Eq. (4.28), is satisfied, and current conservation preserved.

In Table 5.2 we present the contributions of the different components of the longitudinal part of the quark-photon vertex, Eqs. (5.19-5.22), to the pion form factor at zero momentum transfer, using all four dressing functions in the pion BSA. As can be seen, λ^1 contributes the most to $F_\pi(0)$, however it is insufficient to ensure $F_\pi(0) = 1$, as required by current conservation. The contributions from λ^2, λ^3, and λ^4 need to added to bring the value of $F_\pi(0)$ to 1. Note that although the γ_μ part of the vertex does not

	Separate contribution	Accumulated contribution
λ^1	1.1317	1.1317
λ^2	-0.0468	1.0848
λ^3	-0.0848	1.0000
λ^4	0.0000	1.0000
Bare vertex	0.7375	0.7375

Table 5.2.: Contribution to the F_π at $Q^2 = 0$ from the different terms in the Ball-Chiu vertex. Current conservations is fulfilled only when all four terms in the longitudinal piece are taken into account. Compare the contribution of only λ^1 to $F_\pi(0)$ with the bare vertex to see the effect of dressing this last vertex.

preserve electromagnetic current, it provides the most important contribution, as can be seen from row 5 of Table 5.2. The rest is contributed by λ^2, λ^3, λ^4, and by dressing the γ_μ part in such a way that the Ward-Takahashi identity is satisfied.

The conclusion that follow from Tables 5.1,5.2 is that there must be an interconnection between the canonical normalisation condition in the BSA and the Ward-Takahashi identity in order to preserve electromagnetic current. All dressing functions need to be included to ensure this. This relation is similar to that between the truncation in the BSE and that in the quark SDE needed to preserve the (pseudo)Goldstone nature of the pion.

As we mentioned above, when going beyond the rainbow-ladder truncation of the SDE-BSE complex, one must go beyond the impulse approximation in order to ensure electromagnetic current conservation. This is not straightforward however, as there is no identity-like that tells us the type of diagrams that need to be added to the impulse approximation when the Bethe-Salpeter kernel depends on the meson momenta. Therefore, when attempting to ensure charge conservation one must carefully take into account the normalisation condition of the BSA and the WI since these both constrain the meson-photon vertex at zero momentum transfer.

5.7. Summary

The electromagnetic structure of hadrons is encoded in their form factors. These parametrise our ignorance about the distribution of charge and current inside the hadrons. The experimental determination of the pion form factor is a complex endeavour due to the lack of free pions. Of equal complexity is their theoretical prediction in terms of the quarks and gluons of Quantum Chromodynamics. At experimentally accessible momentum transfers, the nonperturbative effects of confinement and bound state structure are dominant and must be taken into account. Due to the strong coupling of this regime, perturbation theory is inapplicable and we lack a systematic theoretical framework for the calculation of the pion form factor. Some modelling of the meson-photon vertex is thus required. This is possible in the SDE-BSE approach to hadron physics. The impulse approximation to the meson-photon vertex has emerged as a good starting point for this, mainly because it automatically satisfies current conservation in conjunction with the rainbow-ladder truncation of the SDE-BSE complex.

Current conservation is of fundamental importance and it can only be guaranteed if there exists an interplay between the Ward-Takahashi identity and the canonical normalisation condition for the meson BSA, as demonstrated in Eqs. (5.34,5.35). The Ward-Takahashi identity will be satisfied if the longitudinal part of the quark-photon vertex is taken to be the Ball-Chiu construction. Additional structure can be added either by solving the quark-photon SDE for the transverse part in an appropriate truncation, or by constraining it using multiplicative renormalisability [124, 125].

Numerical results for the pion form factor have been presented, using the bare and Ball-Chiu vertices. The first of these violates current conservation since it does not satisfy the WTI, and it misses the data completely. The Ball-Chiu vertex improves the situation. It satisfies current conservation because it is designed to do so, however, it is still a little above the experimental data. This is mainly because the transverse part of the quark-photon vertex has been neglected completely. This part should have important contributions to the form factor and to pion charge radius because it contains vector meson poles. Independent of this, more structure can be accommodated into the longitudinal part by dressing the quark propagators and Bethe-Salpeter kernel in a consistent way, as dictated by the axial-vector Ward-Takahashi identity.

Chapter 6.

Pion cloud effects in the quark propagator, meson BSA, and pion form factor

6.1. Introduction

Dynamical chiral symmetry breaking is one of the most important properties of low energy QCD, and its breaking pattern has profound impact on phenomenological quantities, e.g. the appearance of pseudoscalar Goldstone bosons and the non-degeneracy of chiral partners.

The spontaneous breaking of chiral symmetry is a remarkable feature of QCD because it cannot be derived directly from the Lagrangian– it is related to the nontrivial structure of the QCD vacuum, characterised by strong condensates of quarks and gluons. This is quite different from the explicit symmetry breaking, which is put in by hand through the finite quark masses, and appears in a similar way through the Higgs mechanism.

There are two important consequences of the spontaneous breaking of chiral symmetry. The first one is that the valence quarks acquire a dynamical or constituent mass through their interactions with the collective excitations of the QCD vacuum that is much larger than the seed mass present in the Lagrangian. The second one is the appearance of a triplet of pseudoscalar mesons of low mass (π^+, π^-, π^0) which represent the associated Goldstone bosons.

The prominent role played by the pion as the Goldstone boson of spontaneously broken chiral symmetry has its impact on the low-energy structure of hadrons through pion cloud effects in the quark propagation. In full QCD there are hadron contributions to the fully dressed quark-gluon vertex. These effects are generated by the inclusion of dynamical sea quarks in the quark-gluon interaction, and are therefore only present in the unquenched case. It is the aim of this chapter to introduce these pion cloud effects into the quark propagator, and then all the way up into the meson BSA and the pion form factor.

6.2. Pion back reaction into the quark SDE

Within the SDE-BSE complex, pion cloud effects are contained in the structure of the nonperturbative quark-gluon vertex, and quark-antiquark scattering kernel. These two, however, must be consistent as required by the axial-vector Ward-Takahashi identity, Eq. (3.26). Here, we describe the inclusion of the pion back reaction into the quark SDE through the quark-gluon vertex.

6.2.1. Quark-gluon vertex revisited

One of the key quantities in the quark SDE, Eq. (4.1), is the fully-dressed quark-gluon vertex Γ^a_μ. It satisfies its own Schwinger-Dyson equation whose content, which includes various two-, three-, and four-point functions, makes the solution of this equation a very difficult task. The general structure of the full vertex, described in Section 4.3.1, contains contributions from all quark-gluon correlations. In particular, there are hadronic contributions which are generated by dynamical sea quarks, and are therefore present only in the unquenched theory. These contributions should be important at low energies in the (nonperturbative) structure and dynamics of hadrons. Of particular importance are the pion cloud effects [133].

Due to the complexity of this equation, following [38, 42], we neglected in Chapter 4 all explicit contributions to this vertex, and modelled this interaction by dressing the γ_ν-part only, which then was combined with the gluon dressing function $Z(k^2)$ into a phenomenological effective interaction $\mathcal{G}(k^2)$. The full quark-gluon interaction has then been modelled by an effective gluon exchange. This is the so-called rainbow-ladder

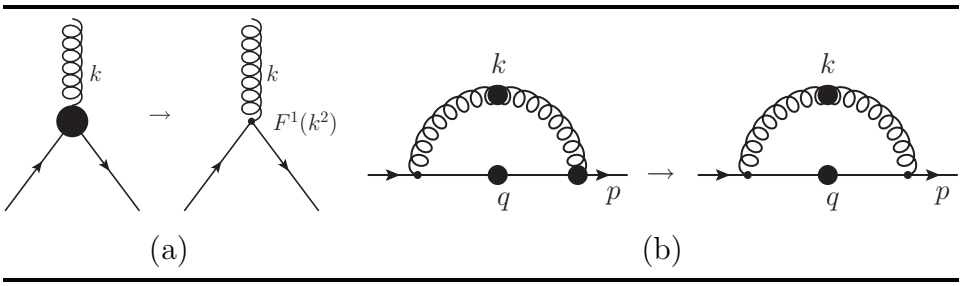

Figure 6.1.: Rainbow truncation of the full quark-gluon vertex. Only the (dressed) γ_ν part of the full interaction is retained. Recall that the full quark-gluon vertex consists of twelve Dirac structures and it receives contributions from all quark-gluon correlations, including hadronic effects.

truncation of the SDE-BSE system that we studied in the previous two chapters of this thesis, and is depicted in Figure 6.1.

More generally, denoting the full quark self-energy by $\sum(p)$, the rainbow truncation of the quark SDE can be summarised as follows. The full quark SDE is given by

$$S^{-1}(p) = Z_2 S^{-1}_{\text{bare}}(p) + \sum(p), \tag{6.1}$$

where $S^{-1}_{\text{bare}}(p) = \mathrm{i}\not{p} + m_{\text{bare}}$ is the inverse bare-quark propagator, and $S^{-1}(p) = \mathrm{i}\not{p}A(p^2) + B(p^2)$ is the inverse fully-dressed quark propagator, completely defined by the dressing functions $A(p^2)$ and $B(p^2)$; Z_2 is the renormalisation constant for the quark field. The quark self-energy $\sum(p)$ is given by

$$\sum(p) = Z_1 \int \frac{\mathrm{d}^4 q}{(2\pi)^4} g^2 D_{\mu\nu}(k) \frac{\lambda^a}{2} \gamma_\mu S(q) \Gamma^a_\nu(k,p), \tag{6.2}$$

where $k = p - q$, and Z_1 is the renormalisation constant for the quark-gluon vertex. As emphasised in Chapter 4, the quark self-energy depends crucially on the full quark-gluon vertex Γ^a_μ and gluon propagator $D_{\mu\nu}$. The latter is given in Landau gauge by

$$D_{\mu\nu}(k) = \frac{Z(k^2)}{k^2}\left(\delta_{\mu\nu} - \frac{k_\mu k_\nu}{k^2}\right). \tag{6.3}$$

The rainbow truncation scheme, depicted in Figure 6.1, consists then in the replacement

$$Z(k^2)\Gamma^a_\nu(k,p) \to \frac{t^a}{2}\gamma_\nu Z(k^2)F^1(k,p) \equiv \frac{\lambda^a}{2}\gamma_\nu Z^{\text{eff}}(k^2) \tag{6.4}$$

in the quark self energy $\sum(p)$, where the effective* gluon dressing function $Z^{\text{eff}}(k^2)$ contains information of the gluon dressing function $Z(k^2)$ and a purely k^2-dependent dressing of the γ_ν-part of the quark-gluon vertex.

The effective gluon dressing function $Z^{\text{eff}}(k^2)$ is also referred to as the effective coupling, since its ultraviolet behaviour has to resemble that of the strong running coupling constant in order to preserve the ultraviolet properties of the quark propagator, see [78] and references therein. By preserving this property, the rainbow approximation then gives reliable results in the ultraviolet, as demonstrated in Chapter 4. In the medium-to-low momentum region, however, one has to resort to a phenomenological modelling of the effective gluon dressing. The model parameters are then fixed either by fitting hadronic observables or lattice QCD data [38, 42, 134, 64].

6.2.2. Hadronic contributions to the quark-gluon vertex

In spite of the success of the rainbow approach [24, 135], by effectively dressing the resulting exchanged gluon, more structure in the quark SDE, other than the γ_ν-part of the quark-gluon vertex, should be important in the intermediate momentum region [57, 136, 54], and in particular for the description of hadron structure and dynamics. Furthermore, the infrared shape of the quark propagator and its analytic structure depend on the details of the quark-gluon vertex [54, 78, 137]. In principle, all twelve Dirac structures can be important in the intermediate momentum region [57, 136, 54]. Additional structure, other than the γ_ν-part, can in principle be incorporated in a consistent way in the quark propagator, and then all the way up into the structure and dynamics of hadrons through the Bethe-Salpeter (BS) kernel, by studying the SDE for the quark-gluon vertex. It is our aim to incorporate hadronic effects, in particular pion cloud effects, into the calculation of electromagnetic form factor for light mesons. The

*In the modelling of[38, 42], that we used in the previous chapters, the renormalised coupling constant squared and the renormalisation constant Z_1 have also been absorbed into $\mathcal{G}(k^2)$, whose model parameters were determined phenomenologically [38, 42].

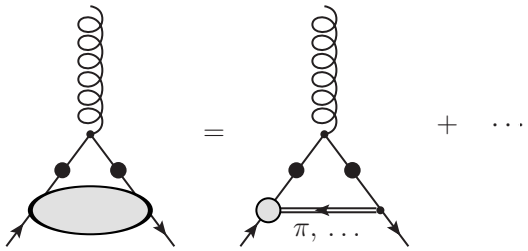

Figure 6.2.: Hadronic contributions to the quark-antiquark scattering kernel in the quark-gluon vertex. The diagram on the left hand side is one of several nonperturbative diagrams in the quark-gluon SDE.

starting point for the inclusion of hadronic effects will be the incorporation of the pion back reaction into the quark propagation. This will be done by extending the rainbow truncation, Figure 6.1, of the quark-gluon vertex by following [78, 137, 138].

In full QCD there are hadronic contributions to the fully dressed quark-gluon interaction. These effects are generated by dynamical sea quarks, and can be accounted for by a particular class of interaction diagrams in the quark-gluon vertex that appear only in unquenched QCD [78].

Of course, unquenching effects are in principle incorporated in rainbow models, Eq. (6.4), via the effective coupling $Z^{\text{eff}}(k^2)$. These models effectively resum additional corrections to the quark-gluon interaction from the Yang-Mills sector, and the inclusion of sea quarks in the gluon polarisation tensor.

Unquenching effects in the SDE-BSE framework have been investigated previously. For example, in [134] unquenching effects in the quark-antiquark Green's function were studied with the aim of providing hadronic intermediate states in bound state calculations, which generate a finite width of meson spectral functions. In[139, 140], dynamical sea quarks in the gluon polarisation were studied, and their effect on light mesons properties were found to be small but not negligible. The unquenching studies of[78, 137, 138], which we follow, are complementary to these.

The particular diagram containing hadronic contributions to the full quark-gluon interaction is given on the left-hand side of Figure 6.2, see [78] for further details. On the right-hand side, this diagram is expanded in terms of resonant and non-resonant contributions, of which only the meson exchange diagram is shown. Other hadronic contributions include baryon and diquark exchanges, and amongst the non-resonant contributions there is a one-gluon exchange between the quark and the antiquark lines, see [78] for further details. However, we are interested only in the dominant [78] meson

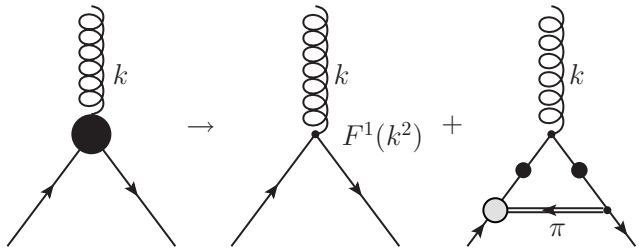

Figure 6.3.: One-pion exchange contribution to the quark-gluon vertex, with the first diagram on the right-hand side representing the rainbow approximation.

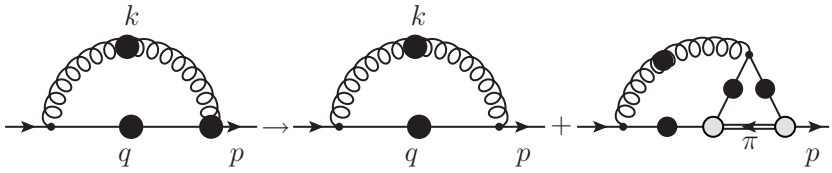

Figure 6.4.: Resulting quark-self energy for the approximated quark-gluon vertex of Figure 6.3. The exchanged gluon in the first diagram is effectively dressed by $Z^{\rm eff}(k^2)$.

exchange diagram, the pion triplet. This contribution requires the solution of the coupled system of the SDE for the quark propagator, and the corresponding BSE for the exchanged meson.

The resulting diagrammatic expression for the quark-gluon vertex is given in Figure 6.3. This approximation for the quark-gluon vertex leads to the two-loop diagram for the quark-self energy given in Figure 6.4. The first term on the right-hand side of Figure 6.4 subsumes gluonic contributions to the quark propagator, effectively dressed by $Z^{\rm eff}(k^2)$. The pion part in Figure 6.4 is more complicated since it involves not only two-loop integrals but also the full pion BSA, which needs to be determined from its Bethe-Salpeter equation. In the earlier work of [78], the loop containing the dressed-gluon was approximated by the pion BSA, using diagrammatic arguments. However, this lead to an overestimation of the back reaction, in disagreement with corresponding lattice QCD results [78]. Good agreement with lattice QCD results for the quark propagator, and meson phenomenology, were obtained [137, 138] by setting this loop equal[†] to $Z_2\tau^i \mathrm{i}\gamma_5$, where $\tau^i\,(i=1,2,3)$ are the generators of flavour $SU(2)$.

[†] A different motivation for simplifying this loop comes from the need to respect the axial-vector Ward-Takahashi identity in the $P^2 \to 0$ limit, and thus preserving the (pseudo)Goldstone nature of the pion. The simplification mentioned above has indeed allowed the construction of a axWTI preserving Bethe-Salpeter kernel [78, 137, 138].

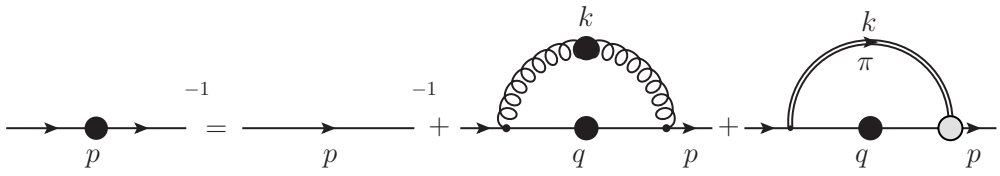

Figure 6.5.: Pion back reaction inclusion into the quark propagation.

After these simplifications, one then arrives at the SDE for the quark propagator, displayed in Figure 6.5,

$$\begin{aligned} S^{-1}(p) =& Z_2 S^{-1}_{\text{bare}} + \int \frac{\mathrm{d}^4 q}{(2\pi)^4} D^{\text{eff}}(k) \frac{\lambda^a}{2} \gamma_\mu S(q) \frac{\lambda^a}{2} \gamma_\nu \\ &+ \int \frac{\mathrm{d}^4 q}{(2\pi)^4} \left\{ \mathrm{i}\tau^i \gamma_5 S(q) \Gamma^i_\pi(\tilde{l}; k) + \mathrm{i}\tau^i \gamma_5 S(q) \Gamma^i_\pi(\hat{l}; -k) \right\} \frac{D_\pi(k)}{2}, \end{aligned} \tag{6.5}$$

where $k = p - q$, $D^{\text{eff}}(k) \equiv \mathcal{G}(k^2) D^{\text{free}}(k)$ is the effectively-dressed gluon propagator of Chapter 4, $\Gamma^i_\pi(p; P) = \tau^i \Gamma_\pi(p; P)$ is the internal pion Bethe-Salpeter amplitude, and $D_\pi(k) = (k^2 + m_\pi^2)^{-1}$ is the propagator for the exchanged pion, where m_π is the internal pion mass. The momenta $\tilde{l}$ and $\hat{l}$ are given in terms of p and q, in such a way that the pion contribution to the self energy is symmetric in p, q. Their explicit expressions are

$$\tilde{l} = (1 - \eta_\pi) p + \eta_\pi q, \quad \hat{l} = (1 - \eta_\pi) q + \eta_\pi p, \tag{6.6}$$

where η_π is the momentum sharing parameter in Γ_π for the exchanged pion. Recall that this pion is not on its mass shell.

In the chiral limit, an exact solution for the amplitudes $E_\pi, \ldots, H_\pi$ in terms of quark dressing functions and regular parts of the isovector axial-vector vertex has been given in Eqs. (3.37-3.40). In particular, the leading dressing function E_π is completely determined in terms of the quark dressing function $B(p^2)$ in the chiral limit, normalised by the chiral limit decay constant f_π. In this limit, the pion BSA amplitude is thus given by

$$\Gamma_\pi(p;P) = \gamma_5 \mathrm{i} \frac{B(p^2)}{f_\pi} + \cdots \tag{6.7}$$

$$\equiv \gamma_5 \mathrm{i} \frac{B(p^2)}{f_\pi}, \tag{6.8}$$

where the ellipsis in Eq. (6.7) denote the contributions from the non-zero dressing functions G_π, F_π, and H_π.

Motivated by Eq. (6.7), and following[78, 137, 138], we will approximate the full pion BSA in the quark self-energy, Eq. (6.5), by its leading amplitude in the chiral limit. We will also use this approximation for the massive internal pion. Evidently, this approximation omits the contributions from the three subleading amplitudes, represented by the ellipsis in Eq. (6.7). However, this approximation is only employed for the internal pion in the quark self-energy, Eq. (6.5).

Substituting Eq. (6.8) for $\Gamma_\pi(p;P)$ into Eq. (6.5), and projecting out the vector and scalar part of the quark propagator we obtain

$$\begin{aligned} A(p^2) &= Z_2 + \frac{C_F}{p^2} \int \frac{\mathrm{d}^4 q}{(2\pi)^4} \frac{\mathcal{G}(k^2)}{k^2} \left\{ -\frac{2}{k^2} \left[p^2 q^2 - (p\cdot q)^2 \right] + 3(p\cdot q) \right\} \sigma_V(q^2) \\ &\quad - \frac{3}{f_\pi} \int \frac{\mathrm{d}^4 q}{(2\pi)^4} \left[B(\tilde{l}^2) + B(\hat{l}^2) \right] \frac{D_\pi(k)}{2} \left(\frac{p\cdot q}{p^2} \right) \sigma_V(q^2) \qquad (6.9) \\ B(p^2) &= Z_4 m(\mu) + 3C_F \int \frac{\mathrm{d}^4 q}{(2\pi)^4} \frac{\mathcal{G}(k^2)}{k^2} \sigma_S(q^2) \\ &\quad - \frac{3}{f_\pi} \int \frac{\mathrm{d}^4 q}{(2\pi)^4} \left[B(\tilde{l}^2) + B(\hat{l}^2) \right] \frac{D_\pi(k)}{2} \sigma_S(q^2), \qquad (6.10) \end{aligned}$$

where the factor of 3 in front of the pion contribution represents the contribution from the pion triplet, which are degenerate in the isospin symmetric limit adopted here. Note that the effective gluon dressing function $\mathcal{G}(k^2)$ of Chapter 4 contains no free parameters. These are preserved from that chapter, and fixed in [38, 42]. Furthermore, the mass of the up quark will preserve its value.

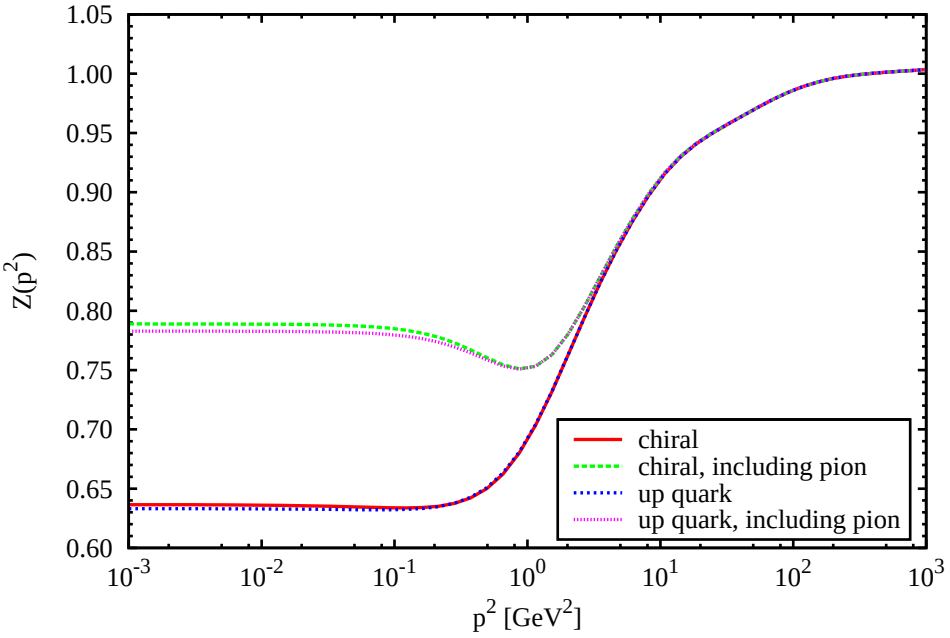

Figure 6.6.: Quark wave function $Z(p^2) = A^{-1}(p^2)$ with and with out the pion back reaction. Results without the pion back-reaction correspond to the rainbow model $\mathcal{G}(k^2)$ studied in the previous two chapters. The parameter $D = 0.93\,\mathrm{GeV}^2$ that defines this model, together with the current up-quark mass $m_u = 3.7\,\mathrm{MeV}$, renormalised at $\mu = 19\,\mathrm{GeV}$, were fixed by the pion mass and decay constant. These parameters are not refitted here after the inclusion of the pion cloud.

6.2.3. Numerical results for the quark propagator

Before attempting a numerical solution of the coupled system Eqs. (6.9,6.10), we need to specify the values for the pion mass m_π in the pion propagator $D_\pi(k)$, and decay constant f_π in the chiral limit for the exchanged pion. We will use the values obtained in Chapter 4 with $D = 0.93\,\mathrm{GeV}^2$ and $m_u = 3.7\,\mathrm{MeV}$. These parameters will be kept fixed in the rest of this thesis. In the chiral limit, we have for the pion mass and decay constant, $m_\pi = 0$ and $f_\pi = 130\,\mathrm{MeV}$, respectively; away from the chiral limit, with the up quark mass $m_u = 3.7\,\mathrm{MeV}$, we will use the physical values, $m_\pi = 138\,\mathrm{MeV}$ and $f_\pi = 132\,\mathrm{MeV}$, for the pion mass and decay constant, respectively. Variations of these numbers do not change the qualitative behaviour of the results with quantitative variations being small [137]. Note that up to here, m_π and f_π are just input parameters describing the internal pion. When we use the quark propagators obtained here, by solving Eqs. (6.9,6.10), into the meson Bethe-Salpeter equation, in the next section, we will study how the pion mass and decay constant change under the influence of pion cloud effects.

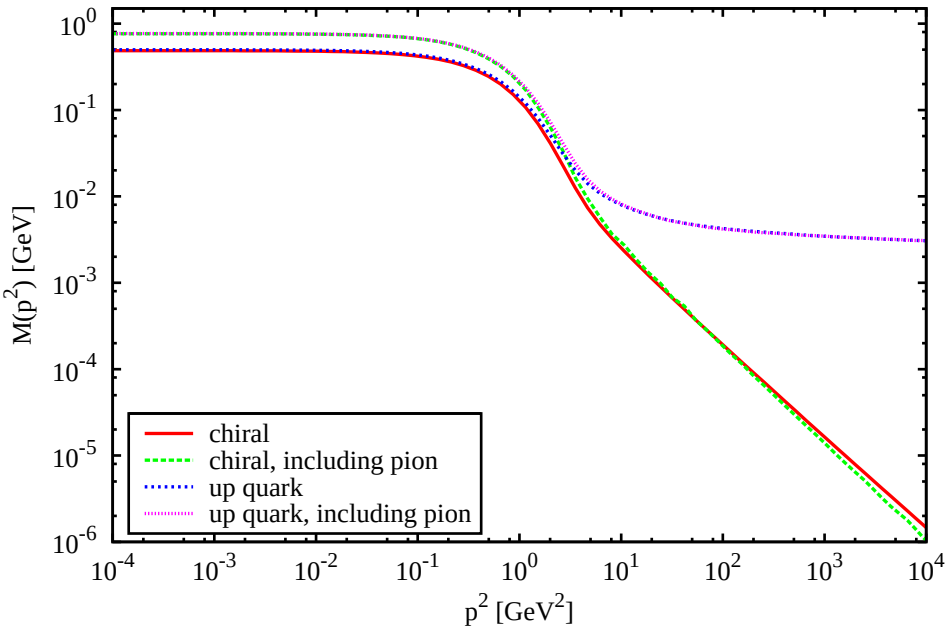

Figure 6.7.: Quark mass function $M(p^2) = B(p^2)/A(p^2)$ with and with out the pion back reaction. Results without the pion back-reaction correspond to the rainbow model $\mathcal{G}(k^2)$ studied in the previous two chapters. The parameter $D = 0.93\,\mathrm{GeV}^2$ that defines this model, together with the current up-quark mass $m_u = 3.7\,\mathrm{MeV}$, renormalised at $\mu = 19\,\mathrm{GeV}$, were fixed by the pion mass and decay constant. These parameters are not refitted here after the inclusion of the pion cloud.

In Figures 6.6,6.7, we present numerical solutions for the dressing functions $Z(p^2) = A^{-1}(p^2)$ and $M(p^2) = B(p^2)/A(p^2)$, after solving Eqs. (6.9,6.10), with and without the pion back-coupling. The explicit current mass of the up quark is $m_u = 3.7\,\mathrm{GeV}$, renormalised at $\mu = 19\,\mathrm{GeV}$. Results without the pion back reaction correspond to the rainbow model studied in the previous chapters with the effective coupling $\mathcal{G}(k^2)$[38, 42].

The inclusion of a finite quark mass in both models adds very little to the quark mass function, making evident the dominance of dynamical over explicit chiral symmetry breaking. Results with and without the pion back-reaction are qualitatively similar. In the ultraviolet region, both the mass function and the quark wave function, are almost identical for the rainbow and beyond the rainbow models. This means that the renormalisation group behaviour of these functions is not altered by the inclusion of the pion back-reaction, and that the approximation $\Gamma_\pi(p;P) \approx \gamma_5 \mathrm{i} B(p^2)/f_\pi$ captures the correct behaviour at large momenta, both at and away from the chiral limit.

$m_f(\mu)$ [MeV]	M^E [GeV]	M^E [GeV] Including π	$-\langle\overline{q}q\rangle^0$	$-\langle\overline{q}q\rangle^0$ Including π
0.0	0.391	0.527	$(0.227\ \text{GeV})^3$	$(0.203\ \text{GeV})^3$
3.7	0.400	0.531	-	-

Table 6.1.: Euclidean mass function, M^E, and chiral quark condensate $-\langle\overline{q}q\rangle^0$, with and without the inclusion of the pion back-reaction.The current up-quark mass is $m_u = 3.7\,\text{MeV}$, renormalised at $\mu = 19\,\text{GeV}$.

In the presence of explicit chiral symmetry breaking, the quark mass function in the far ultraviolet is given by Eq. (4.20) [72, 73], whereas when dynamical chiral symmetry breaking takes place, it is given by

$$M(p^2) \overset{p^2\gg\Lambda_{\rm QCD}^2}{=} \frac{2\pi^2\gamma_m}{3}\frac{1}{p^2}\frac{-\langle\overline{q}q\rangle^0}{\left[\frac{1}{2}\ln\left(p^2/\Lambda_{\rm QCD}^2\right)\right]^{1-\gamma_m}}, \tag{6.11}$$

where $\langle\overline{q}q\rangle^0$ is the renormalisation-point-independent chiral vacuum quark condensate. Consequently, one can determine the value of the chiral quark condensate by fitting Eq. (6.11) to the asymptotics of our chiral limit numerical solutions, Figure 6.7. In this way, we can determine quantitatively the effect of including the pion back-reaction into the quark SDE. Explicit values for the chiral quark condensate and Euclidean mass are given in Table 6.1, where we also include results for the rainbow model. From Table 6.1, we can see that the value of the chiral quark condensate has decreased by the inclusion of the back-reaction of the pion, in agreement with the results of [137].

6.3. Hadronic unquenching effects into the Bethe-Salpeter kernel

We now turn our study to meson bound states. Here, we would like to study the influence of the pion back-reaction into the static and dynamic properties of mesons, in particular the pion. The pion back-reaction enters in two ways into the Bethe-Salpeter equation. In the first one, in an indirect way through the quark propagator for the constituent quark and antiquark, as we described in the previous section. Here, the effective one-

gluon exchange and one-pion exchange are resummed to all orders through the solution of the quark SDE. In the second one, in a direct way through the Bethe-Salpeter kernel. Following [78, 137, 138] we explain how this can be done.

As we have already discussed, meson bound states are described by the Bethe-Salpeter equation (BSE), depicted in Figure 4.8,

$$[\Gamma_{\rm H}(p;P)]_{tu} = \int \frac{{\rm d}^4 q}{(2\pi)^4} \, [K(p,q;P)]_{tu;rs} \left[S^a(q_+)\Gamma_{\rm H}(q;P)S^b(q_-)\right]_{sr} , \tag{6.12}$$

where $H = (a\bar{b})$ indicates the flavour structure of the meson, $\Gamma_{\rm H}(p;P)$ is the meson Bethe-Salpeter amplitude (BSA) describing the bound state, $S^f(q_\pm)$ is the propagator for a dressed quark, and $K(p,q;P)_{tu;rs}$ is the quark-antiquark scattering kernel that contains, in principle, all the information about the quark-antiquark interaction. Latin indices indicate the colour, flavour, and Dirac structure. Momentum conservation entails $q_+ = q + \eta P$, $q_+ = q - (1-\eta)P$, and similarly for $p_\pm$, with $P = p_+ - p_-$. The parameter $\eta \in [0,1]$ describes the meson momentum sharing between the quark-antiquark pair. Observables, however, do not depend on this, see Tables 4.3,4.4.

As explained in Chapter 4, the BSE is a parametric eigenvalue equation, with discrete solutions $P^2 = -m_H^2$, where $m_{\rm H}$ is the mass of the bound state, with the lowest mass solutions corresponding to the physical ground state in a particular channel. Once the quark propagators and the Bethe-Salpeter kernel are known, the BSE can be solved with the use of the numerical procedure given in Appendix A.

Chiral symmetry constrains the Bethe-Salpeter kernel through the axial-vector Ward-Takahashi identity (axWTI),

$$\int \frac{{\rm d}^4 q}{(2\pi)^4} K_{tu;rs}(k,q;P) \left[\gamma_5 T^H S(q_-) + S(q_+)\gamma_5 T^H\right]_{sr} = \left[\Sigma(k_+)\gamma_5 T^H + \gamma_5 T^H \Sigma(k_-)\right]_{tu} , \tag{6.13}$$

providing a relation between the kernel in the quark SDE, through the quark self-energy $\sum(p)$, and that in the BSE. Any truncation of these equations must preserve this relation

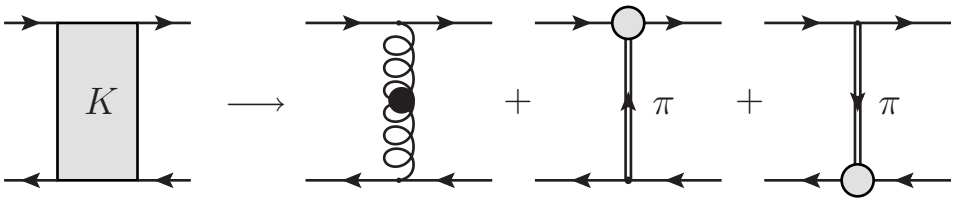

Figure 6.8.: Pion cloud effects into the quark-antiquark scattering kernel, as required by the axWTI, Eq. (6.13).

if the pattern of chiral symmetry breaking is to be satisfied. This implies that to a given kernel in the quark SDE corresponds a particular truncation of the Bethe-Salpeter kernel.

In the rainbow truncation of the quark SDE, Eq. (6.4) and Figure 6.1, this relation can be easily satisfied by

$$K^{\text{gluon}}(p,q;P)_{tu;rs} = -\frac{Z^{\text{eff}}(k^2)}{k^2}\left(\delta_{\mu\nu} - k_\mu k_\nu\right)\left[\frac{\lambda^a}{2}\gamma_\mu\right]_{ts}\left[\frac{\lambda^a}{2}\gamma_\nu\right]_{ru}, \tag{6.14}$$

where $k = p - q$, and $Z^{\text{eff}}(k^2) \equiv Z_1 g^2 F^1(k^2) Z(k^2)$. In our case, Z_1 and g^2 are absorbed into the model parameters for $\mathcal{G}(k^2)$. The resulting BSE includes an effective one-gluon exchange between the constituent quark-antiquark pair, thus providing the "ladder". The solution of the ladder-truncated BSE then corresponds to a resummation of this (infinite) gluon ladder.

As detailed in [78], the construction of a Bethe-Salpeter kernel corresponding to the pion-exchange part is more complicated. There, diagrammatic arguments were used to come up with a kernel that satisfies Eq. (6.13) in the $P^2 \to 0$ limit. In order to satisfy the axial-vector Ward-Takahashi identity, the expression for the quark self-energy containing two loops, Figure 6.4, had to be simplified to the one-loop expression of the third diagram on the right-hand of Figure 6.5, in order to ensure Eq. (6.13). The resulting Bethe-Salpeter kernel, depicted in Figure 6.8, is

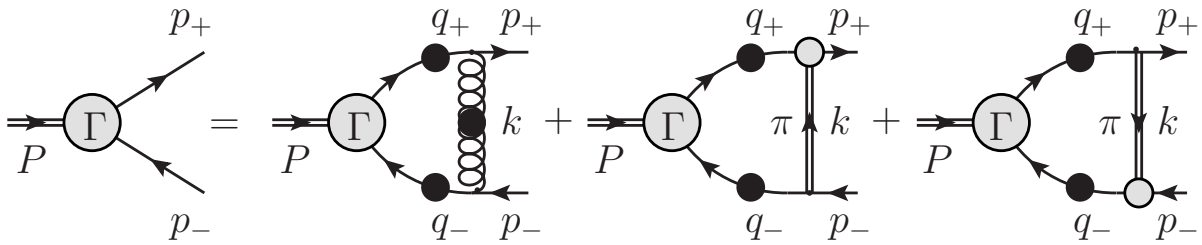

Figure 6.9.: Inclusion of the pion back reaction in the BSE as dictated by the axWTI. Quark propagators contain pion cloud effects implicitly through the solution of the quark SDE.

$$
\begin{aligned}
K^{\text{pion}}_{tu;rs}(p,q;P) = \Big\{ & \left[\Gamma^i_\pi\left(\tilde{l}^-;k\right)\right]_{ts}\left[\mathrm{i}\tau^i\gamma_5\right]_{ru} \\
& + \left[\Gamma^i_\pi\left(\hat{l}^-;-k\right)\right]_{ts}\left[\mathrm{i}\tau^i\gamma_5\right]_{ru} \\
& + \left[\mathrm{i}\tau^i\gamma_5\right]_{ts}\left[\Gamma^i_\pi\left(\tilde{l}^+;k\right)\right]_{ru} \\
& + \left[\mathrm{i}\tau^i\gamma_5\right]_{ts}\left[\Gamma^i_\pi\left(\hat{l}^+;-k\right)\right]_{ru}\Big\}\frac{D_\pi(k)}{4},
\end{aligned}
\tag{6.15}
$$

where $k = p-q$, and the relative momenta in the exchanged pion are given by $\tilde{l}^+ = \tilde{l}+\eta P$, $\tilde{l}^- = \tilde{l}-(1-\eta)P$, and similarly for $\hat{l}^\pm$, with $\tilde{l}$ and $\hat{l}$ as in Eq. (6.6). The gluon exchange part of the Bethe-Salpeter kernel is given by Eq. (6.14)

Finally, the Bethe-Salpeter equation beyond the rainbow-ladder is given by

$$
\begin{aligned}
\left[\Gamma_{\mathrm{H}}(p;P)\right]_{tu} = \int \frac{\mathrm{d}^4q}{(2\pi)^4} & \left\{K^{\text{gluon}}(p,q;P) + K^{\text{pion}}(p,q;P)\right\}_{tu;rs} \\
& \times \left[S^a(q_+)\Gamma_{\mathrm{H}}(q;P)S^b(q_-)\right]_{sr},
\end{aligned}
\tag{6.16}
$$

with $K^{\text{gluon}}(p,q;P)$ and $K^{\text{pion}}(p,q;P)$ given by Eqs. (6.14,6.15), respectively. The resulting diagrammatic expression for the BSE is given in Figure 6.9.

The rainbow-ladder kernel $K^{\text{gluon}}(p,q;P)$ is independent of the total meson momenta P. However, $K^{\text{pion}}(p,q;P)$ depends on P through the relative momenta of the exchanged pion, $l^{\tilde{\pm}}$ and $l^{\hat{\pm}}$, giving rise to a complicated expression for the canonical normalisation condition for the BSA, see Figure 6.10:

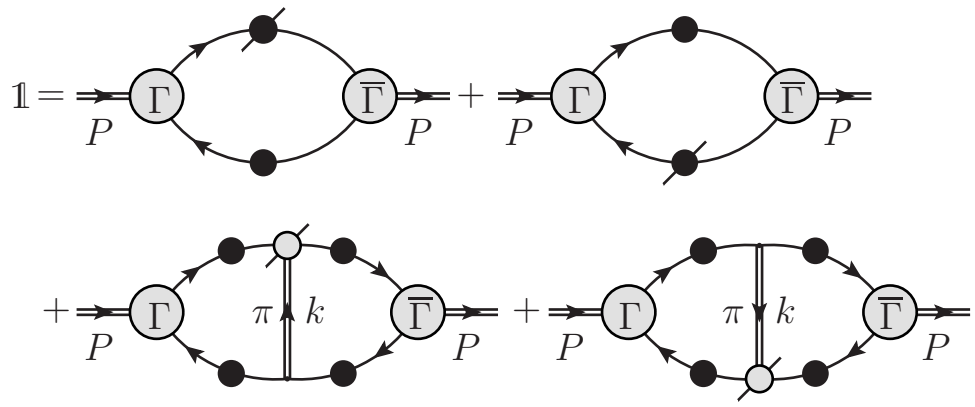

Figure 6.10.: Canonical normalisation condition for the meson BSA, after adding a one-pion exchange into the rainbow-ladder kernel. This results in a P-dependent kernel.

$$
\begin{aligned}
2P_\mu = \int \frac{\mathrm{d}^4q}{(2\pi)^4} \Bigg\{ & \mathrm{Tr}\left[\overline{\Gamma}_H(q;-P)\frac{\partial S^a(q_+)}{\partial P_\mu}\Gamma_{\mathrm{H}}(q;P)S^b(q_-)\right] \\
& + \mathrm{Tr}\left[\overline{\Gamma}_H(q;-P)S^b(q_+)\Gamma_{\mathrm{H}}(q;P)\frac{\partial S^b(q_-)}{\partial P_\mu}\right]\Bigg\} \\
+ \iint \frac{\mathrm{d}^4p}{(2\pi)^4}\frac{\mathrm{d}^4q}{(2\pi)^4} & \left[\overline{\chi}_H(q;-P)\right]_{sr}\left[\frac{\partial K^{\mathrm{pion}}(p,q;P)}{\partial P_\mu}\right]_{tu;rs}\left[\chi_H(p;P)\right]_{ut},
\end{aligned}
\tag{6.17}
$$

where $\chi_H(q;P) = S^a(q_+)\Gamma_{\mathrm{H}}(q;P)S^b(q_-)$ is the bound state wave function, and $\overline{\Gamma}_H(q;-P)^t = C^{-1}\Gamma_{\mathrm{H}}(-q;-P)C$, with $C = \gamma_2\gamma_4$ the charge conjugation matrix, and X^t denoting the transpose of the matrix X.

The problem with the expression Eq. (6.17) is the two-loop integral that must be evaluated numerically. Decomposing the measure into hyperspherical coordinates, where none of the angles may be evaluated trivially, results in the need to evaluate an eight dimensional integral numerically. Since this is forbidding, we turn our attention to an alternative but equivalent normalisation condition.

Using the artificial eigenvalue λ we have introduced into the BSE, one may use the equivalent [30, 31] normalisation condition

$$
\left(\frac{1}{\lambda}\frac{d\lambda}{dP^2}\right)^{-1} = \int \frac{\mathrm{d}^4q}{(2\pi)^4}\mathrm{Tr}\left[S^a(q_+)\Gamma_{\mathrm{H}}(q;P)S^b(q_-)\overline{\Gamma}_H(q;-P)\right], \tag{6.18}
$$

	Experiment (estimates) [MeV]	$\omega = 0.4$ [GeV] $D = 0.93$ [GeV^2]	Including π
$m_{u/d}$ [MeV]	5-10	3.7	-
m_π [MeV]	138.5	138	124
f_π [MeV]	130.7	131	147 (146)

Table 6.2.: Pion cloud effects into the pion mass and decay constant, compared to the rainbow-ladder model. The current quark mass is given at the renormalisation point $\mu = 19\,\mathrm{GeV}$. The number in parenthesis in the leptonic decay constant is the value for f_π that results when the two-loop integral in Eq. (6.17) is ignored. It thus seems a very good approximation to neglect this term altogether. Note that after including pion cloud effects the parameter $m_{u/d}$, ω, and D are not refitted.

with $P^2 = -m_H^2$. This evidently requires less numerical effort, and can simply be applied to all truncations of the Bethe-Salpeter kernel. We therefore use this expression for the normalisation of Γ_H instead. It is important to note that both normalisation conditions are equivalent in the sense that both ensure that the residue of the four-point quark-antiquark Green's function, at the pion pole, is unity.

We present our results for the pion mass m_π and decay constant f_π in Table 6.2. The mass and decay constant characterising the pion being exchanged are fixed to $m_\pi = 138.5\,\mathrm{MeV}$ and $f_\pi = 132\,\mathrm{MeV}$ for the massive pion, and to $m_\pi = 0$ and $f_\pi = 130\,\mathrm{MeV}$ in the chiral limit, as obtained in the rainbow-ladder truncation of the SDE-BSE system. These will be our reference point. Recall that the BSA of the exchanged pion was approximated with its leading amplitude $E_\pi(p;P) = B(p^2)/f_\pi$. However, it has to be stressed that this is done for the internal pion only.

The values for the parameters defining the effective coupling $\mathcal{G}(k^2)$ are $\omega = 0.4\,\mathrm{GeV}$ and $D = 0.93\,\mathrm{GeV}^2$[‡]. Recall that these parameters, together with $m_u = 3.7\,\mathrm{MeV}$, at the renormalisation point $\mu = 19\mathrm{GeV}$, were fixed in such a way that the the experimental values for the pion mass and decay constant were reproduced. As can be seen from Table 6.2, including the pion exchange into the SDE-BSE system gives rise to an attractive effect, reducing the pion mass from $m_\pi = 138\,\mathrm{MeV}$ to $m_\pi = 124\,\mathrm{MeV}$, that is, a 11 % reduction. Recall that the meson mass m_H is determined solely by the condition $\lambda(P^2 = -m_H^2) = 1$, see Figure 6.11, that is, it does not depend at all on the

[‡]We can in principle re-calculate ω and D such that the experimental values for the mass and decay constant of the pion are well reproduced. This will, of course, modify their values in the rainbow-ladder model. As we consider the rainbow-ladder model our starting point we do not do this.

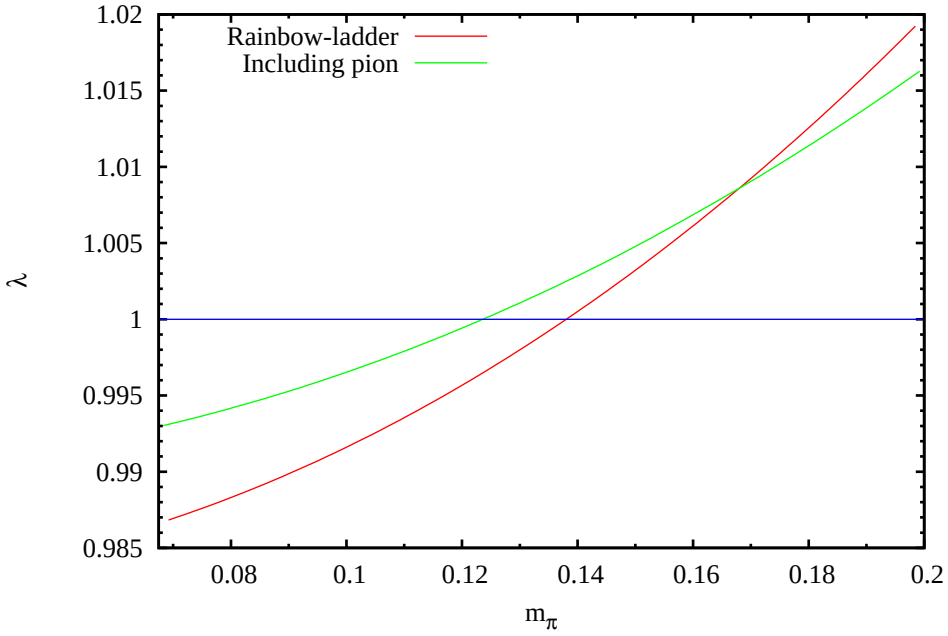

Figure 6.11.: Evolution of λ as a function of the pion mass m_π in the rainbow-ladder truncation, and by adding effects of the pion back reaction. We can see that the λ has to be determined quite precisely.

normalisation of the meson BSA. However, the decay constant does. From the canonical normalisation condition, we see that it depends on the value of the two-loop integral, see Figure 6.10. On the other hand, from the alternative normalisation condition, we see that it depends on the derivative of the artificial eigenvalue, evaluated at the meson mass shell, see Eq. (6.18). These two expressions must give the same normalisation constant. For the decay constant we also see a significant change, 12 %, going from 131 MeV to 147 MeV. In Table 6.2, we also present results for the pion decay constant calculated with the BSA normalised according the full normalisation of Eq. (6.18), and with a ladder-type normalisation that results by neglecting the explicit two-loop integral in Figure 6.10. From this, we can see that there is no significant change in f_π when we use the full normalisation condition, Eq. (6.18), or a ladder-type normalisation, suggesting that we can neglect the two-loop integral in the canonical normalisation condition. Even though there is no problem now in calculating the normalisation constant for the BSA, neglecting the two-loop integral in the canonical normalisation condition can be useful when we consider the pion-photon vertex.

6.4. Electromagnetic form factor

In Section 5.5.3, we saw how important the normalisation condition for the pion BSA was in ensuring current conservation. There, the impulse approximation for the pion-photon vertex reduced to the canonical normalisation condition for the pion BSA, in the limit in which the photon momentum vanished. This meant that, in this limit, the photon only probes the overall electric charge of the pion, given as the sum of the electric charges of the up and antidown quarks. Furthermore, in the impulse approximation the photon interacted only with the up and antidown quarks, as suggested by the ladder-type normalisation condition, Eq. (4.28). Writing the meson-photon vertex in terms of the quark-photon vertex meant that we were able to use the Ward-Takahashi identity, and specially the Ward identity, to write a zero-momentum quark-photon vertex in terms of the derivative of the inverse quark propagator, Eq. (5.14), eventually reducing the impulse approximation for the meson-photon vertex to the canonical normalisation condition for the pion BSA. This general procedure only applied to the case in which the Bethe-Salpeter kernel was independent of the meson momenta, where the two-loop integrals in the canonical normalisation identically vanished.

When we include the pion back-reaction into the quark propagator, and then for consistency into the Bethe-Salpeter kernel, however, the Bethe-Salpeter kernel is no longer independent of the meson momenta. This in turn implies that the two-loop integral term in the normalisation condition no longer vanishes, and the meson-photon vertex cannot be simply written as the sum of just two terms, one where the photon couples to the quark, and another where the photon couples to the antiquark, but it must include, somehow, a term where the photon couples to the (internal) pion being exchanged. In analogy with the impulse approximation, the two-loop integral term in the normalisation condition suggests that we add a term to the impulse approximation where the zero-momentum photon couples to the BSA for the exchanged pion. However, we will immediately face the problem of how to write such a term for nonzero photon momenta, since we lack a diagrammatic expression for the BSA-photon coupling, see the last two terms in Figure 6.10.

We have seen in Table 6.2 that it does not make a difference for the pion decay constant whether we normalise the BSA with the full normalisation condition, Eq. (6.18), or with the ladder-type normalisation, obtained by neglecting the two-loop diagrams in Eq. (6.17). This clearly indicates that the two-loop integrals do not contribute much to the normalisation constant. By using Eqs. (6.18,6.17), we can indeed calculate the

contribution of the two-loop integrals to the normalisation constant, without actually calculating any two-loop integral. For this, we write the canonical normalisation condition as

$$2P^2 = \frac{1}{N^2}\left[I(P^2) + D(P^2)\right], \tag{6.19}$$

where $P^2 = -m_H^2$ is the on-shell meson momenta, N is the full normalisation constant for the meson BSA , $I(P^2)$ represents the one-loop integrals in Eq. (6.17), and $D(P^2)$ the two-loop integrals in the same equation. These are given in terms the unnormalised BSA, obtained as the solution of the homogeneous bound state equation. Similarly, we can write the alternative normalisation condition, Eq. (6.18), as

$$\left(\frac{1}{\lambda}\frac{d\lambda}{dP^2}\right)^{-1}\Bigg|_{P^2=-m_H^2} = \frac{1}{N^2}J(P^2). \tag{6.20}$$

Since both, Eq. (6.19) and Eq. (6.20), give the same normalisation constant, we can compare the two-loop integrals $D(P^2)$ to the one-loop integrals in Eq. (6.17). From Eqs. (6.19,6.20), we obtain

$$\frac{D(P^2)}{I(P^2)} = \frac{2P^2}{I(P^2)}\left(\frac{1}{\lambda}\frac{d\lambda}{dP^2}\right)J(P^2) - 1, \tag{6.21}$$

with $P^2 = -m_H^2$. In the ladder truncation of the BSE, D/I is zero. With $m_\pi = 0.124\,\mathrm{GeV}$, in the beyond rainbow-ladder we find

$$\frac{D(P^2)}{I(P^2)} = -1.885\times10^{-2}, \quad \left(\frac{N_{\mathrm{ladder}}}{N_{\mathrm{full}}}\right)^2 = 1.019, \tag{6.22}$$

where N_{ladder} is the normalisation constant obtained with the ladder-type normalisation, i.e. by neglecting two-loop integrals,

$$2P^2 = \frac{1}{N_{\text{ladder}}^2} I(P^2), \tag{6.23}$$

and N_{full} that with the full normalisation, Eq. (6.19) or Eq. (6.20). From Eq. (6.21), we see that normalisation condition is dominated by the one-loop integrals, that is, the two-loop integrals add very little to the normalisation constant, in fact less than 2 %, and therefore do not contribute much to the static properties of the pion, as can be seen in Table 6.2. It thus, might be a good idea to neglect the two-loop integrals altogether. We stress that calculating the normalisation constant is not a problem, specially now that we have an alternative condition, but we recall that the canonical normalisation condition suggests the kind and type of diagrams that need to be added to the meson-photon vertex when trying to preserve electromagnetic charge, as discussed in Section 5.5.3. In other words, if we normalise the BSA with the full normalisation, we will need to add a term to the meson-photon vertex where the photon couples to the pion being exchanged, and we want to avoid that in the first place.

6.4.1. A hybrid approach

We have explained above that when using a meson-momenta-dependent kernel, we cannot avoid the two-loop integral appearing in the canonical normalisation condition, the last two terms in Figure 6.10. Consequently, when attempting to write an expression for the meson-photon vertex, this normalisation condition itself suggests that we take into account a term in the meson-photon vertex where the photon couples to the pion being exchanged[§]. In fact, this is required for consistency between the beyond-rainbow-ladder and the beyond-impulse approximations. In this way, we ensure, at the same time, a correctly normalised meson BSA and electromagnetic current conservation. Physically, this suggests that we consider, somehow, the case where the photon couples directly to the pion being exchanged.

For simplicity, consider the diagram of Figure 6.12. We would like to add this diagram to the impulse approximation, Figure 5.7, of the pion-photon vertex. In Figure 6.12, the internal $\pi\pi\gamma$ vertex will be calculated in the impulse approximation, as we have described in Section 5.5. However, there are two important things to be stressed. The first one is that the external pions are not on shell. The second is that this is a hybrid approach

[§]This will inevitably lead to a two-loop integral, something we would like to avoid.

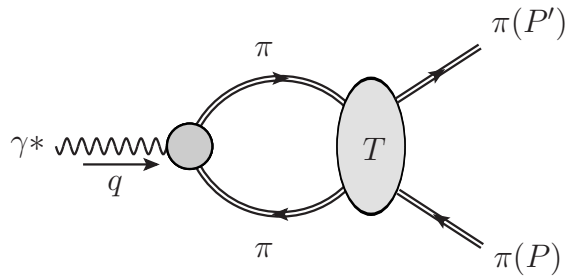

Figure 6.12.: Pion loop contribution to the electromagnetic pion form factor. T is the $\pi\pi$ scattering amplitude.

where only part of it is correctly described in the SDE-BSE approach, while the rest is *modelled* using chiral perturbation theory input. Therefore it cannot be considered a rigorous SDE-BSE application, and the results should be interpreted with due care. The intention of this section is to see how the effects of explicit pion exchange in the pion-meson vertex can be incorporated, before presenting the results in the SDE-BSE approach in Section 6.4.2. A similar approach has been presented in [141]

We approximate the pion loop contribution to the connected $\pi\pi\gamma$ vertex as

$$\Lambda_\mu^{ij\text{loop}}(P,P';Q) = \epsilon^{3kl}\int \frac{\mathrm{d}^4k}{(2\pi)^4} T^{ijkl}(s,t,u) D_\pi(k_-) D_\pi(k_+) \Lambda_\mu^{\text{IA}}(k_-,k_+;Q), \tag{6.24}$$

where Λ_μ^{IA} is the impulse approximation to the pion-photon vertex of Section 5.5, and $T^{ijkl}(s,t,u)$ is the $\pi\pi$ scattering amplitude, a function of the Mandelstam variables, and $D_\pi(k) = (k^2+m_\pi^2)^{-1}$ is the pion propagator for the internal pion.

The $\pi\pi$ scattering amplitude $T^{ijkl}(s,t,u)$ can be written in terms of a single scalar function $A(s,t,u)$ as [142, 8]

$$\begin{aligned} T^{ijkl}(s,t,u) =& \text{Amp}(\pi^i(p_1)\pi^j(p_2)\to\pi^k(p_3)\pi^l(p_4)) \\ =& A(s,t,u)\delta^{ij}\delta^{kl} + A(t,s,u)\delta^{ik}\delta^{jl} + A(u,t,s)\delta^{il}\delta^{jk}, \end{aligned} \tag{6.25}$$

where

$$s=(p_1+p_2)^2, \quad t=(p_1-p_3)^2, \quad u=(p_1-p_4)^2, \tag{6.26}$$

are the usual Mandelstam variables. Furthermore, the various amplitudes of definite isospin can also written in terms of this function as [142, 8]

$$\begin{aligned} T^0(s,t,u) &= 3A(s,t,u) + A(t,s,u) + A(u,t,s), && (6.27)\\ T^1(s,t,u) &= A(t,s,u) - A(u,t,s), && (6.28)\\ T^2(s,t,u) &= A(t,s,u) + A(u,t,s). && (6.29) \end{aligned}$$

Chiral perturbation theory input

Note that in Eq. (6.24) the ϵ^{3kl} factor allows only for a $I = 1$ isospin, forbidding the ρ^0-photon mixing that is contained in the transverse part of the quark-photon vertex. Since $q_\mu \Lambda_\mu^{\rm IA} = 0$, see Eq. (5.35), we can write

$$\Lambda_\mu^{ij\,\rm loop}(P,P';Q) = \epsilon^{3ij} T_\mu(P,P') F_\pi^{\rm loop}(Q^2), \tag{6.30}$$

with

$$\begin{aligned} q_\mu T_\mu(P,P';Q) &= 0,\\ T_\mu(P,P';Q) &= \frac{2}{Q^2}\left[P_\mu\,(P'\cdot Q) - P'_\mu\,(P\cdot Q)\right]. \end{aligned} \tag{6.31}$$

Setting $i = 1$ and $j = 2$, and contracting Eq. (6.30) with $V_\mu \equiv (P' - P)_\mu$, we have

$$F_\pi^{\rm loop}(Q^2) = \frac{V_\mu(P,P')\Lambda_\mu^{\rm loop}(P,P';Q)}{V(P,P')\cdot T(P,P')}, \tag{6.32}$$

where we have put the external pions on shell, $P^2 = P'^2 = -m_\pi^2$. Writing $\Lambda_\mu^{\rm IA}(k_-,k_+;Q)$ as in Eq. (6.30), we can write $F_\pi^{\rm loop}$ in terms of the pion form factor in the impulse approximation:

$$F_\pi^{\rm loop}(Q^2) = \int \frac{{\rm d}^4k}{(2\pi)^4} T^{I=1}(s,t,u) D_\pi(k_-) D_\pi(k_+) \frac{V_\mu(P,P')T_\mu(k_-,k_+)}{V_\nu(P,P')T_\nu(P,P')} F_\pi^{\rm IA}(k_-^2, k_-\cdot k_+, k_+^2)$$
$$= \int \frac{{\rm d}^4k}{(2\pi)^4} T^{I=1}(s,t,u) D_\pi(k_-) D_\pi(k_+) \left(\frac{-k\cdot P}{m_\pi^2 + \frac{1}{4}Q^2}\right) F_\pi^{\rm IA}(k_-^2, k_-\cdot k_+, k_+^2), \tag{6.33}$$

where $F_\pi^{\rm IA}(k_-^2, k_-\cdot k_+, k_+^2)$ is the electromagnetic form factor for off shell (internal) pions in the impulse approximation, and $T^{I=1}(s,t,u)$ is the $\pi\pi$ scattering amplitude for isospin $I=1$, Eq. (6.28). In principle, given these two quantities we should be able to calculate $F_\pi^{\rm loop}(Q^2)$ by performing the one-loop integral Eq. (6.33). However, it is difficult to calculate these quantities, one reason being that the internal pions are not on shell. The quantity $F_\pi^{\rm IA}(k_-^2, k_-\cdot k_+, k_+^2)$ can be calculated in the impulse approximation of Section 5.5, however numerical problems (e.g. sampling the quark propagators and pion BSA for large and complex momenta, as required by the loop integration) prohibit this. Thus, for practical reasons we approximate $F_\pi^{\rm IA}(k_-^2, k_-\cdot k_+, k_+^2)$ by its on-shell value, i.e.

$$F_\pi^{\rm IA}(k_-^2, k_-\cdot k_+, k_+^2) \to F_\pi^{\rm IA}(Q^2), \tag{6.34}$$

where $Q^2 = (P'-P)^2$. The quantity $T^{I=1}(s,t,u) = A(t,s,u) - A(u,t,s)$ can in principle be calculated in chiral perturbation theory[142, 8]. At lowest order in chiral perturbation theory [142, 8]

$$A(s,t,u) = -\frac{1}{f_\pi^2}(s - m_\pi^2), \tag{6.35}$$

where f_π and m_π are the physical pion decay constant and mass, respectively. This expression is valid only for small momenta however, as dictated by chiral perturbation theory [142, 8]. We can extend $A(s,t,u)$ above, by introducing an effective parameter m_σ into it:

	$\Lambda^2 = \infty$		$\Lambda^2 = 1\,\mathrm{GeV}^2$	
	$m_\sigma\,[\mathrm{GeV}^2]$	$r_\pi^2\,[\mathrm{fm}^2]$	$m_\sigma\,[\mathrm{GeV}^2]$	$r_\pi^2\,[\mathrm{fm}^2]$
$r^2_{\pi,\mathrm{exp}}$ [84]	0.559	0.440	0.667	0.440
Amendiola et al [85]	0.668	0.510	0.875	0.500

Table 6.3.: Fitted m_σ using low-Q^2 data on F_π [85] and the experimental pion charge radius value $r^2_{\pi,\mathrm{exp}} = 0.44\,\mathrm{fm}^2$ [84].

$$A(s,t,u) = \frac{1}{f_\pi^2}\left(\frac{s+m_\pi^2}{1+\frac{s}{m_\sigma^2}}\right), \tag{6.36}$$

provided that $s/m_\sigma^2 \ll 1$, where we have written Eq. (6.36) in Euclidean space.

We now define the net $\pi\pi\gamma$ vertex as the sum of the impulse approximation contribution, Eq. (5.26), and the pion loop contribution of Eq. (6.24), as

$$\Lambda_\mu^{ij}(P,P';Q) = \epsilon^{3ij}\Lambda^{\mathrm{IA}}(P,P';Q) + \Lambda_\mu^{ij\mathrm{loop}}(P,P';Q). \tag{6.37}$$

Defining a form factor for each vertex, as in Eq. (6.30), we can write the total form factor as

$$\begin{aligned} F_\pi(Q^2;m_\sigma) =& F_\pi^{\mathrm{IA}}(Q^2) + F_\pi^{\mathrm{loop}}(Q^2) \\ =& F_\pi^{\mathrm{IA}}(Q^2)\left[1 + \int^\Lambda \frac{\mathrm{d}^4k}{(2\pi)^4} T^{I=1}(s,t,u) D_\pi(k_-) D_\pi(k_+)\left(\frac{-k\cdot P}{m_\pi^2 + \frac{1}{4}Q^2}\right)\right] \\ =& F_\pi^{\mathrm{IA}}(Q^2)\left[1 + W(Q^2;m_\sigma)\right], \end{aligned} \tag{6.38}$$

where we have used Eqs. (6.33,6.34) in factoring F_π^{IA} out in the second line, and Λ is a momentum cut-off for the evaluation of Eq. (6.38) in spherical coordinates . Recall that the impulse approximation to the pion form factor, $F_\pi^{\mathrm{IA}}(Q^2)$, satisfies current conservation, that is, it satisfies $F_\pi^{\mathrm{IA}}(Q^2=0) = 1$. Therefore, in order to ensure current

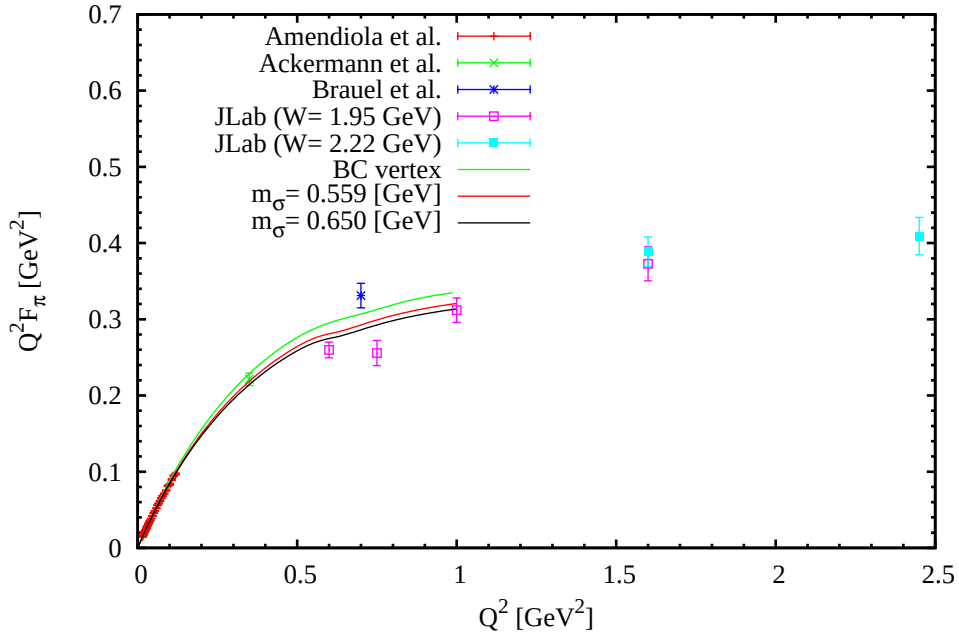

Figure 6.13.: Pion form factor given by Eq. (6.39) in the hybrid approach, with $\Lambda = \infty$.

conservation, $F_\pi(Q^2 = 0; m_\sigma) = 1$, in this hybrid approach, we redefine $W(Q^2; m_\sigma)$ by subtracting its value at $Q^2 = 0$. Our final expression for the form factor is

$$F_\pi(Q^2; m_\sigma) = F_\pi^{\rm IA} \left[1 + W(Q^2; m_\sigma) - W(Q^2 = 0; m_\sigma)\right], \tag{6.39}$$

where

$$W(Q^2; m_\sigma) = \int^\Lambda \frac{{\rm d}^4 k}{(2\pi)^4} T^{I=1}(s,t,u) D_\pi(k_-) D_\pi(k_+) \left(\frac{-k \cdot P}{m_\pi^2 + \frac{1}{4}Q^2}\right). \tag{6.40}$$

We recall that m_σ in $W(Q^2; m_\sigma)$ is an effective parameter that needs to be specified. We can obtain m_σ either by fitting $F_\pi(Q^2; m_\sigma)$ in Eq. (6.39) to low-Q^2 data on F_π, or by fitting the squared charge radius $r_\pi^2(m_\sigma)$, obtained with $F_\pi(Q^2; m_\sigma)$, to the experimental value $r_\pi^2 = 0.44\,{\rm fm}^2$. In this way, we obtain the values presented in Table 6.3. Note that in Eq. (6.39) we have to specify the cutoff Λ in the loop integration. The fitted value of m_σ will depend on this. In Table 6.3 we present values for $\Lambda = \infty$, and $\Lambda = 1\,{\rm GeV}$, a characteristic hadronic scale. We note that $W(Q^2; m_\sigma)$ is finite for $\Lambda = \infty$. In

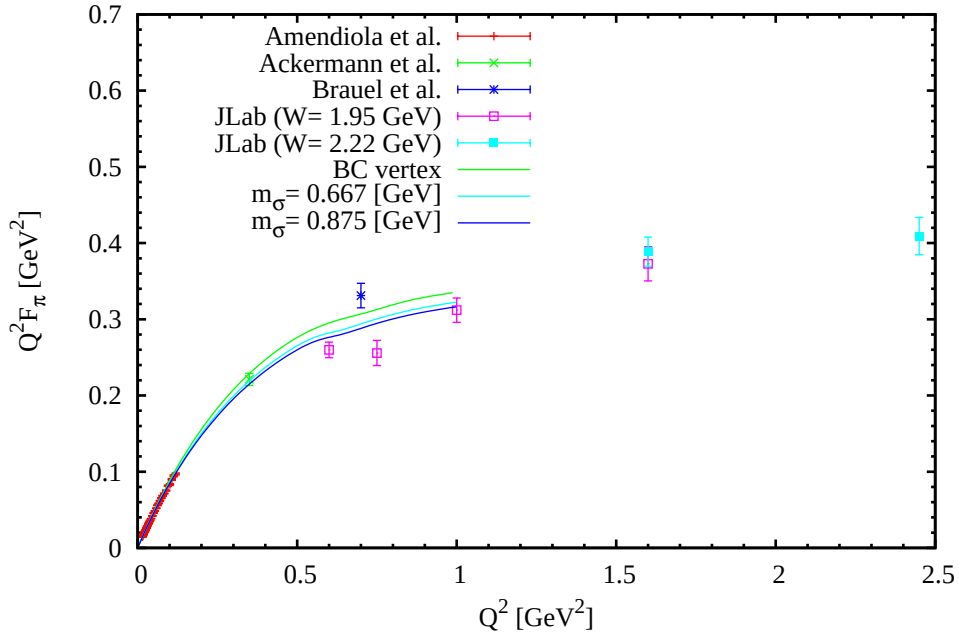

Figure 6.14.: Pion form factor given by Eq. (6.39) in the hybrid approach, with $\Lambda = 1\,\mathrm{GeV}$.

Figures 6.13,6.14, we present the respective pion form form factors for $Q^2 \in [0\text{-}1]\,\mathrm{GeV}^2$, compared to the experimental data, and to the impulse approximation of Chapter 5. From these figures, we can clearly see that the pion loop lowers the value of F_π in the region studied, with a magnitude dependent on Q^2. For $Q^2 > 1\,\mathrm{GeV}^2$ we need the pion form factor in the impulse approximation, unfortunately numerical problems prohibit its reliable calculation. From Figures 6.13,6.14, it is expected that $F_\pi(Q^2; m_\sigma)$ continues to decrease, however, it is not known in advance at which value of Q^2 it will "connect" to the perturbative result. Clearly, more work on this approach needs to be done. Furthermore, from Figures 6.13,6.14 we see that the "quark core" of the meson BSA contributes the most to the form factor, in qualitative agreement with the findings of [141], where it was found that the pion loop contributes less than 15 % to the squared pion charge radius. Finally, we stress that this hybrid calculation is only a qualitative way of estimating the pion loop contributions to the pion form factor, compared to the impulse approximation, not a rigorous calculation.

Going beyond the impulse approximation for the calculation of the electromagnetic form factor, builds additional structure into the pion BSA, whose BSA is a ladder quark-antiquark bound state, i.e. it represents the "quark core" of the pion. As we have seen, this quark core provides a very good description of static and dynamic properties of the pion, away from resonance contributions. Adding the pion loop contribution is a first

step in allowing this ladder quark-antiquark bound state to dress itself with a cloud of ladder mesonic bound states. In the framework of the BSE, this corresponds to going beyond the rainbow-ladder approximation. Indeed, this modification could be built into the pion BSE (and for consistency into the quark SDE) and would lead to a dependence on the centre-of-mass momentum P in the Bethe-Salpeter kernel, thus changing the normalisation obtained in Eq. (4.28), as we have seen in the previous section.

6.4.2. Pion cloud effects in the pion form factor

In the SDE-BSE approach, pion cloud effects enter into the pion-photon vertex in various ways: they are resummed in the quark propagators connecting pion Bethe-Salpeter amplitudes in Figure 6.15, by solving the quark SDE; through the pion Bethe-Salpeter amplitudes themselves by solving the Bethe-Salpeter equation; and possibly (explicitly) through the interaction of the virtual photon with the pion being exchanged. As we have emphasised in Section 5.5.1, there is an interplay between the canonical normalisation condition for the meson BSA and the type of diagrams that need to be considered in the meson-photon vertex, at and away from $Q^2 = 0$. For the rainbow-ladder truncation of the Bethe-Salpeter kernel of Chapter 4, we saw that it was sufficient to add only two diagrams to the meson-photon vertex: one where the photon couples to the quark, and one where the photon couples to the anti-quark, as in Figure 6.15. Using the Ward identity, we reduced these two diagrams to the normalisation condition of the pion BSA, automatically obtaining electromagnetic charge conservation, see Eqs. (5.34,5.35). This general result holds only when the Bethe-Salpeter kernel is independent of the meson momenta however, and the resulting approximation to the meson-photon vertex is called the impulse approximation, see Figure 6.15.

Based on the results of Table 6.2, we see that the two-loop integral in the canonical normalisation condition does not contribute much to the normalisation of the pion BSA, that is, the normalisation condition is dominated by the first two terms in Eq. (6.17), those that contain a derivative with respect to P^2 on the quark propagator. By neglecting the two-loop-integral terms in Eq. (6.17), we are left with a ladder-type normalisation condition. Once again, we stress that there is no problem in calculating the full normalisation of the BSA, since we now have an alternative normalisation condition, Eq. (6.18), that can be calculated easily. The "problem" with this normalisation condition is that it does not suggest which diagrams to add to the meson-photon vertex when trying to ensure electromagnetic current conservation: at $Q^2 = 0$, the normalisation condition for

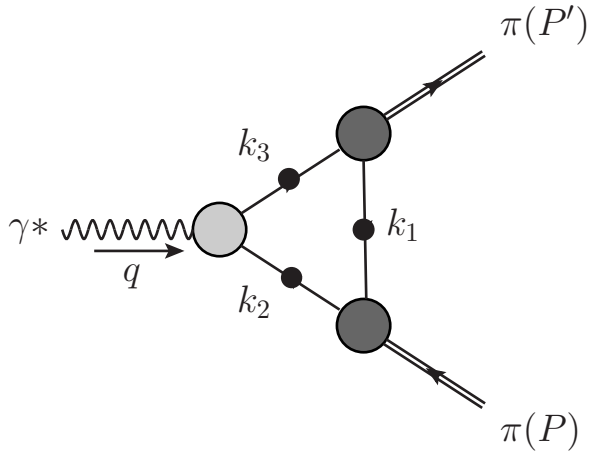

Figure 6.15.: Impulse approximation to the pion-photon vertex. All quantities have built-in nonperturbative dressing effects, including pion cloud effects.

the meson BSA and the expression for the meson-photon vertex should be "consistent", in such a way that they ensure electromagnetic current conservation automatically. This is why we are still keeping the canonical normalisation condition.

Independent of the contribution of the two-loop integral to the normalisation condition, Eq. (6.17), we define the pion-photon vertex by the impulse approximation, Figure 6.15, as we did in Chapter 5. In this approximation, the meson-photon vertex is written as the sum of two terms,

$$\Lambda_\mu^\pi(P,P';Q) = \hat{Q}^u \Lambda_\mu^{\pi,u}(P,P';Q) + \hat{Q}^{\overline{d}} \Lambda_\mu^{\pi,\overline{d}}(P,P';Q), \tag{6.41}$$

where $\Lambda_\mu^{\pi,u}(P,P';Q)$ is the contribution to the meson-photon vertex from the diagram where the photon couples to the up quark, and $\Lambda_\mu^{\pi,\overline{d}}(P,P';Q)$ that where the photon couples to the down antiquark; $\hat{Q}^u$ and $\hat{Q}^{\overline{d}}$ are the electromagnetic charges of the quark and the antiquark, respectively. Isospin symmetry ensures that $\Lambda_\mu^{\pi,u}(P,P';Q) = \Lambda_\mu^{\pi,\overline{d}}(P,P';Q)$. Explicitly, we have

$$\begin{aligned}\Lambda_\mu^{\pi,\overline{d}}(P,P';Q) = N_c \int \frac{\mathrm{d}^4\ell}{(2\pi)^4} \mathrm{Tr}\Big[& S^u(k_1)\Gamma^\pi(k_1,k_2;P) S^d(k_2) \\ & \mathrm{i}\Gamma_\mu^d(k_2,k_3;Q) S^d(k_3) \overline{\Gamma}^\pi(\hat{k};-P')\Big],\end{aligned} \tag{6.42}$$

	Rainbow-Ladder	Beyond-Rainbow-Ladder	
	ladder norm.	ladder norm.	full norm.
Ball-Chiu vertex	1.000	1.000	1.019
Bare vertex	0.736	0.836	0.852

Table 6.4.: F_π at $Q^2 = 0$ in the impulse approximation of the pion-photon vertex for the Ball-Chiu and the bare vertices. The BSA is normalised with a ladder-type normalisation, Eq. (6.23), in the first two columns, and with the full normalisation, Eq. (6.20), in the last column. In the Rainbow-Ladder truncation of the Bethe-Salpeter kernel, the two-loop integral term is zero, and therefore the ladder-type normalisation is exact. In the Beyond-Rainbow-Ladder truncation this term is not zero, however its contribution is negligible, as we can see.

where N_c is the number of colours, the trace is performed over Dirac indices, and ℓ is an appropriate loop integration variable. In $\Gamma^\pi(k_1, k_2; P)$, k_1 is the momentum of the quark, and k_2 that of the antiquark, such that $k_1 - k_2 = P$, and $P^2 = -m_\pi^2$. For a ladder-normalised $\Gamma^\pi(k_1, k_2; P)$, Eq. (6.42) and the Ward-Takahashi identity ensure electromagnetic current conservation. The normalisation of $\Gamma^\pi(k_1, k_2; P)$ is of ladder type only if we neglect the two-loop integrals in Eq. (6.17). Eq. (6.42) defines our approximation for the pion-photon vertex, however, we still need to see whether it preserves electromagnetic current conservation automatically, that is, if it gives $F_\pi(0)$=1. In Eq. (6.42), $\Gamma^\pi(k_1, k_2; P)$ is the correctly normalised BSA, normalised according to Eq. (6.17), or equivalently with Eq. (6.18). Eq. (6.18) is the full normalisation condition, however, we are not guaranteed $F_\pi(0) = 1$ automatically. On the other hand, even though the ladder-type normalisation is not the correct one, it ensures $F_\pi(0) = 1$ by construction, and, as we have seen, neglecting the two-loop integrals in calculating static properties of the pion does not make any significant difference.

In Table 6.4, we present results for $F_\pi(0)$ using the Ball-Chiu and bare vertices for the quark-photon vertex. In the first column of Table 6.4, we present the results of Chapter 5, where the ladder-truncation of the BSE, and the impulse approximation of the pion-photon vertex, exactly give $F_\pi(0) = 1$ for the Ball-Chiu vertex. In the second column, we give our results for $F_\pi(0)$ for the same vertices, but with the pion BSA normalised with a ladder-type normalisation, that is, we have neglected the two-loop integrals in Eq. (6.17). We can see that current conservation is satisfied, and we knew this beforehand, since the impulse approximation and a ladder-type normalisation of the BSA are consistent, in the sense that they guarantee $F_\pi(0) = 1$. Since the bare vertex

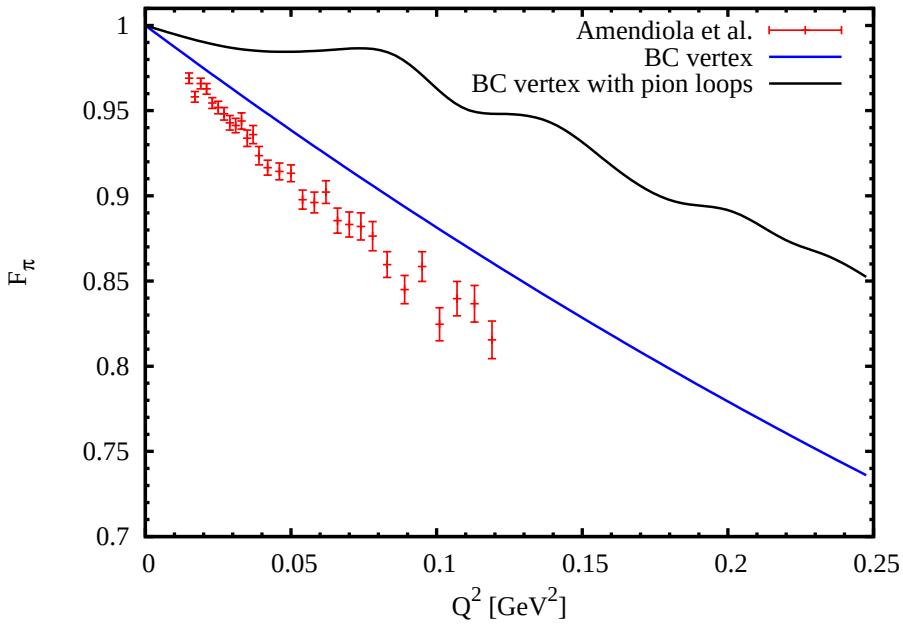

Figure 6.16.: Implicit inclusion of pion cloud effects into the pion form factor through the dressed quark propagators and the pion BSA. The structure of the pion-photon vertex is that of the impulse approximation.

does not satisfy the WTI, it is not constrained to have any fixed value at $Q^2 = 0$. Adding pion cloud effects to the impulse approximation increases the bare-vertex value of $F_\pi(0)$ by 14 % with respect to the results of the first column. Finally, in the last column, we present the same calculation as in column two, but this time the pion BSA is normalised using the full normalisation condition, that is, the contribution of the two-loop integrals is taken into account. For both vertices, we see a very small increase in $F_\pi(0)$, supporting the results of Table 6.2. The most important result is that the impulse approximation of the pion-photon vertex still preserves electromagnetic charge automatically, even if the normalisation condition of the pion BSA is not of ladder type. This is because the contribution of the two-loop integrals is negligible.

In Figure 6.17, we present numerical results for the pion form factor in the impulse approximation, Figure 6.15, using the Ball-Chiu and bare vertices for the quark-photon vertex. Pion cloud effects entered in this calculation in various ways: through the quark propagators, Eq. (6.5), connecting the pion BSA in the pion-photon vertex, see Figure 6.15; through the quark-photon vertex with the Ball-Chiu construction; and through the BSA, via the constituent quark propagators in the BSE, Eq. (6.12), and the Bethe-Salpeter kernel, Eq. (6.15). These results are compared to those of Chapter 5,

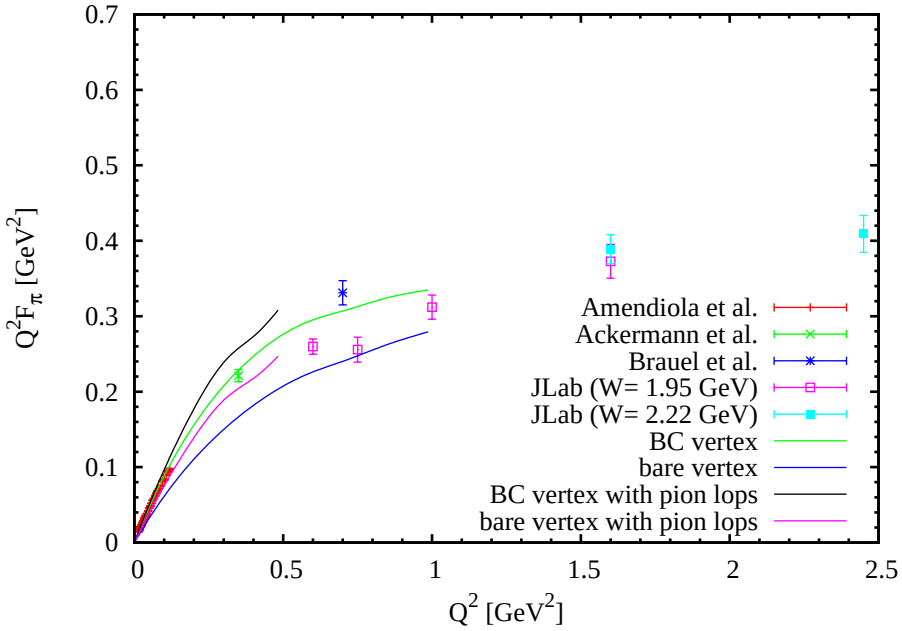

Figure 6.17.: Implicit inclusion of pion cloud effects into the pion form factor through the dressed quark propagators and the pion BSA. The structure of the pion-photon vertex is that of the impulse approximation.

and with experimental data. The new results are given on the $Q^2 \in [0\text{-}0.5]\,\mathrm{GeV}^2$ range only. Compared to the calculation of Chapter 5, the qualitative behaviour of $Q^2 F_\pi$ remains the same, at least for this Q^2 range, the only difference being the magnitude of $Q^2 F_\pi$ for both the Ball-Chiu and bare vertices. However, a closer look to the low-Q^2 momentum region, see Figure 6.16, shows that the pion cloud effects could have important contributions to the slope of F_π at $Q^2 = 0$, and therefore to the charge radius of the pion. An explicit verification of this is therefore necessary. For $Q^2 > 0.5\,\mathrm{GeV}^2$ we should expect a similar behaviour as well, due to the fact that we are using the same approximation for the pion-photon vertex, namely, the impulse approximation, and the pion cloud effects preserve the ultraviolet behaviour of the quark propagators. However, in order to make this evident, the quark propagators need to be sampled for large complex momenta, a complicated task with our current numerical procedure. Therefore, it seems that the impulse approximation to the pion-photon vertex needs to be supplemented with more structure, other than that accommodated in the quark propagators and the Bethe-Salpeter kernel, consistent with current conservation. On a deeper level, the quark-photon vertex should be obtained by solving its Schwinger-Dyson equation, thus incorporating more structure into the vertex, and vector meson bound states. On the other hand, going beyond the rainbow-ladder truncation, and

therefore beyond the impulse approximation, should also be an improvement. However, the numerical complexity of the problem then grows quickly, since we will be faced with the need to evaluate two-loop integrals numerically.

6.5. Summary

We have introduced pion cloud effects into the quark SDE and pion BSE through the quark-gluon vertex by following [78, 137, 138], and then extended these into the calculation of the electromagnetic form factor of the pion.

We found that the inclusion of pion cloud effects into the quark propagation have little effect in the behaviour of the quark dressing functions, these being largely constrained by perturbative QCD at ultraviolet momenta, and the dynamical generation of a large constituent-quark mass in the infrared region.

After the inclusion of pion cloud effects into the quark propagation, we have calculated the influence of these effects into the static properties of the pion, namely its mass and decay constant, without any readjustment of model parameters for the effective gluon dressing function. Compared to the rainbow-ladder truncation alone, the pion cloud has a considerable effect on these quantities, around 12 % change, with a decrease in the pion mass and an increase in the pion decay constant. However, a refitting of the model parameters for the gluon interaction, which are the only parameters since the pion cloud effects do not contain any adjustable parameter, should bring the values of these quantities back to their experimental values.

Furthermore, we have extended the pion cloud effects to the calculation of the electromagnetic form factor of the pion. Due to the negligible contribution of the two-loop integrals in the canonical normalisation condition for the pion BSA, see Eq. (6.22), we have written the pion-photon vertex in terms of the impulse approximation, neglecting a possible explicit coupling of the photon with the pion cloud, which could have considerable effects away from $Q^2 = 0$. The pion cloud effects therefore were confined to the quark propagators, pion BSA, and dressed quark-photon vertex. Even though we have simplified the pion BSA for the pion cloud, we have found that the qualitative behaviour of $Q^2 F_\pi(Q^2)$ does not change by the inclusion of these effects, see Figure 6.17. The quantitative difference on the region studied, compared to the rainbow-ladder truncation, might be due to the fact that the model parameters for the effective gluon

dressing function were not refitted. Nevertheless, a closer look to the low-Q^2 momentum region, see Figure 6.16, shows that the pion cloud effects have important contributions to the slope of F_π at $Q^2 = 0$, and therefore to the charge radius of the pion. An explicit evaluation of this is thus necessary.

In making the above observations, however, we have to keep in mind the simplifications we have made. There are three main simplifications which will need to be addressed in future work. The first one has to do with the representation of the virtual pion BSA. This has been replaced by its leading amplitude in the chiral limit, i.e. $\Gamma_\pi(p;P) \approx \gamma_5 \mathrm{i}B(p^2)/f_\pi$. Here, the remaining tensor structures could have sizable effects in both the static and dynamic properties of the pion. The second simplification is concerned with the neglecting of the explicit coupling of the photon with the virtual pion BSA. Although at $Q^2 = 0$ this term contributes little to the form factor and the normalisation condition of the BSA, it could have important effects away from $Q^2 = 0$. In the third simplification we have made, the transverse part of the dressed quark-photon vertex has been neglected completely. This should be important in the low-Q^2 region at and beyond the impulse approximation for the pion-photon vertex. The inclusion of a transverse part of the quark-photon vertex could be realised in the near future, either by solving its SDE or by employing existing models in the literature[124, 125]. This should be particularly important since the transverse part of the quark-photon vertex contains vector meson bound states.

Chapter 7.

Conclusions

The SDE-BSE is a well founded continuum approach to nonperturbative hadron physics. Indeed, they are a natural framework for the exploration of strong QCD since they provide access to infrared as well as ultraviolet momenta, thus giving a clear connection with processes that are well understood because QCD is asymptotically free. Moreover, the SDE are the generating tool for perturbation theory.

However, the SDE-BSE form an infinite tower of coupled n-point functions that must be truncated in order to define a tractable problem. That is, we have to make an ansatz for the n-point functions whose SDE are not explicitly solved for, thereby introducing a *model dependence* that is difficult to quantify. Furthermore, drawing a connection between QCD (in the form of the SDE for the nonperturbative quarks and gluons) and hadron observables (e.g. in the form of the meson BSE) is difficult, and that is why modelling remains a keystone is the SDE-BSE approach to hadron physics. Phenomenological input is proving useful in designing an effective quark-antiquark interaction, and quantitative comparisons between the SDE-BSE and lattice-QCD studies are today complementing the (SDE-BSE) approach.

Independent of the complexity of the truncation scheme designed for the SDE-BSE system, it has to respect some general features of the strong interactions, such as chiral symmetry and its breaking pattern. This is achieved by ensuring that the approach respects the corresponding Ward-Takahashi identities. In considering the chiral symmetry of QCD, we focused on the axial-vector Ward-Takahashi identity (axWTI). When chiral symmetry is dynamically broken, we found a number of relations between the fundamental theory and bound state properties: an explicit relation between the kernel in the meson BSE and that in the quark SDE that must be preserved by any truncation scheme; the homogeneous, flavour-nonsinglet, BSE has a massless pseudoscalar solution

with its leading amplitude given completely in terms of the nonzero scalar part of the quark propagator; and a mass formula for the flavour-nonsinglet pseudoscalar mesons in terms of the current-quark masses and the chiral quark condensate. These general results have provided important guidance in determining the structure of the BSE kernel, and have been a useful test for further approximations made.

In this thesis we have extensively studied the rainbow-ladder truncation scheme of the SDE-BSE system, complemented with a successful phenomenological quark-antiquark effective interaction, by calculating static and dynamic properties of the pion. First, we have defined the rainbow truncation of the quark SDE, and then presented numerical solutions to the resulting equations for various quark flavours, from the chiral limit to the strange quark mass. We have shown that chiral symmetry breaking is a nonperturbative phenomenon, impossible at any order in perturbative QCD, and that such an effect is possible in the rainbow truncation scheme with a phenomenologically motivated effective quark-antiquark interaction. Additionally, we have shown that dynamical chiral symmetry breaking is a mass generating mechanism. Indeed, it can take the almost massless light-quarks of perturbative QCD and turn them into the massive constituent-quarks whose mass sets the scale which characterises the spectrum of the strong interaction. This phenomenon is understood via the QCD's gap equation, the solution of which gives a quark mass function with a momentum dependence that connects the perturbative and nonperturbative, constituent-quark domains. This actually happened thanks to the fact that the effective quark-antiquark interaction reduced to the perturbative result in the ultraviolet.

By solving the axial-vector Ward-Takahashi identity, we have obtained the Bethe-Salpeter kernel that ensures the preservation of the generalised Gell-Mann–Oakes-Renner relation. Once we have obtained the ladder Bethe-Salpeter kernel, we have solved the Bethe-Salpeter integral eigenvalue equation numerically for the pion and kaon, and systematically calculated their static properties. Despite the fact that the light-quarks are made heavier, the mass of the pion, in particular, remained unnaturally small. This, too, is due to the fact that the rainbow-ladder truncation preserves the chiral symmetry breaking pattern of QCD encoded in the axWTI. This demonstrated that the rainbow-ladder truncation scheme is a good starting point for the investigation of the static properties of ground state pseudoscalar mesons, and that it can be used as a firm foundation for future improvements, as well as for the investigation of the dynamic properties of the pion.

The theoretical determination of the pion form factor, in terms of the electromagnetic interaction between its nonperturbative constituent-quarks and the photon, is a difficult task. At experimentally accessible momentum transfers, the nonperturbative effects of confinement and bound state structure must be taken into account. Due to the inapplicability of perturbative QCD in this momentum regime, modelling of the pion-photon vertex is required. We showed that this is possible in the SDE-BSE approach to hadron physics by means of the impulse approximation to the meson-photon vertex. In fact, this approximation has emerged as a good starting point for this, mainly because, as we have shown explicitly, it automatically satisfies current conservation in conjunction with the rainbow-ladder truncation of the SDE-BSE complex. We have shown that electromagnetic current conservation can only be guaranteed automatically if there exists an interplay between the vector Ward-Takahashi identity (WTI) and the canonical normalisation condition for the meson BSA. The vector WTI will be satisfied if the longitudinal part of the quark-photon vertex is taken to be the Ball-Chiu construction, leaving the transverse part largely unconstrained. In the impulse approximation, additional structure to the meson-photon vertex can be added through the quark-photon vertex, either by solving the quark-photon SDE for transverse part in an appropriate truncation scheme or by constraining it using multiplicative renormalisability.

We have presented numerical results for the pion form factor in the impulse approximation using the bare and Ball-Chiu vertices for the quark-photon vertex on the $Q^2 \in [0\text{-}1]\,\mathrm{GeV}^2$ region. The first of these violates current conservation since it does not satisfy the WTI, and it misses the data completely. The Ball-Chiu vertex improves the situation. It satisfies current conservation because it is designed to do so, however, it is still a little above the experimental data on the region studied. This is mainly because the transverse part of the quark-photon vertex has been neglected completely. This part should have important contributions to the form factor and charge radius of the pion because it contains vector meson poles. Independent of this, more structure can be accommodated into the longitudinal part of the vertex by dressing the quark propagators and Bethe-Salpeter kernel in a consistent way, as dictated by the axial-vector Ward-Takahashi identity, and then using the Ball-Chiu vertex construction.

In connection with the perturbative prediction for F_π, the diagrammatic expression for the pion-photon vertex in the impulse approximation is similar to the perturbative one. The difference being that in the impulse approximation we take into account the nonperturbative effects of gluon dressing in the quark-gluon vertex, quark-photon vertex, constituent quark propagators, and pion BSA by modelling the infrared part of

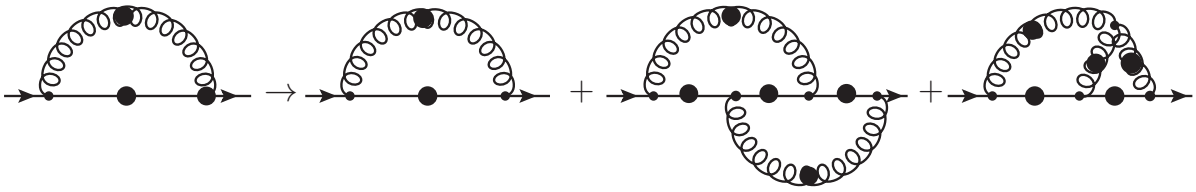

Figure 7.1.: Nonperturbative one-loop corrections to the quark-gluon vertex in the quark self-energy.

the effective quark-antiquark interaction. Since the rainbow-ladder truncation preserves the ultraviolet behaviour of QCD, we are guaranteed to recover the leading power-law of F_π at large Q^2. Unfortunately, an explicit verification of this, and the value of Q^2 at which this happens, is difficult since numerical accuracy at such Q^2 is problematic.

Following the observation above, that more structure can be accommodated into the longitudinal part of the vertex by using the Ball-Chiu construction, we have introduced pion cloud effects into the quark SDE and pion BSE through the quark-gluon vertex, and then all the way up into the pion electromagnetic form factor using the impulse approximation for the pion-photon vertex. Even though we have approximated the pion BSA for the virtual pion by its leading amplitude in the chiral limit, it seems, according to the numerical results presented, that the introduction of pion cloud effects, as we have done it here, do not change the qualitative behaviour of the quark propagators and pion form factor, the former being largely constrained by perturbative QCD and dynamical chiral symmetry breaking. For the static properties of the pion (m_π and f_π), we have seen a considerable variation in their values, as compared to their rainbow-ladder results, however, a readjustment of the effective gluon dressing parameters should bring them back to their experimental values.

For the pion form factor, on the other hand, incorporating the transverse part of the quark-photon vertex should be important at and beyond the impulse approximation. This will add a richer structure to the vertex, and because it contains vector meson bound states it will also be relevant for the pion charge radius. Moreover, going beyond the impulse approximation to the pion-photon vertex, in accordance with electromagnetic current conservation, should be important as well, since the Q^2 behaviour of the pion form factor would be modified, at least in principle.

In particular, starting with the quark SDE, the inclusion of the one-loop corrections to the quark-gluon vertex in the quark self-energy should be relevant, see Figure 7.1, both for the static and dynamic properties of mesons. According to the axial-vector

Ward-Takahashi identity, Eq. (3.26), these one-loop (nonperturbative) corrections to the quark-gluon vertex would require 5 additional two-loop diagrams in the ladder Bethe-Salpeter kernel [131] in order to preserve the chiral symmetry breaking pattern of the strong interactions. The resulting BSE kernel will now become dependent on the total meson momenta, implying a quite complicated canonical normalisation condition for the BSA. In fact, this introduces 4 extra terms in the normalisation condition [131] for the meson BSA. Furthermore, according to the vector Ward-Takahashi identity, this will require 4 additional diagrams to be added to the impulse approximation of the pion-photon vertex in order to ensure electromagnetic current, Eq. (5.31). As can be inferred from Figure 7.1, and subsequent diagrams for the BSE kernel, and pion-photon vertex diagrams, every step, from the calculation of the quark propagators to the pion-photon vertex, will present significant technical, nevertheless, some progress is being made in current exploratory studies [143, 144].

The Schwinger-Dyson equation for the quark propagator has been one of the main objects studied in this thesis. We have seen that it is closely related to the meson Bethe-Salpeter equation, not only because it is one of its main inputs, but also because the kernels of these two integral equations must be related according to the chiral symmetry properties of the strong interactions implied by the axial-vector Ward-Takahashi identity. The quark SDE is also crucially related to the full gluon propagator and quark-gluon vertex. These two objects combine nonperturbatively to give the quark propagator its spectral properties. Due to the complexity of the SDE-BSE system, tractability requieres us to adopt a more model dependent approach. Probably, by systematically incorporating all the relevant Ward-Takahashi identities of the theory, this model dependence can be reduced. In fact, the rainbow-ladder truncation scheme of the SDE-BSE is the leading-order term of a nonperturbative symmetry-preserving truncation scheme of the SDE-BSE [145]. This truncation scheme may be described as a dressed-loop expansion of quark-gluon vertex. Its diagrammatic expansion yields an ordered truncation of the SDE-BSE that, term by term, guarantees the preservation of vector and axial-vector Ward-Takahashi identities. The nonperturbative one-loop corrections to the quark-gluon vertex in the quark self-energy described above are the next-to-leading terms in this dressed-loop expansion. The advantage of this truncation scheme is that it is systematic and satisfies the Ward-Takahashi identities mentioned above, thus ensuring the Goldstone character of the pion, and electromagnetic current conservation automatically. Unfortunately, at every order of the truncation, an ansatz for the gluon dressing function is required. Here is where the phenomenological and lattice-QCD input enter, providing insight for the modelling of the gluon dressing func-

tion. Hopefully by blending the systematics of this truncation scheme with the insight of fully nonperturbative lattice-QCD, we might arrive at a robust truncation scheme capable of describing quantitatively many phenomena in hadron physics.

Appendix A.

Numerical solution to the Bethe-Salpeter equation

A.1. Numerical solution of the rainbow-ladder truncated BSE in the pseudoscalar channel

The Bethe-Salpeter equation (BSE) is a homogeneous eigenvalue equation that admits solutions only for discrete values of the meson momenta squared $P^2 = -m_H^2$, where m_H is the mass of the meson under consideration. In order to facilitate the numerical solution of this equation we modify it by introducing a fictitious eigenvalue $\lambda(P^2)$ into Eq. (6.12),

$$\lambda(P^2)\left[\Gamma_H(p;P)\right]_{tu} = \int \frac{\mathrm{d}^4 q}{(2\pi)^4}\left[K(p,q;P)\right]_{tu;rs}\left[S^a(q_+)\Gamma_H(q;P)S^b(q_-)\right]_{sr}, \qquad \text{(A.1)}$$

where q is the relative momenta between the quark and the antiquark, $q_+ = q + \eta P$, and $q_- = q - (1-\eta)P$, such that $P = q_+ - q_-$ is the meson momenta with $P^2 = -m_H^2$ fixed. The original problem is recovered when $\lambda = 1$ at the meson mass shell $P^2 = -m_H^2$.

The general structure of the Bethe-Salpeter amplitude (BSA), $\Gamma_H(p;P)$, for the meson under consideration will depend on its quantum numbers, such as flavour, Dirac, and CPT transformations[27]. Scalar and pseudoscalar mesons are characterised by four Lorentz-scalar dressing functions, see Eq. (A.4), while vector mesons are characterized by eight. We denote these generically by $F_H^\alpha(p;P)$.

A.1.1. Rainbow-Ladder Kernel

In this appendix we will solve the BSE for a pseudoscalar meson in the rainbow-ladder truncation by explicitly applying the general method described in Section 4.4.2.

In principle, the only input quantities to the bound state equation, Eq. (A.1), are the quark-antiquark scattering kernel, $[K(p,q;P)]_{tu;rs}$, and the constituent dressed-quark propagators, S^a and S^b. However, these quantities are part of an infinite tower of coupled nonlinear integral equations, and a truncation scheme must be introduced in order to obtain a tractable problem.

The rainbow-ladder truncation scheme of the SDE-BSE complex is a scheme that preserves essential properties of the strong interactions such as chiral symmetry and its breaking pattern, as dictated by the axial-vector Ward-Takahashi identity Eq. (3.26). This truncation has been successfully applied to the study of pseudoscalar and vector mesons, as discussed in Chapter 4. In this truncation the Bethe-Salpeter kernel is given by the effective one-gluon exchange kernel [38, 42]

$$K(p,q;P)_{tu;rs} = -\mathcal{G}(k^2) D^{\text{free}}_{\mu\nu}(k) \left[\frac{\lambda^i}{2}\gamma_\mu\right]_{ts} \left[\frac{\lambda^i}{2}\gamma_\nu\right]_{ru}, \tag{A.2}$$

where $k = p - q$, $D^{\text{free}}_{\mu\nu}(k)$ is the free gluon propagator in Landau gauge, and $\mathcal{G}(k^2)$ is the effective coupling of Eq. (4.15). The quark propagators are obtained as solutions of the quark SDE in the rainbow truncation.

In this truncation, the full BSE, Eq. (A.1), takes the form

$$\begin{aligned}\lambda(P^2)\Gamma_H(p;P) &= -\int \frac{\mathrm{d}^4q}{(2\pi)^4}\mathcal{G}(k^2)D^{\text{free}}_{\mu\nu}(k)\frac{\lambda^i}{2}\gamma_\mu S^a(q_+)\Gamma_H(q;P)S^b(q_-)\gamma_\nu\frac{\lambda^i}{2} \\ &= \int \frac{\mathrm{d}^4q}{(2\pi)^4} D^{\text{phen}}_{\mu\nu}(k)\gamma_\mu S^a(q_+)\Gamma_H(q;P)S^b(q_-)\gamma_\nu,\end{aligned} \tag{A.3}$$

where $D^{\text{phen}}_{\mu\nu}(k) \equiv -C_F\mathcal{G}(k^2)D^{\text{free}}_{\mu\nu}(k)$ is a "phenomenologically" dressed gluon propagator.

A.1.2. Pseudoscalar Bethe-Salpeter amplitude

In the pseudoscalar channel ($J^P = 0^-$) the lowest mass solutions are the pion and kaon mesons, with valence flavour structure $u\overline{d}$ and $u\overline{s}$, respectively. The general form of the meson BSA in this channel is given by [27]

$$\begin{aligned}\Gamma_H(p;P) &= \gamma_5 \left[\mathrm{i}E_H(p;P) + \not{P}F_H(p;P)\right. \\ &\qquad \left. + \not{p}(p\cdot P)G_H(p;P) + \sigma_{\mu\nu}p_\mu P_\nu H_H(p;P)\right] \\ &= \sum_{\alpha=1}^{4} F_H^\alpha(p;P)A^\alpha(p;P),\end{aligned} \tag{A.4}$$

where we have defined

$$\begin{aligned}A^\alpha(p;P) &= \gamma_5\left\{\mathrm{i}\mathbb{1},\ \not{P},\ \not{p}(p\cdot P),\ \sigma_{\mu\nu}p_\mu P_\nu\right\}, \\ F_H^\alpha(p;P) &= \left\{E_H(p;P),\ F_H(p;P),\ G_H(p;P),\ H_H(p;P)\right\}.\end{aligned} \tag{A.5}$$

The functions $F_H^\alpha(p;P)$ are Lorentz-scalar dressing functions, that is, $F_H^\alpha(p;P) = F_H^\alpha(p^2, p\cdot P; P^2)$, with $P^2 = -m_H^2$ fixed.

A.1.3. Projecting out $\boldsymbol{F_H^\alpha(p;P)}$

We solve the BSE for $\Gamma_H(p;P)$ using matrix methods as follows. First, we project the BSE onto the Lorentz-scalar dressing functions $F_H^\alpha(p;P)$ using appropriate projectors. We denote these by $P^\alpha(p;P)$, $\alpha = 1,\ldots,4$.

In general, the Lorentz-Dirac basis $\{A^\alpha(p;P),\ \alpha = 1,\ldots,4\}$ is not orthogonal with respect to the Dirac trace. Thus, in order to project out the Lorentz-scalar dressing functions $F_H^\alpha(p;P)$ we need to construct these projectors such that

$$F_H^\alpha(p;P) = \frac{1}{4}\mathrm{Tr_D}\left[P^\alpha(p;P)\Gamma_H(p;P)\right], \text{for} \quad \alpha = 1,\ldots,4, \tag{A.6}$$

where $\mathrm{Tr_D}$ is the Dirac trace. Finding these projectors is of course equivalent to a change of basis for $\Gamma_H(p;P)$. Write $P^\alpha(p;P)$, $\alpha = 1,\ldots,4$, in terms of the basis $\{A^\alpha(p;P),\, \alpha = 1,\ldots,4\}$ as

$$P^\alpha(p;P) = \sum_{\beta=1}^{4} P^{\alpha\beta}(p;P) A^\beta(p;P), \tag{A.7}$$

where $P^{\alpha\beta}(p;P)$ are the coefficients for the change of basis. Substituting Eq. (A.7) into the right hand side of Eq. (A.6), we see that the coefficients $P^{\alpha\beta}(p;P)$ are obtained by solving

$$\frac{1}{4}\sum_{\beta=1}^{4} P^{\alpha\beta}(p;P)\mathrm{Tr_D}\left[A^\beta(p;P)A^\gamma(p;P)\right] = \delta^{\alpha\gamma}, \tag{A.8}$$

or in matrix notation

$$\mathcal{P}\mathcal{A} = \mathbb{1} \Rightarrow \mathcal{P} = \mathcal{A}^{-1}, \tag{A.9}$$

where the matrix elements $\mathcal{A}^{\alpha\beta}$ are

$$\begin{aligned}\mathcal{A}^{\alpha\beta}(p;P) &\equiv \frac{1}{4}\mathrm{Tr_D}\left[A^\alpha(p;P)A^\beta(p;P)\right] \\ &= \begin{bmatrix} -1 & 0 & 0 & 0 \\ 0 & -P^2 & -(p\cdot P)^2 & 0 \\ 0 & -(p\cdot P)^2 & -p^2(p\cdot P)^2 & 0 \\ 0 & 0 & 0 & p^2P^2 - (p\cdot P)^2 \end{bmatrix}.\end{aligned} \tag{A.10}$$

By calculating the inverse of $\mathcal{A}$ we find

$$\mathcal{P}^{\alpha\beta} = \left(\mathcal{A}^{-1}\right)^{\alpha\beta} = \begin{bmatrix} (\mathcal{A}^{11})^{-1} & 0 & 0 & 0 \\ 0 & \mathcal{A}^{33}\Delta^{-1} & -\mathcal{A}^{23}\Delta^{-1} & 0 \\ 0 & -\mathcal{A}^{32}\Delta^{-1} & \mathcal{A}^{22}\Delta^{-1} & 0 \\ 0 & 0 & 0 & (\mathcal{A}^{44})^{-1} \end{bmatrix}, \tag{A.11}$$

with $\Delta = \mathcal{A}^{33}\mathcal{A}^{22} - \mathcal{A}^{32}\mathcal{A}^{23}$.

A.1.4. Preparing the numerical kernel I

With the projectors $P^\alpha(p;P)$ found explicitly, we can now project out the dressing functions $F_H^\alpha(p;P)$. Multiply Eq. (A.3) by $(1/4)P^\alpha(p;P)$, take the Dirac trace, and use Eq. (A.6) to obtain

$$\lambda(P^2)F_H^\alpha(p;P) = \int \frac{\mathrm{d}^4q}{(2\pi)^4} K^{\alpha\beta}(p,q;P)F_H^\beta(q;P), \tag{A.12}$$

where we have suppressed summation symbols, and

$$K^{\alpha\beta}(p,q;P) \equiv D_{\mu\nu}^{\mathrm{phen}}(k)\frac{1}{4}\mathrm{Tr}_{\mathrm{D}}\left[P^\alpha(p;P)\gamma_\mu S^a(q_+)A^\beta(q;P)S^b(q_-)\gamma_\nu\right]. \tag{A.13}$$

Eq. (A.12) is a system of four coupled integral equations for the dressing functions $F_H^\alpha(p;P)$.

A.1.5. Momentum frame

We use the rest frame of the meson to solve Eq. (A.12). In Euclidean metric this frame is given by

$$P_\mu = (\mathrm{i}m_H, 0, 0, 0), \tag{A.14}$$

with $P^2 = -m_H^2$ the meson mass shell. In the same metric, the integration measure and loop integration variables are [1, 3]

$$\begin{aligned} \int \frac{\mathrm{d}^4 q}{(2\pi)^4} &= \frac{1}{(2\pi)^4}\frac{1}{2}\int_0^\infty \mathrm{d}q^2 q^2 \int_0^\pi \mathrm{d}\theta \cos^2\theta \int_0^\pi \mathrm{d}\phi \cos\phi \int_0^{2\pi} \mathrm{d}\psi, & \text{(A.15)} \\ \text{where } q_\mu &= \sqrt{q^2}(\cos\theta,\ \sin\theta\cos\phi,\ \sin\theta\sin\phi\cos\psi,\ \sin\theta\sin\phi\sin\psi), & \text{(A.16)} \end{aligned}$$

from which follows that $q \cdot P = \mathrm{i}m_H\sqrt{q^2}\cos\theta$, and therefore the Lorentz-scalar dressing functions $F_H^\alpha(p;P)$ depend only on two variables, one radial and one angular(the ψ integration is trivial, giving an overall contribution of 2π). The numerical integration in Eq. (A.12) is straightforward and is performed using standard Gauss quadrature techniques [82].

A.1.6. Chebyshev decomposition

The system of Eq. (A.12) can now be solved directly for the scalar dressing functions $F_H^\alpha(p;P)$ depending on two variables, p^2 and $p \cdot P$, and labelled by P^2, as an integral eigenvalue equation. This has a high demand of computer memory and computing time. However, in order to elucidate the angular dependence of the Lorentz-scalar dressing functions $F_H^\alpha(p;P)$, and save on computing resources, we expand these in terms of Chebyshev polynomials in the angle $\widehat{p \cdot P} \equiv p \cdot P/|pP| = \cos\theta = z$ as*

$$F_H^\alpha(p^2, p\cdot P; P) = \sum_{m=0}^{\infty}{}' F_{H,m}^\alpha(p^2; P^2) T_m(z), \quad \text{with} \quad P^2 = -m_H^2, \tag{A.17}$$

*In practice the number of Chebyshev polynomials needed in Eq. (A.17) to produce converged results is quite low. For example, the numerical results presented in Figures A.1,A.2 were obtained by using only 4 Chebyshev polynomials in the decomposition of the dressing functions. See also Tables 4.3,4.4

where the prime indicates that the zeroth Chebyshev coefficient is halved. The functions $F^{\alpha}_{H,m}(p^2;P^2)$ can be further projected out using the orthonormal properties of the Chebyshev polynomials T_m,

$$\int_{-1}^{1} \mathrm{d}z\, W(z) T_m(z) T_n(z) = \begin{cases} 0 & : m \neq n \\ \pi & : m = n = 0 \\ \pi/2 & : m = n \neq 0, \end{cases} \tag{A.18}$$

where $W(z) = (1-z^2)^{1/2}$ is the weight function. The Chebyshev moments for $F^{\alpha}_{H}(p;P)$ are thus given by

$$F^{\alpha}_{H,m}(p^2;P^2) = \left(\frac{\pi}{2}\right)^{-1} \int_{-1}^{1} \mathrm{d}z\, W(z) T_m(z) F^{\alpha}_{H}(p^2, p\cdot P; P^2),\ \alpha = 1,\ldots,4, \tag{A.19}$$

with $z = \cos\theta = p\cdot P/|pP| = \widehat{p\cdot P}$.

A.1.7. Preparing the numerical kernel II

Projecting out Eq. (A.12) onto the Chebyshev moments we have

$$\begin{aligned} \lambda(P^2) F^{\alpha}_{H,m}(p^2;P^2) = & \left(\frac{\pi}{2}\right)^{-1} \int_{-1}^{1} \mathrm{d}z\, W(z) T_m\left(\widehat{p\cdot P}\right) \\ & \int \frac{\mathrm{d}^4 q}{(2\pi)^4} K^{\alpha\beta}(p,q;P) \sum_{n=0}^{\infty}{}' T_n\left(\widehat{q\cdot P}\right) F^{\beta}_{H,n}(q^2;P^2) \\ = & \int \mathrm{d}q^2 q^2 K^{\alpha\beta}_{mn}(p^2,q^2;P) F^{\beta}_{H,n}(q^2;P^2), \end{aligned} \tag{A.20}$$

where it is obvious what $K^{\alpha\beta}_{mn}(p^2,q^2;P)$ is. With the angular dependence made explicit, we can evaluate numerically the non-trivial angular integrals appearing after the first equal sign in Eq. (A.20). The result of this is contained in $K^{\alpha\beta}_{mn}(p^2,q^2;P)$. By matching the external radial points, p_i^2, to the integration nodes for the numerical radial integral, q_j^2, we can arrange Eq. (A.20) in the form of an eigenvalue matrix equation for the Cheby-

shev moments. The Bethe-Salpeter amplitude $\Gamma_H(p;P)$ is thus effectively projected out onto the decomposition $F^{\alpha}_{H,m}(p_i^2;P^2)$. Schematically we are solving

$$\lambda(P^2)\mathbf{F} = \mathbf{K}\mathbf{F} \tag{A.21}$$

for the eigenvector $\mathbf{F}$ made up of Chebyshev moments as a parametric equation of $P^2 = -m_H^2$. The required physical solution corresponds to $\lambda = 1$, with the lowest mass solution being the ground state in any particular channel.

A.1.8. Iterative numerical solution

The bound state BSE equation, Eq. (A.1), has now the form of a standard eigenvalue equation, Eq. (A.21), which can be solved with the use of standard numerical techniques. We are only interested in the eigenvalue $\lambda = 1$ with the lowest mass and its corresponding eigenvector. In the pseudoscalar channel these are the pion and the kaon. Finding this eigenvalue, and its associated eigenvector, is done iteratively by studying the evolution of the eigenvalue closest to one with respect to the pseudoscalar meson mass. The pseudoscalar meson mass is that for which $\lambda = 1$ at $P^2 = -m_H^2$. This is equivalent to finding the root of $f(m_H)$, defined by

$$f(m_H) = \lambda(P^2 = -m_H^2) - 1. \tag{A.22}$$

As we are only interested in the $\lambda = 1$ eigenvalue of $\mathbf{K}$, it will be a waste of time to find all the eigenvalues first and then search for the one that is closest to one. The task of finding *only* the closest eigenvalue to one is performed by using the standard inverse iteration method. In general, this method will converge to the closest eigenvalue to ρ, and is based on the following algorithm [146]:

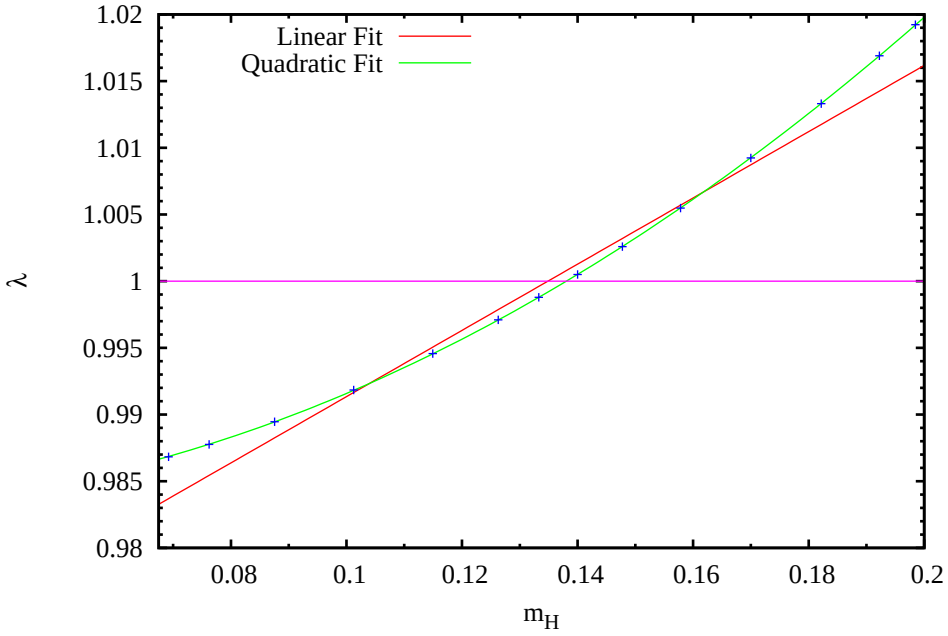

Figure A.1.: Evolution of $\lambda(P^2 = -m_H^2)$ for the pion together with Linear and quadratic fits to the numerical data. The value of m_H that corresponds to the intersection with $\lambda = 1$ is the pion mass; $m_\pi = 0.1385\,\mathrm{GeV}$.

Inverse Iteration:

Choose ϵ, $\mathbf{V}_0$, ρ; Set r_0, $k = 0$

Solve $\mathbf{LU} = \mathbf{K} - \rho\mathbf{1}$ (LU decomposition of the right-hand side)

Repeat

$$\begin{aligned} &k = k + 1 \\ &\text{Solve } (\mathbf{K} - \rho\mathbf{1})\mathbf{Z}_k = \mathbf{V}_{k-1} \\ &r_k = \mathbf{V}_{k-1}^T \mathbf{Z}_k \\ &\mathbf{V}_k = \mathbf{Z}_k / ||\mathbf{Z}_k||_2 \end{aligned} \tag{A.23}$$

Until $|r_k - r_{k-1}| < \epsilon$,

$\lambda = 1/r_k + \rho, \quad \mathbf{F} = \mathbf{V}_k.$

This algorithm is based on the well-known power method which converges to the largest eigenvalue of a matrix [146]. The shift ρ above is chosen in such a way that $(\lambda - \rho)^{-1}$ is the largest eigenvalue of $(\mathbf{K} - \rho\mathbf{1})^{-1}$. Using this algorithm we can, in principle, find all eigenvalues of $\mathbf{K}$. If $\rho \approx \lambda$, then $(\lambda - \rho)^{-1}$ is likely to be the largest eigenvalue,

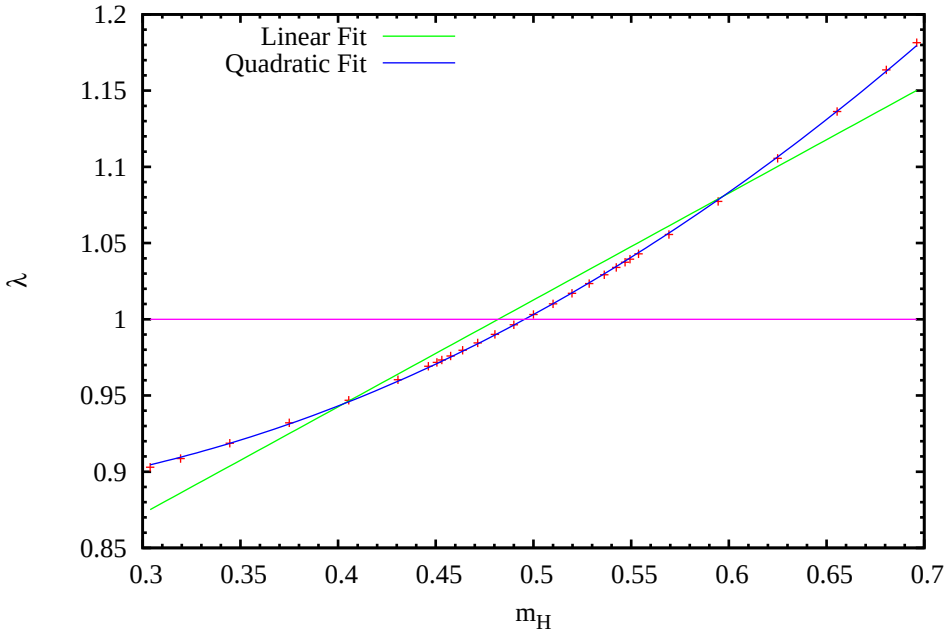

Figure A.2.: Evolution of $\lambda(P^2 = -m_H^2)$ for the kaon together with Linear and quadratic fits to the numerical data. The value of m_H that corresponds to the intersection with $\lambda = 1$ is the kaon mass; $m_K = 0.496\,\text{GeV}$.

hence for good choices of ρ the inverse iteration will converge rapidly. However, choosing a good ρ requires some previous knowledge of the eigenvalues. For this reason, the inverse iteration method is generally used when an estimate of an eigenvalue has been obtained from another algorithm. In this situation, the inverse iteration can be used to improve the eigenvalue estimation as well as to compute the associated eigenvector. Luckily, we know that $\lambda = 1$, and just need to tune m_H such that this occurs. Therefore we put $\rho = 1$ in Eq. (A.23).

In Figures A.1,A.2 we present the evolution of the closest eigenvalue to 1 obtained with the inverse iteration algorithm, Eq. (A.23), for the pion and kaon. The mass of the pseudoscalar meson is that for which $\lambda = 1$. In this way, for the pion we have $m_\pi = 0.1385\,\text{GeV}$, while for the kaon $m_K = 0.496\,\text{GeV}$.

The inverse iteration algorithm gives also the eigenvector $\mathbf{F}$ for the Chebyshev moments. Once these are obtained, the Chebyshev sum in Eq. (A.17) is performed using the Clenshaw's recurrence formula, as discussed in [82]. The normalized Γ_H is then used for the calculation of pseudoscalar observables.

Bibliography

[1] M. E. Peskin and D. V. Schroeder, "An Introduction to quantum field theory,". Reading, USA: Addison-Wesley (1995) 842 p.

[2] L. D. Faddeev and V. N. Popov, "Feynman diagrams for the Yang-Mills field," *Phys. Lett.* **B25** (1967) 29–30.

[3] T. Muta, "Foundations of quantum chromodynamics. Second edition," *World Sci. Lect. Notes Phys.* **57** (1998) 1–409.

[4] J. Nyiri, (ed.), "The Gribov theory of quark confinement,". River Edge, USA: World Scientific (2001) 296 p.

[5] V. N. Gribov, "Quantization of non-Abelian gauge theories," *Nucl. Phys.* **B139** (1978) 1.

[6] B. L. Ioffe, V. S. Fadin, and L. N. Lipatov, "Quantum Chromodynamics: Perturbative and Nonperturbative Aspects," *Camb. Monogr. Part. Phys. Nucl. Phys. Cosmol.* **30** (2010) 1–585, `arXiv:hep-ph/0000000`.

[7] A. Bassetto, I. Lazzizzera, and R. Soldati, "Absence of Gribov copies in the spacelike planar gauge," *Phys. Lett.* **B131** (1983) 177.

[8] J. F. Donoghue, E. Golowich, and B. R. Holstein, "Dynamics of the standard model," *Camb. Monogr. Part. Phys. Nucl. Phys. Cosmol.* **2** (1992) 1–540.

[9] M. Dine, "The strong CP problem," `arXiv:hep-ph/0011376`.

[10] K. Huang, "Quarks, Leptons and Gauge Fields,". Singapore, Singapore: World Scientific (1982) 281p.

[11] W. Weise, "The QCD vacuum and its hadronic excitations," `arXiv:nucl-th/0504087`.

[12] P. van Baal, "The QCD vacuum," *Nucl. Phys. Proc. Suppl.* **63** (1998) 126–137,

arXiv:hep-lat/9709066.

[13] S. Weinberg, "The U(1) Problem," *Phys. Rev.* **D11** (1975) 3583–3593.

[14] J. C. Collins, "The problem of scales: Renormalization and all that," arXiv:hep-ph/9510276.

[15] J. C. Collins, "Renormalization. An introduction to renormalization, the renormalization group, and the operator product expansion,". Cambridge, Uk: Univ. Pr. (1984) 380p.

[16] S. Capstick *et al.*, "Key issues in hadronic physics," arXiv:hep-ph/0012238.

[17] D. Drechsel and T. Walcher, "Hadron structure at low Q^2 ," *Rev. Mod. Phys.* **80** (2008) 731–785, arXiv:0711.3396 [hep-ph].

[18] I. Aznauryan *et al.*, "Theory Support for the Excited Baryon Program at the Jlab 12 GeV Upgrade," arXiv:0907.1901 [nucl-th].

[19] P. Hagler, "Hadron structure from lattice quantum chromodynamics," *Phys. Rept.* **490** (2010) 49–175, arXiv:0912.5483 [hep-lat].

[20] D. B. Renner, "Status and prospects for the calculation of hadron structure from lattice QCD," arXiv:1002.0925 [hep-lat].

[21] F. Gross, "Relativistic quantum mechanics and field theory,". New York, USA: Wiley (1993) 629 p.

[22] G. Eichmann, "Hadron properties from QCD bound-state equations," arXiv:0909.0703 [hep-ph].

[23] A. Holl, C. D. Roberts, and S. V. Wright, "Hadron physics and Dyson-Schwinger equations," arXiv:nucl-th/0601071.

[24] P. Maris and C. D. Roberts, "Dyson-Schwinger equations: A tool for hadron physics," *Int. J. Mod. Phys.* **E12** (2003) 297–365, arXiv:nucl-th/0301049.

[25] E. E. Salpeter and H. A. Bethe, "A Relativistic equation for bound state problems," *Phys. Rev.* **84** (1951) 1232–1242.

[26] M. Gell-Mann and F. Low, "Bound states in quantum field theory," *Phys. Rev.* **84** (1951) 350–354.

[27] C. H. Llewellyn-Smith, "A relativistic formulation for the quark model for

mesons," *Ann. Phys.* **53** (1969) 521–558.

[28] C. D. Roberts, M. S. Bhagwat, A. Holl, and S. V. Wright, "Aspects of hadron physics," *Eur. Phys. J. ST* **140** (2007) 53–116, arXiv:0802.0217 [nucl-th].

[29] C. D. Roberts and A. G. Williams, "Dyson-Schwinger equations and their application to hadronic physics," *Prog. Part. Nucl. Phys.* **33** (1994) 477–575, arXiv:hep-ph/9403224.

[30] N. Nakanishi, "Normalization Condition and Normal and Abnormal Solutions of the Bethe-Salpeter Equation," *Phys. Rev.* **138** (1965) B1182–B1192.

[31] N. Nakanishi, "Normalization Condition and Normal and Abnormal Solutions of the Bethe-Salpeter Equation. II," *Phys. Rev.* **139** (1965) B1401–B1406.

[32] E. V. Shuryak, "The QCD vacuum, hadrons and the superdense matter," *World Sci. Lect. Notes Phys.* **71** (2004) 1–618.

[33] V. A. Miransky, "Dynamical symmetry breaking in quantum field theories,". Singapore, Singapore: World Scientific (1993) 533 p.

[34] T. P. Cheng and L. F. Li, "Gauge Theory of Elementary Particle Physics,". Oxford, UK: Clarendon (1984) 536 P. (Oxford Science Publications).

[35] S. Narison, "QCD as a theory of hadrons: from partons to confinement," *Camb. Monogr. Part. Phys. Nucl. Phys. Cosmol.* **17** (2002) 1–779, arXiv:hep-ph/0205006.

[36] T.-W. Chiu and T.-H. Hsieh, "Light quark masses, chiral condensate and quark-gluon condensate in quenched lattice QCD with exact chiral symmetry," *Nucl. Phys.* **B673** (2003) 217–237, arXiv:hep-lat/0305016.

[37] R. Williams, "Schwinger-Dyson equations in QED and QCD: The Calculation of fermion-antifermion condensates,".

[38] P. Maris and C. D. Roberts, "pi and K meson Bethe-Salpeter amplitudes," *Phys. Rev.* **C56** (1997) 3369–3383, arXiv:nucl-th/9708029.

[39] J. M. Cornwall, "Dynamical Mass Generation in Continuum QCD," *Phys. Rev.* **D26** (1982) 1453.

[40] H. Pagels, "Dynamical Chiral Symmetry Breaking in Quantum Chromodynamics," *Phys. Rev.* **D19** (1979) 3080.

[41] P. Maris, C. D. Roberts, and P. C. Tandy, "Pion mass and decay constant," *Phys. Lett.* **B420** (1998) 267–273, arXiv:nucl-th/9707003.

[42] P. Maris and P. C. Tandy, "Bethe-Salpeter study of vector meson masses and decay constants," *Phys. Rev.* **C60** (1999) 055214, arXiv:nucl-th/9905056.

[43] R. Alkofer and L. von Smekal, "The infrared behavior of QCD Green's functions: Confinement, dynamical symmetry breaking, and hadrons as relativistic bound states," *Phys. Rept.* **353** (2001) 281, arXiv:hep-ph/0007355.

[44] A. S. Kronfeld and C. Quigg, "Resource Letter: Quantum Chromodynamics," arXiv:1002.5032 [hep-ph].

[45] A. Efremov and A. Radyushkin, "Perturbative QCD of hard and soft processes," *Mod. Phys. Lett.* **A24** (2009) 2803–2824, arXiv:0911.1195 [hep-ph].

[46] L. Chang, Y.-X. Liu, M. S. Bhagwat, C. D. Roberts, and S. V. Wright, "Dynamical chiral symmetry breaking and a critical mass," *Phys. Rev.* **C75** (2007) 015201, arXiv:nucl-th/0605058.

[47] M. S. Bhagwat and P. C. Tandy, "Analysis of full-QCD and quenched-QCD lattice propagators," *AIP Conf. Proc.* **842** (2006) 225–227, arXiv:nucl-th/0601020.

[48] P. O. Bowman *et al.*, "Unquenched quark propagator in Landau gauge," *Phys. Rev.* **D71** (2005) 054507, arXiv:hep-lat/0501019.

[49] M. S. Bhagwat, M. A. Pichowsky, C. D. Roberts, and P. C. Tandy, "Analysis of a quenched lattice-QCD dressed-quark propagator," *Phys. Rev.* **C68** (2003) 015203, arXiv:nucl-th/0304003.

[50] P. Maris, A. Raya, C. D. Roberts, and S. M. Schmidt, "Facets of confinement and dynamical chiral symmetry breaking," *Eur. Phys. J.* **A18** (2003) 231–235, arXiv:nucl-th/0208071.

[51] R. Alkofer, W. Detmold, C. S. Fischer, and P. Maris, "Analytic properties of the Landau gauge gluon and quark propagators," *Phys. Rev.* **D70** (2004) 014014, arXiv:hep-ph/0309077.

[52] R. Alkofer, W. Detmold, C. S. Fischer, and P. Maris, "Analytic structure of the Landau gauge gluon propagator," *AIP Conf. Proc.* **756** (2005) 272–274, arXiv:hep-ph/0411367.

[53] R. Alkofer, W. Detmold, C. S. Fischer, and P. Maris, "Analytic structure of the gluon and quark propagators in Landau gauge QCD," *Nucl. Phys. Proc. Suppl.* **141** (2005) 122–127, arXiv:hep-ph/0309078.

[54] R. Alkofer, C. S. Fischer, F. J. Llanes-Estrada, and K. Schwenzer, "The quark-gluon vertex in Landau gauge QCD: Its role in dynamical chiral symmetry breaking and quark confinement," *Annals Phys.* **324** (2009) 106–172, arXiv:0804.3042 [hep-ph].

[55] C. S. Fischer, "Non-perturbative propagators, running coupling and dynamical mass generation in ghost - antighost symmetric gauges in QCD," arXiv:hep-ph/0304233.

[56] J. Skullerud and A. Kizilersu, "Quark-gluon vertex from lattice QCD," *JHEP* **09** (2002) 013, arXiv:hep-ph/0205318.

[57] J. I. Skullerud, P. O. Bowman, A. Kizilersu, D. B. Leinweber, and A. G. Williams, "Nonperturbative structure of the quark gluon vertex," *JHEP* **04** (2003) 047, arXiv:hep-ph/0303176.

[58] J.-I. Skullerud, P. O. Bowman, A. Kizilersu, D. B. Leinweber, and A. G. Williams, "Quark-gluon vertex in arbitrary kinematics," *Nucl. Phys. Proc. Suppl.* **141** (2005) 244–249, arXiv:hep-lat/0408032.

[59] J. Skullerud, P. O. Bowman, and A. Kizilersu, "The nonperturbative quark gluon vertex," arXiv:hep-lat/0212011.

[60] A. Cucchieri and T. Mendes, "What's up with IR gluon and ghost propagators in Landau gauge? A puzzling answer from huge lattices," *PoS* **LAT2007** (2007) 297, arXiv:0710.0412 [hep-lat].

[61] S. Bethke, "The 2009 World Average of $\alpha_s(M_Z)$," *Eur. Phys. J.* **C64** (2009) 689–703, arXiv:0908.1135 [hep-ph].

[62] P. Jain and H. J. Munczek, "Calculation of the pion decay constant in the framework of the Bethe-Salpeter equation," *Phys. Rev.* **D44** (1991) 1873–1879.

[63] H. J. Munczek and P. Jain, "Relativistic pseudoscalar q anti-q bound states: Results on Bethe-Salpeter wave functions and decay constants," *Phys. Rev.* **D46** (1992) 438–445.

[64] R. Alkofer, P. Watson, and H. Weigel, "Mesons in a Poincare covariant

Bethe-Salpeter approach," *Phys. Rev.* **D65** (2002) 094026, arXiv:hep-ph/0202053.

[65] M. R. Frank and C. D. Roberts, "Model gluon propagator and pion and rho meson observables," *Phys. Rev.* **C53** (1996) 390–398, arXiv:hep-ph/9508225.

[66] R. Alkofer and C. D. Roberts, "Calculation of the anomalous $\gamma\pi^* \to \pi\pi$ form factor," *Phys. Lett.* **B369** (1996) 101–107, arXiv:hep-ph/9510284.

[67] A. Holl, A. Krassnigg, and C. D. Roberts, "Pseudoscalar meson radial excitations," *Phys. Rev.* **C70** (2004) 042203, arXiv:nucl-th/0406030.

[68] A. Holl, A. Krassnigg, P. Maris, C. D. Roberts, and S. V. Wright, "Electromagnetic properties of ground and excited state pseudoscalar mesons," *Phys. Rev.* **C71** (2005) 065204, arXiv:nucl-th/0503043.

[69] A. Krassnigg, "Excited mesons in a Bethe-Salpeter approach," *PoS* **CONFINEMENT8** (2008) 075, arXiv:0812.3073 [nucl-th].

[70] A. Krassnigg, "Survey of J=0,1 mesons in a Bethe-Salpeter approach," *Phys. Rev.* **D80** (2009) 114010, arXiv:0909.4016 [hep-ph].

[71] M. S. Bhagwat and P. Maris, "Vector meson form factors and their quark-mass dependence," *Phys. Rev.* **C77** (2008) 025203, arXiv:nucl-th/0612069.

[72] H. D. Politzer, "Effective Quark Masses in the Chiral Limit," *Nucl. Phys.* **B117** (1976) 397.

[73] V. A. Miransky, "On dynamical chiral symmetry breaking," *Phys. Lett.* **B165** (1985) 401–404.

[74] J. Skullerud, D. B. Leinweber, and A. G. Williams, "Nonperturbative improvement and tree-level correction of the quark propagator," *Phys. Rev.* **D64** (2001) 074508, arXiv:hep-lat/0102013.

[75] P. O. Bowman, U. M. Heller, D. B. Leinweber, and A. G. Williams, "Modelling the quark propagator," *Nucl. Phys. Proc. Suppl.* **119** (2003) 323–325, arXiv:hep-lat/0209129.

[76] P. O. Bowman, U. M. Heller, D. B. Leinweber, A. G. Williams, and J.-b. Zhang, "Infrared and ultraviolet properties of the Landau gauge quark propagator," *Nucl. Phys. Proc. Suppl.* **128** (2004) 23–29, arXiv:hep-lat/0403002.

[77] J. D. Bjorken and S. Drell, *Relativistic Quantum Fields*. McGraw-Hill, New York, first ed., 1965.

[78] C. S. Fischer, D. Nickel, and J. Wambach, "Hadronic unquenching effects in the quark propagator," *Phys. Rev.* **D76** (2007) 094009, arXiv:0705.4407 [hep-ph].

[79] H. J. Munczek, "Dynamical chiral symmetry breaking, Goldstone's theorem and the consistency of the Schwinger-Dyson and Bethe- Salpeter Equations," *Phys. Rev.* **D52** (1995) 4736–4740, arXiv:hep-th/9411239.

[80] J. M. Cornwall, R. Jackiw, and E. Tomboulis, "Effective Action for Composite Operators," *Phys. Rev.* **D10** (1974) 2428–2445.

[81] A. Krassnigg and C. D. Roberts, "DSEs, the pion, and related matters," *Fizika* **B13** (2004) 143–152, arXiv:nucl-th/0308039.

[82] W. H. Press, S. A. Teukolsky, W. T. Veterling, and B. P. Flannery, "Numerical Recipes in Fortran 90: The Art of parallel scientific computing," *Cambridge University Press (UK)* **vol 2** (1996) 935–1447.

[83] F. Halzen and A. D. Martin, "Quarks and Leptons: An introductory course in modern particle physics,". New York, Usa: Wiley (1984) 396p.

[84] S. R. Amendolia *et al.*, "Measurement of the pion form-factor in the timelike region for q^2 values between 0.1-GeV/c^2 and 0.18-GeV/c^2," *Phys. Lett.* **B138** (1984) 454.

[85] **NA7** Collaboration, S. R. Amendolia *et al.*, "A Measurement of the Space - Like Pion Electromagnetic Form-Factor," *Nucl. Phys.* **B277** (1986) 168.

[86] K. Huang, "Quarks, Leptons and Gauge Fields,". Singapore, Singapore: World Scientific 2nd ed (1992) 333p.

[87] G. P. Lepage and S. J. Brodsky, "Exclusive Processes in Quantum Chromodynamics: Evolution Equations for Hadronic Wave Functions and the Form-Factors of Mesons," *Phys. Lett.* **B87** (1979) 359–365.

[88] G. P. Lepage and S. J. Brodsky, "Exclusive Processes in Perturbative Quantum Chromodynamics," *Phys. Rev.* **D22** (1980) 2157.

[89] N. Isgur and C. H. Llewellyn Smith, "Asymptopia in High q^2 Exclusive Processes in QCD," *Phys. Rev. Lett.* **52** (1984) 1080.

[90] N. Isgur and C. H. Llewellyn Smith, "Perturbative QCD in exclusive processes," *Phys. Lett.* **B217** (1989) 535–538.

[91] N. Isgur and C. H. Llewellyn Smith, "The Applicability of Perturbative QCD to Exclusive Processes," *Nucl. Phys.* **B317** (1989) 526–572.

[92] L. M. Barkov *et al.*, "Electromagnetic Pion Form-Factor in the Timelike Region," *Nucl. Phys.* **B256** (1985) 365–384.

[93] **DM2** Collaboration, D. Bisello *et al.*, "The pion electromagnetic form facror in the timelike energy range 1.35-GeV ¡= $\sqrt{S}$ ¡= 2.4-GeV," *Phys. Lett.* **B220** (1989) 321.

[94] M. R. Whalley, "A Compilation of data on hadronic total cross-sections in e+ e- interactions," *J. Phys.* **G29** (2003) A1–A133.

[95] S. R. Amendolia *et al.*, "A measurement of the pion charge radius," *Phys. Lett.* **B146** (1984) 116.

[96] **Jefferson Lab** Collaboration, G. M. Huber *et al.*, "Charged pion form factor between Q^2=0.60 and 2.45 GeV^2. II. Determination of, and results for, the pion form factor," *Phys. Rev.* **C78** (2008) 045203, arXiv:0809.3052 [nucl-ex].

[97] **Jefferson Lab** Collaboration, H. P. Blok *et al.*, "Charged pion form factor between Q^2=0.60 and 2.45 GeV^2. I. Measurements of the cross section for the ^{1}H$(e, e'\pi^+)n$ reaction," *Phys. Rev.* **C78** (2008) 045202, arXiv:0809.3161 [nucl-ex].

[98] G. M. Huber *et al.*, "Measurement of the charged pion form factor to high q^2,". http://www.jlab.org/exp_prog/generated/12GeV/apphallc.html.

[99] **The Jefferson Lab F(pi)** Collaboration, J. Volmer *et al.*, "Measurement of the charged pion electromagnetic form factor," *Phys. Rev. Lett.* **86** (2001) 1713–1716, arXiv:nucl-ex/0010009.

[100] **Jefferson Lab F(pi)** Collaboration, V. Tadevosyan *et al.*, "Determination of the pion charge form factor for Q^2=0.60- 1.60 GeV^2," *Phys. Rev.* **C75** (2007) 055205, arXiv:nucl-ex/0607007.

[101] **Jefferson Lab F(pi)-2** Collaboration, T. Horn *et al.*, "Determination of the Charged Pion Form Factor at Q^2=1.60 and 2.45 (GeV/c)^2," *Phys. Rev. Lett.* **97** (2006) 192001, arXiv:nucl-ex/0607005.

[102] M. Vanderhaeghen, M. Guidal, and J. M. Laget, "Regge description of charged pseudoscalar meson electroproduction above the resonance region," *Phys. Rev.* **C57** (1998) 1454–1457.

[103] G. F. Chew and F. E. Low, "Unstable particles as targets in scattering experiments," *Phys. Rev.* **113** (1959) 1640–1648.

[104] G. M. Huber, "Recent experimental results for the π^+ electric form factor from Jefferson Lab," *J. Phys. Conf. Ser.* **69** (2007) 012015.

[105] P. Brauel *et al.*, "Pi- Electroproduction Off Deuterium Above the Resonance Region," *Phys. Lett.* **B65** (1976) 184–186.

[106] P. Brauel *et al.*, "Separation of Sigma-L and Sigma-u in pi+ Electroproduction Above the Resonance Region," *Phys. Lett.* **B69** (1977) 253.

[107] C. J. Bebek *et al.*, "Further measurements of forward-charged-pion electroproduction at large κ^2," *Phys. Rev.* **D9** (1974) 1229–1242.

[108] C. J. Bebek *et al.*, "Measurement of the pion form-factor up to $q^2 = 4$- GeV^2," *Phys. Rev.* **D13** (1976) 25.

[109] C. J. Bebek *et al.*, "Electroproduction of single pions at low epsilon and a measurement of the pion form-factor up to $q^2 = 10$- GeV^2," *Phys. Rev.* **D17** (1978) 1693.

[110] H. Ackermann *et al.*, "Determination of the Longitudinal and the Transverse Part in pi+ Electroproduction," *Nucl. Phys.* **B137** (1978) 294.

[111] F. Gutbrod and G. Kramer, "The k-squared dependence of the transverse pion electroproduction cross-section in a generalized born term model," *Nucl. Phys.* **B49** (1972) 461–474.

[112] F. A. Berends, "Forward charged-pion electroproduction from fixed-momentum-transfer dispersion relations," *Phys. Rev.* **D1** (1970) 2590–2594.

[113] http://www.jlab.org/ mack/FPI_PHASE2/.

[114] http://www.jlab.org/12GeV/.

[115] E. S. Smith, "The 12 GeV JLab Upgrade Project," *Nucl. Phys.* **A827** (2009) 599c–604c, `arXiv:0901.3249 [nucl-ex]`.

[116] E. S. Smith, "Physics prospects with the JLab 12-GeV upgrade," *Nucl. Phys.* **A721** (2003) 198–205.

[117] K. de Jager, "Future research program at JLab: 12-GeV and beyond," *Nucl. Phys.* **A805** (2008) 494–501.

[118] M. Guidal, J. M. Laget, and M. Vanderhaeghen, "Pion and kaon photoproduction at high energies: Forward and intermediate angles," *Nucl. Phys.* **A627** (1997) 645–678.

[119] M. R. Frank, "Nonperturbative aspects of the quark - photon vertex," *Phys. Rev.* **C51** (1995) 987–998, `arXiv:nucl-th/9403009`.

[120] P. Maris and P. C. Tandy, "The quark photon vertex and the pion charge radius," *Phys. Rev.* **C61** (2000) 045202, `arXiv:nucl-th/9910033`.

[121] C. J. Burden and C. D. Roberts, "Gauge covariance and the fermion - photon vertex in three- dimensional and four-dimensional, massless quantum electrodynamics," *Phys. Rev.* **D47** (1993) 5581–5588, `arXiv:hep-th/9303098`.

[122] Y. Takahashi, "On the generalized Ward identity," *Nuovo Cim.* **6** (1957) 371.

[123] J. C. Ward, "An Identity in Quantum Electrodynamics," *Phys. Rev.* **78** (1950) 182.

[124] D. C. Curtis and M. R. Pennington, "Truncating the Schwinger-Dyson equations: How multiplicative renormalizability and the Ward identity restrict the three point vertex in QED," *Phys. Rev.* **D42** (1990) 4165–4169.

[125] A. Kizilersu and M. R. Pennington, "Building the Full Fermion-Photon Vertex of QED by Imposing Multiplicative Renormalizability of the Schwinger-Dyson Equations for the Fermion and Photon Propagators," *Phys. Rev.* **D79** (2009) 125020, `arXiv:0904.3483 [hep-th]`.

[126] J. S. Ball and T.-W. Chiu, "Analytic Properties of the Vertex Function in Gauge Theories. 1," *Phys. Rev.* **D22** (1980) 2542.

[127] F. T. Hawes and M. A. Pichowsky, "Electromagnetic form factors of light vector mesons," *Phys. Rev.* **C59** (1999) 1743–1750, `arXiv:nucl-th/9806025`.

[128] A. Krassnigg and P. Maris, "Pseudoscalar and vector mesons as q anti-q bound states," *J. Phys. Conf. Ser.* **9** (2005) 153–160, `arXiv:nucl-th/0412058`.

[129] P. Maris, "Meson elastic and transition form factors," arXiv:nucl-th/0209048.

[130] P. Maris and P. C. Tandy, "The pi, K+, and K0 electromagnetic form factors," *Phys. Rev.* **C62** (2000) 055204, arXiv:nucl-th/0005015.

[131] P. Maris and P. C. Tandy, "QCD modeling of hadron physics," *Nucl. Phys. Proc. Suppl.* **161** (2006) 136–152, arXiv:nucl-th/0511017.

[132] G. A. Miller, M. Strikman, and C. Weiss, "Pion transverse charge density from timelike form factor data," arXiv:1011.1472 [hep-ph].

[133] A. W. Thomas, "The Pion Cloud: Insights into Hadron Structure," *Prog. Theor. Phys.* **168** (2007) 614, arXiv:0711.2259 [nucl-th].

[134] P. Watson and W. Cassing, "Unquenching the quark antiquark Green's function," *Few Body Syst.* **35** (2004) 99–115, arXiv:hep-ph/0405287.

[135] R. Alkofer, G. Eichmann, A. Krassnigg, and D. Nicmorus, "Hadron properties from QCD bound-state equations: A status report," *Chin. Phys.* **C34** (2010) 1175, arXiv:0912.3105 [hep-ph].

[136] A. Kizilersu, D. B. Leinweber, J.-I. Skullerud, and A. G. Williams, "Quark-gluon vertex in general kinematics," *Eur. Phys. J.* **C50** (2007) 871–875, arXiv:hep-lat/0610078.

[137] C. S. Fischer, D. Nickel, and R. Williams, "On Gribov's supercriticality picture of quark confinement," *Eur. Phys. J.* **C60** (2008) 1434–6052, arXiv:0807.3486 [hep-ph].

[138] C. S. Fischer and R. Williams, "Beyond the rainbow: effects from pion back-coupling," *Phys. Rev.* **D78** (2008) 074006, arXiv:0808.3372 [hep-ph].

[139] C. S. Fischer, P. Watson, and W. Cassing, "Probing unquenching effects in the gluon polarisation in light mesons," *Phys. Rev.* **D72** (2005) 094025, arXiv:hep-ph/0509213.

[140] C. S. Fischer and R. Alkofer, "Non-perturbative Propagators, Running Coupling and Dynamical Quark Mass of Landau gauge QCD," *Phys. Rev.* **D67** (2003) 094020, arXiv:hep-ph/0301094.

[141] R. Alkofer, A. Bender, and C. D. Roberts, "Pion loop contribution to the electromagnetic pion charge radius," *Int. J. Mod. Phys.* **A10** (1995) 3319–3342,

arXiv:hep-ph/9312243.

[142] J. Bijnens, P. Dhonte, and P. Talavera, "pi pi scattering in three flavour ChPT," *JHEP* **01** (2004) 050, arXiv:hep-ph/0401039.

[143] C. S. Fischer and R. Williams, "Probing the gluon self-interaction in light mesons," *Phys. Rev. Lett.* **103** (2009) 122001, arXiv:0905.2291 [hep-ph].

[144] R. Williams and C. S. Fischer, "Bethe-Salpeter equations: mesons beyond the rainbow-ladder truncation," arXiv:0912.3711 [hep-ph].

[145] A. Bender, C. D. Roberts, and L. Von Smekal, "Goldstone Theorem and Diquark Confinement Beyond Rainbow- Ladder Approximation," *Phys. Lett.* **B380** (1996) 7–12, arXiv:nucl-th/9602012.

[146] J. W. Demmel, "Applied Numerical Linear Algebra,". Society for Industrial Mathematics (1997) 431 p.

List of figures

List of tables